TAU AND NEURODEGENERATION: NEUROIMAGING, GENES, AND BIOMARKERS

Kacie Danielle Deters

Submitted to the faculty of the University Graduate School
in partial fulfillment of the requirements
for the degree
Doctor of Philosophy
in the Program of Medical Neuroscience,
Indiana University

August 2017

Accepted by the Graduate Faculty of Indiana University, in partial fulfillment of the requirements for the degree of Doctor of Philosophy.

Ruben Vidal, Ph.D., Chair

Andrew J. Saykin, Psy.D.

Martin Farlow, M.D.

Doctoral Committee

Shannon L. Risacher, Ph.D.

June 29, 2017

Kwangsik Nho, Ph.D.

Sujuan Gao, Ph.D.

Dedication

This dissertation is dedicated to all those who were told they won't, they can't, and they shouldn't…because you can.

Acknowledgements

I would first like to thank my family. My mother who sacrificed so much for me to get a decent education. My aunt Cheryl Deters who has always been my cheerleader and my Disneyland buddy. The love and support of my family knows no bounds and I am forever grateful for what they have given me.

I would like to acknowledge Dr. Andrew J. Saykin and the amazing research environment he has created for students. Dr. Saykin took me in as lowly Master's student with zero neuroscience or imaging experience and has provided me with everything I needed to be a real, certified scientist. His kindness, calmness, peacefulness, and mentorship has led me to the successful future that awaits me. Dr. Shannon Risacher, words can't describe how much her mentorship, leadership, and friendship have helped me get through this degree. Like Dr Saykin, her peacefulness and kindness is just what I needed in my life. As her first trainee, all I can say is, she rocks. I have no doubt in my mind that Shannon will make a great mentor to any student who comes her way. Both Drs. Saykin and Risacher are beyond smart, beyond kind, and beyond friendly.

My committee members have always been there when I needed help and have continued to provide advice and support over the years: Dr. Ruben Vidal, Dr. Martin Farlow, Dr. Kwangsik Nho, and Dr. Sujuan Gao. John West, Brad Glazier, and Marian Helms have to be some of the most positive people I know. They may not know the impact they had, but when I was in panic mode and needed their assistance, talking to any of them always made life better. Additionally, other members of the Saykin lab and collaborators, both past and present, including Dr. Sungeun Kim, Dr. Shanker Swaminathan, Dr. Brenna McDonald, Dr. Kelly Nudelman, Tamiko R. Magee, Eileen Tallman, and Dr. Li Shen for their contributions to my research. Furthermore, it takes a team to do great science. A would like to thank all those who contributed their time and

efforts to helping me publish including Dr. Frederick W Unverzagt, Dr. David A Kareken, Dr. Gary D Hutchins, Dr. Karmen K Yoder, Dr. Jill R Murrell, Dr. Salvatore Spina, Francine Epperson, Dr. Adrian Oblak, Dr. Kimberly Quaid, Dr. Kaj Blennow, Dr. Henrik Zetterberg, Dr. Leslie Shaw, Dr. John Trojanowski, and Dr. Michael Weiner, and especially Dr. Bernardino Ghetti for providing the neuropathology analysis. I would like to thank the GSS and MSTD family members and ADNI and IMAS participants for their participation in our research.

Next up, my Indy friends. Joey Contreras, Jason Kwon, Christine VanArsdall, Zahi Abdul Sater, and Jeff Willy, thank you for always drinking with me! Without you all in Indy, I don't think I would've made it through the program with my sanity intact. Jenya Chumin, without those nerf guns, I would've gone bonkers! Naomie Olivos, we met in Cali, and now you are stuck with me for life; that in itself says what you mean to me. Yohance Allette, no matter what our future holds for us both, your support and the support of your family was more than I asked for, and I will forever hold that memory in heart.

Monica Henry, thank you for your friendship and your encouragement. You are a wonderful human being and your support through the years has meant the world. You have and will continue to always be a positive influence in everyone's life that you enter.

My friends in other states: Marisa Hughes and family, Morena Duwe, Dominick Gray, Jennifer Welsh, The Therrio family, Susie Harvey, Janell Williams, The Ortega family, Cierra Jamerson, Sade Sparks, Uche Egeonuigwe, and Echo Dickerson. I have known each of you almost ten years or more and having friends like you has made all the difference. All of you have always cheered me on and more importantly, we have maintained our friendship thousands of miles apart. Thank you.

I would not have been able to complete my dissertation if it weren't for the various forms of financial support. The research was supported in part by grants from

the National Institute on Aging (P30 AG10133, R01 AG19771, R36 AG053445, and K01 AG049050), the Alzheimer's Association, the National Library of Medicine (R01 LM011360), the Indiana University Health-Indiana University School of Medicine Strategic Research Initiative, and the Indiana Clinical and Translational Science Institute (CTSI). Additionally, the Alzheimer's Disease Neuroimaging Initiative (ADNI) (National Institutes of Health Grant U01 AG024904) and DOD ADNI (Department of Defense award number W81XWH-12-2-0012). ADNI is funded by the National Institute on Aging, the National Institute of Biomedical Imaging and Bioengineering, and through generous contributions from the following: AbbVie, Alzheimer's Association; Alzheimer's Drug Discovery Foundation; Araclon Biotech; BioClinica, Inc.; Biogen; Bristol-Myers Squibb Company; CereSpir, Inc.; Cogstate; Eisai Inc.; Elan Pharmaceuticals, Inc.; Eli Lilly and Company; EuroImmun; F. Hoffmann-La Roche Ltd and its affiliated company Genentech, Inc.; Fujirebio; GE Healthcare; IXICO Ltd.; Janssen Alzheimer Immunotherapy Research & Development, LLC.; Johnson & Johnson Pharmaceutical Research & Development LLC.; Lumosity; Lundbeck; Merck & Co., Inc.; Meso Scale Diagnostics, LLC.; NeuroRx Research; Neurotrack Technologies; Novartis Pharmaceuticals Corporation; Pfizer Inc.; Piramal Imaging; Servier; Takeda Pharmaceutical Company; and Transition Therapeutics. The Canadian Institutes of Health Research is providing funds to support ADNI clinical sites in Canada. Private sector contributions are facilitated by the Foundation for the National Institutes of Health (www.fnih.org). The grantee organization is the Northern California Institute for Research and Education, and the study is coordinated by the Alzheimer's Therapeutic Research Institute at the University of Southern California. ADNI data are disseminated by the Laboratory for Neuro Imaging at the University of Southern California.

Kacie Danielle Deters

TAU AND NEURODEGENERATION: NEUROIMAGING, GENES, AND BIOMARKERS

The pathway leading from soluble and monomeric to hyperphosphorylated, insoluble and filamentous tau protein is at the center of many human neurodegenerative diseases, collectively referred to as tauopathies, such as Alzheimer disease (AD). In this report, we discuss the role of neuroimaging, genetics, and biomarkers in better understanding the underlying brain changes in tauopathies. In Chapters 1 and 2, we review current knowledge of tauopathies, the protein tau and FDG PET studies in AD. In Chapter 3, we investigate glucose metabolism using [^{18}F]FDG PET in a family with multiple systems tauopathy with presenile dementia (MSTD), a primary tauopathy cause by a mutation in *MAPT*. The results from this study suggest that mutation carriers have lower [^{18}F]FDG uptake, which may precede clinical onset. In Chapter 4, we assessed brain glucose metabolism using [^{18}F]Fluorodeoxyglucose (FDG) positron emission tomography (PET) in individuals with Gerstmann–Sträussler–Scheinker Disease (GSS) with the *PRNP* F198S mutation. The results from this study suggest hypometabolism in the cerebellar and striatal regions, which may be preceded by hypermetabolism. This chapter also evaluated if [^{11}C]Pittsburgh Compound B (PiB) PET is capable of detecting PrP-amyloid in GSS in individuals with the *PRNP* P102L and F198S mutations. The results from this study suggest that [^{11}C]PiB is not suitable for *in vivo* assessment of PrP-amyloid plaques in GSS. In Chapter 5, we examine a correlation between two peripheral markers of axonal degeneration, plasma tau and neurofilament light (NFL), and MRI. The results from this study suggest that plasma NFL may be a more specific marker for neurodegeneration relative to plasma tau. In Chapter 6, we attempted to create a tau biological network from gene and protein databases and literature search. We identified over 150 genes that are related to tau protein or *MAPT* that are involved in different

biological functions. Overall, the results of this report support the notion that using a combination of techniques may help model progression of tau pathology. Future studies may establish additional markers that may be used in combination with some of these measures as tools for diagnosis and for the evaluation of treatment efficacy in therapeutic trials.

Ruben Vidal, Ph.D., Chair

Table of Contents

List of Tables

List of Figures

List of Abbreviations

1.5T	1.5 Tesla
21F12	Amyloid-beta antibody
3R	3 microtubule-binding repeats
3T	3 Tesla
4R	4 microtubule-binding repeats
ABri	Amyloid-BRI
AC	Asymptomatic carrier
AD	Alzheimer's disease
ADNI	Alzheimer's Disease Neuroimaging Initiative
ANCOVA	Analysis of covariance
ANOVA	Analysis of variance
APOE	Apolipoprotein E
APOE ε4	Apolipoprotein E epsilon 4 allele
APP	Amyloid precursor protein
APrP	Prion protein-amyloid
AT8	Tau antibody
Aβ	Amyloid-beta
Aβ-	Amyloid-beta negative
Aβ+	Amyloid-beta positive
BA	Brodmann area
BACE1	Beta-secretase amyloid precursor protein cleaving enzyme
BRI2	Integral transmembrane protein 2B
BSB	(*trans*, *trans*),-1-bromo-2,5-bis-(3-hydroxycarbonyl-4-hydroxy)styrylbenzene[4′-(methylamino)phenyl] benzothiazole
BTA-1	Thioflavin T derivative [4′-(methylamino)phenyl] benzothiazole

bvFTD	Behavioral variant frontotemporal dementia
CBD	Corticobasal degeneration
CDR-SB	Clinical dementia rating - sum of boxes
CI	Confidence interval
CNS	Central nervous system
COWA	Controlled oral word association test
CSF	Cerebrospinal fluid
DNA	Deoxy-riboculeic acid
Dom.	Dominant
DTI	Diffusion tensor imaging
ELISA	Enzyme-linked immunosorbent assay
EMCI	Early mild cognitive impairment
EOAD	Early onset Alzheimer's disease
F	Female
F198S	Phenylalanine to serine at codon 198
FDA	Food and Drug Administration
FDG	Fluoro-deoxyglucose
FTD	Frontotemporal dementia
FTDP-17	Frontotemporal dementia and parkinsonism linked to chromosome 17
FWE	Family-wise error correction
FWHM	Full width at half maximum
GM	Grey matter
GMD	Grey matter density
GSS	Gerstmann-Sträussler-Scheinker disease
GWAS	Genome wide association studies
H&E	Hematoxylin and eosin

H1	Haplotype 1
H2	Haplotype 2
IADC	Indiana Alzheimer Disease Center
IMAS	Indiana Memory and Aging Study
k	Minimum cluster threshold
LD	Linkage disequilibrium
LFG-H&E	Luxol fast blue with hematoxylin & eosin
LLOQ	Lower Limit of Qantification
LMCI	Late mild cognitive impairment
LOAD	Late onset Alzheimer's disease
LOD	Limit of Detection
M	Male
M	Methionine
MAF	Minor allele frequency
MAPT	Microtubule-associated protein tau gene
MCI	Mild cognitive impairment
mL	Milliliter
MMSE	Mini-mental state exam
MNI	Montreal Neurologic Institute
MPRAGE	Magnetization-prepared rapid gradient-echo
MR	Magnetic resonance
MRI	Magnetic resonance imaging
MSTD	Multiple systems tauopathy with presenile dementia
MTL	Medial temporal lobe
NC	Non-carrier
NFL	Neurofilament light chain

NFT	Neurofibrillary tangles
NIA	National Institute on Aging
NIH	National Institute of Health
Non-dom	Non-dominant
O-GlcNAc	O-linked β-N-acetylglucosamine
P102L	Proline to leucine at codon 102
PART	Primary age-related tauopathy
PBR	Peripheral benzodiazepine binding site
PDPK	Proline-directed protein kinases
PET	Positron emission tomography
pg	Picogram
PGRN	Progranulin
PHF	Paired helical filament
PI	Principal investigator
PIB	Pittsburgh Compound B
PRNP	Prion protein gene
PrP	Prion protein
PSEN1	Presenilin 1
PSEN2	Presenilin 2
PSP	Progressive supranuclear palsy
p-tau	Phosphorylated-tau
RNA	Ribonucleic acid
ROI(s)	Region(s) of interest
SC	Symptomatic carrier
SD	Standard deviation
SE	Standard error

SF	Straight filaments
Simoa	Single molecule array
SNP(s)	Single nucleotide polymorphism(s)
SPM8	Statistical Parametric Mapping 8
SUVR	Standardized uptake value ratio
tICV	Intracranial volume
TSPO	Translocator protein
t-tau	Total-tau
UTR	Untranslated region
V	Valine
VBM	Voxel-based morphometry
WM	White matter

Chapter 1: Introduction

Tau is a microtubule-associated protein first discovered in 1975 by Weingarten and colleagues [1]. Shortly thereafter, tau was discovered to be a mainly axonal phosphoprotein [2, 3]. By the mid- to late-1980's, tau was identified as the core protein in the neurofibrillary tangles of Alzheimer's disease (AD) [4-8]. At first, interest in tau was low after it was demonstrated tau pathology was second to amyloid-beta (Aβ) pathology in AD. However, in the mid- to late-1990's, interest in tau skyrocketed when tau pathology and mutations were discovered in neurodegenerative diseases with no amyloid pathology [9-12]. These diseases became collectively known as frontotemporal dementia with parkinsonism linked to chromosome 17 (FTDP-17) [13]. Interestingly, both AD and FTDP-17 show tau that is abnormally hyperphosphorylated. Now, several other neurodegenerative disorders linked to aggregates of hyperphosphorylated tau in neurons and/or glial cells have been identified and are collectively referred to as "tauopathies" [14].

1.1 The Microtubule-Associated Protein Tau

The Tau Gene

The tau protein is encoded by the microtubule-associated protein tau (*MAPT*) gene. The *MAPT* gene spans 16 exons and is located at chromosome 17q21 [15]. *MAPT* undergoes alternative splicing of exons 2, 3, and 10, which results in a total of six normally expressed isoforms ranging from 352-441 amino acids in the central nervous system (CNS). The exclusion or inclusion of exon 10 determines whether the tau protein will contain three (3R) or four (4R) repeat microtubule-binding domains, respectively. The healthy adult brain has an equal ratio of 3R:4R tau. The presence of the extra microtubule-binding repeat increases the affinity of 4R tau isoforms for tubulin [16]. In

addition, “big tau” is a tau isoform in peripheral neurons that project very long axons with large diameters. Big tau has an extra N-terminal region encoded by exon 4a and is not transcribed in the human brain [17, 18].

Rare mutations in *MAPT* have been identified as the main causative agent in some neurodegenerative disorders, such as some forms of corticobasal degeneration, progressive supranuclear palsy, and frontotemporal dementia [9, 19, 20]. Most mutations are located in or around exon 10 and promote exon 10 inclusion, thus leading to an overproduction of 4R tau isoform. The finding that genetic variations in *MAPT* may be the primary cause of neurodegeneration in these disorders suggests the potential that *MAPT* loci may play a pathogenic role in other neurodegenerative diseases associated with tau. However, detecting an association between *MAPT* and other neurodegenerative diseases may be hindered if the genetic variant is rare or if the genetic variant interacts with other genetic variants to cause the disease or disease-associated traits.

A 900kb inversion covers the *MAPT* region, generating a 1.8Mb region of linkage disequilibrium defined by two major haplotypes, H1 and H2, in individuals of European descent [21, 22]. The H1 haplotype contains multiple polymorphisms, exhibits linkage disequilibrium, and contains many sub-haplotypes compared to H2, which is a single un-recombining haplotype. H1 has been linked to familial and sporadic neurodegenerative disorders such as progressive supranuclear palsy, corticobasal degeneration, Parkinson’s disease, and frontotemporal dementia [9, 22-24].

Tau Protein and Function

Tau is a natively unfolded protein that is highly soluble due to its hydrophilic character. Little secondary structure exists except for β-structure in the R2 and R3 microtubule binding repeats which enables self-assembly into filaments [25]. The tau

protein has four main domains that mediate function: (1) the negatively charged, acidic N-terminal domain, which projects away from the negatively charged microtubule and is thought to be involved in microtubule spacing; (2) the proline-rich region, which is involved in cell signaling; (3) the positively charged microtubule binding repeat region, which binds to the inner surface of microtubules and may also play a role in scaffolding and signal transduction; and, (4) the C-terminal domain, which regulates microtubule polymerization by acting as an electrostatic zipper [1, 26]. Tau also plays a fundamental role in several other cellular processes such as axonal elongation and transport and neurite polarity.

Sorting Mechanisms of Tau Protein

Tau is mainly expressed in neurons and is primarily found in neuronal axons in the CNS, although small amounts of tau have been identified in the somatodendritic compartments and the nucleus [27, 28]. Little is known regarding the sorting mechanism of tau but evidence suggests that the distribution could occur at either the mRNA or protein level. Tau mRNA has been discovered in axons, and it is thought that transport to the axon may be mediated by a 3' – untranslated region (UTR) axonal localization signal [29, 30]. Additionally, preferential translation of tau mRNA in the axon, owing to a 5' - UTR terminal oligopyrimine tract, mediates mammalian target of rapamycin-governed protein synthesis, which is important in regulating the cell cycle [31]. At the protein level, it has been hypothesized that tau is degraded faster in non-axonal compartments or that tau has a higher affinity for axonal microtubules over dendritic microtubules [32]. Furthermore, a retrograde barrier at the axon initial segment was also suggested as potential factor keeping tau in the axonal compartment [33].

Post-translational Modifications

Tau protein is heavily regulated by post-translational modifications. Probably the most important of these modifications is phosphorylation, which negatively regulates tau solubility, cellular distribution, association with microtubules, and interaction with binding partners [34]. There are 85 serine, threonine, and tyrosine phosphorylation sites on the longest isoform of tau, the majority of which are located around the microtubule-binding domains. Phosphorylation of tau is developmentally regulated with high tau phosphorylation observed from the embryonic stage through synaptogenesis [35]. Then, in the normal adult human brain, tau phosphorylation decreases to approximately 2-4 mole phosphate attached per molecule of tau.

Tau is mainly phosphorylated by proline-directed protein kinases (PDPK), including glycogen synthase kinase 3 beta, cyclin-dependent kinase 5, and mitogen activated protein kinases, but several non-PDPK, such as calcium/calmodulin-dependent kinase II and protein kinase C, also phosphorylate tau [36-39]. Tau dephosphorylation is mainly regulated by phosphatases; protein phosphatase 2A accounts for about 70% of tau phosphatase activity [40]. Additionally, tau conformation can affect phosphorylation [41].

Tau protein can also undergo several other post-translational modifications including ubiquitination, glycosylation, acetylation, methylation, nitration, isomerization, sumoylation, and truncation [42]. The phosphorylation of tau can be influenced by other post-translational modifications. For example, O-GlcNAcylation, a type of O-glyocsylation, attaches O-linked β-N-acetylglucosamine (O-GlcNAc) to some seronine/threonine phosphorylation sites of tau [43]. Thus, O-GlcNAcylated tau competes with the phosphate groups that occupy the same sites, consequently reducing tau phosphorylation at this location. Abnormal post-translational modifications to tau

usually enhance or suppress phosphorylation, promote or prevent tau aggregation, or alter tau conformation, contributing to the pathological state of tau.

Tau Aggregation

The exact trigger for tau aggregation is unknown. Tau function is tightly regulated by phosphorylation, and hyperphosphorylation of tau leads to microtubule destabilization and missorting of tau into the somatodendritic compartment [44]. The hyperphosphorylated tau then undergoes a conformational change enabling self-assembly into filaments. Polymerization of tau forms paired helical filaments (PHF) or straight filaments (SF), with the core of each composed of the microtubule-binding repeats. Tau in solution forms a “paperclip” conformation where the C-terminus is folded onto the microtubule-binding repeat domain, and the N-terminus is folded over the C-terminus. This conformation is thought to prevent aggregation since the microtubule-binding repeats are less accessible [45]. Abnormal hyperphosphorylation in the N- and C-terminus cause the “paperclip” confirmation to loosen, thus exposing the microtubule-binding repeats for aggregation, forming the PHF/SF core [46]. PHF and SF further aggregate to form neurofibrillary tangles (NFT) or neuropil threads that are characteristic of several tauopathies. Biochemically, tau aggregates can be composed of an equal ratio of 3R:4R, 4R>>3R, or 3R>>4R.

While it has yet to be determined if abnormal phosphorylation alone triggers tau aggregation, it is likely that cofactors or interactions with other molecules also have an effect. Even so, destabilization of microtubules and the subsequent impairment of axonal transport due to tau hyperphosphorylation appear to be the critical steps leading to neuronal demise. After tangle-bearing cells die, the tangles remain in the extracellular space as “ghost tangles.” While NFTs have been strongly correlated with dementia and neurodegeneration [47], relatively new evidence suggests that tau toxicity does not

require the formation of fibrillar tau. Instead, several reports have proposed prefibrillar oligomeric tau as the toxic tau species, which were detected and isolated in the early stages of aggregation [48].

The presence of NFTs does not necessarily indicate dementia or disease. Pathological studies have consistently shown tau pathology in cognitively healthy young and older adults [49-51]. In general, tau pathology restricted to subcortical regions in the absence of amyloid pathology was associated with normal aging and was termed primary age-related tauopathy (PART) [52]. On the other hand, tau pathology found outside subcortical regions is usually associated with cognitive impairment and disease.

Propagation of Tau

Similar to the mechanism of tau sorting, little is known regarding the process by which physiological and pathophysiological tau spreads. While tau is mainly an intracellular protein, new reports suggest that tau can spread via synaptic and non-synaptic mechanisms. For example, exosomal and ectosomal tau release has been observed [53]. Additionally, synaptic stimulation was shown to enhance tau release to the extracellular space, as measured in brain interstitial fluid [54, 55]. Current research also suggests tau pathology may spread through the brain in a prion-like manner, inducing tau fibrillization cell-to-cell and in anatomically connected brain regions, which could also be mediated by tau oligomers [56-60]. The pattern by which tau pathology progresses is highly disease-specific.

Tauopathy Classification

Sporadic and familial tauopathies are quite heterogeneous and can be classified by clinical, neuropathological, and biochemical characteristics. For example, when tau pathology is the salient neuropathological insult, the disorder is classified as a “primary

tauopathy." When tau pathology is associated with another pathology, as seen in AD, the disorder is classified as a "secondary tauopathy." Tau pathology can also be classified according to the predominant tau isoform. Class I tauopathies include all six tau isoforms and can have an equal ratio of 3R:4R, including AD and some cases of FTDP-17 [61-63]. Class II and Class III tauopathies are predominantly composed of 4R tau isoforms and 3R tau isoforms, respectively [9, 64]. Finally, Class IV tauopathy is represented by a disease called myotonic dystrophy which excludes exons 2, 3, and 10 [65].

1.2 Primary and Secondary Familial Tauopathies

Primary familial tauopathies are caused by an autosomal-dominant mutation in the tau gene (*MAPT*) [66]. The majority of these are FTDP-17 diseases. The tau mutations in FTDP-17 are either missense, deletion, or silent mutations in the regions surrounding exon 10 and most of these mutations lead to an increase in the 4R:3R ratio. Different tau mutations give rise to variable clinical and neuropathological phenotypes of FTDP-17 [67]. Clinical phenotypes can include behavioral changes, psychiatric symptoms, cognitive decline, extrapyramidal signs, epilepsy, and/or motor neuron disease. Neuropathologically, all tau filaments are hyperphosphorylated. The clinical and neuropathological phenotypes of FTDP-17 often overlap with those of Pick disease, corticobasal degeneration, or progressive supranuclear palsy [68].

Secondary tauopathies can be caused by autosomal-dominant mutations in genes other than *MAPT*. For example, mutations in the prion protein (PrP) gene (*PRNP*) or the integral transmembrane protein 2B (*BRI2*) gene can also lead to amyloid (APrP and ABri respectively) and NFT formation [63, 69]. Additionally, mutations in the presenlin-1 (*PSEN1*), presenlin-2 (*PSEN2*), and amyloid precursor protein (*APP*) genes lead to Aβ and NFT deposition associated with familial AD (*see section 1.3*) [70-74].

Interestingly, the tau pathology seen in disorders associated with *PRNP* and *BRI2* mutations are biochemically and structurally similar to that seen in AD [62, 63, 75, 76]. These findings also give credence to the amyloid cascade hypothesis, in which tau pathology occurs as a consequence of amyloid pathology [77]. Clinically, these mutations present with various phenotypes but commonly exhibit cognitive decline and ataxia. Genetic tests allow for accurate diagnosis of these familial tauopathies.

1.3 Alzheimer's Disease

The most common tauopathy is AD. AD is a progressive neurodegenerative disorder that affects millions of people worldwide that is characterized by a decline in memory and cognitive disturbances in multiple domains, including language, orientation, and judgment. AD in individuals over the age of 65 is referred to as late-onset AD (LOAD) while those under the age of 65 are classified has having early-onset AD (EOAD) [78]. More than half of the cases of EOAD are caused by single-gene mutations and are termed familial AD. Currently, LOAD can only be diagnosed post-mortem by identifying two key pathological features, intracellular NFTs and extracellular Aβ plaques [47, 79-83].

NFTs in AD have both 3R and 4R isoforms of hyperphosphorylated tau protein. Although the full relationship between NFTs and AD is not completely understood, studies have suggested that initiation of NFTs may be induced by Aβ plaques [84, 85]. NFTs spread in a well-defined pattern called Braak stages [47, 86]. Tau pathology is first observed in the transentorhinal region (stage 1 and 2), then progresses to the limbic regions and the hippocampus (stage 3 and 4), and finally the neocortex (stage 5 and 6). NFTs have been consistently correlated with neurodegeneration and cognitive status [87, 88].

Aβ plaques are a result of the accumulation of an insoluble form of Aβ, a product of amyloidogenic processing of *APP*, and are thought to be the causative pathologic agent in AD. The amyloidogenic processing pathway occurs when APP is cleaved by β-secretase and subsequently cleaved by γ-secretase releasing the amyloidogenic Aβ peptide and the N-terminal soluble APPβ [89]. The major β-secretase and rate-limiting enzyme responsible for generating the Aβ peptide is the β-secretase APP cleaving enzyme (BACE1). When BACE1 was deleted in a mouse model, Aβ was not produced making BACE1 a possible therapeutic target for AD [90]. The enzyme responsible for the γ-secretase cleavage of *APP* is the product of *PSEN1* and *PSEN2*, a secondary γ-secretase. The non-amyloidogenic processing pathway of APP occurs when an α-secretase cleaves APP within the Aβ domain, therefore eliminating the formation of the detrimental form of the protein. Several different Aβ species exist with a great degree of heterogeneity at the N- and C-terminus of the peptide. The most abundant species is $A\beta_{1\text{-}40}$, while the most neurotoxic but less abundant form is $A\beta_{1\text{-}42}$. $A\beta_{1\text{-}42}$ pathology is highest in the frontal cortex but is seen throughout the cortex in AD [91].

Clinical diagnosis of LOAD is usually a result of exclusion of other dementias. Diagnostic criteria for possible, probable, or definite LOAD involves a combination of medical history, clinical examination, neuropsychological testing, and other laboratory assessments [78]. However, the sensitivity and specificity for these methods are relatively low and diagnostic accuracy rates are ≤90%. In an attempt to predict those most likely to be diagnosed with LOAD, researchers and clinicians have defined a transitional state between normal aging and dementia, referred to as mild cognitive impairment (MCI) [92]. Individuals may be diagnosed with MCI if they present with cognitive complaints from the individual, an informant, or a clinician and abnormal age-adjusted memory or other cognitive domain performance, but proceed with normal daily

activities and are non-demented. Individuals with MCI are at high risk for LOAD, with a conversion rate of up to 15% per year [92].

Mutations within AD-related genes contribute to the majority of familial EOAD cases. As previously mentioned, mutations within the gene responsible for Aβ production, *APP,* and other genes that encode enzymes that cleave within the *APP* gene, *PSEN1,* and *PSEN2* contribute to EOAD [71, 72]. However, no such gene mutations have been identified in patients with LOAD. Although mutations within *MAPT* have been identified and are the main causative agent in other neurodegenerative disorders as described in sections 1.1 and 1.2, none thus far have been associated with AD. Currently, the only gene with a high risk association to LOAD is the apolipoprotein E (*APOE*) gene, and more specifically, the ε4 allele of *APOE* [93]. Subjects that are ε4 positive for both alleles are eight times more likely to develop AD than those with the ε2 and ε3 genotypes, thus increasing risk for AD from 20% to 91% [93].

Recent advances in molecular genetics, such as linkage studies and genome wide association studies (GWAS), have identified several other candidate genes which are associated with LOAD risk; however, their combined predictive value remains quite low (for review see [94]). More recently, studies have had success with finding new genetic risk factors associated to AD-related phenotypes rather than just disease presence or absence, which was historically the primary outcome variable used in most genetic studies [95-97]. Using biomarkers of AD pathology (tau and Aβ) increases the power of genetic studies for identifying novel genes and improves the biological interpretability of the potential effect of identified genetic variants. Identification of this class of biomarker based genotype-phenotype association is likely to provide clues to the pathogenesis of AD, help identify potential novel therapeutic targets, and aid in the early detection and clinical diagnosis of AD.

1.4 Neuroimaging

Great effort has been put forth to develop methods to study neuronal insults and proteinopathies in the living brain. The development of noninvasive neuroimaging techniques to study structural, functional, and molecular alterations in disease has allowed for the development of hypothetical models to describe the ongoing series of brain changes that may occur over decades and exist well before symptoms appear in neurodegenerative diseases [98]. These findings have given scientists new insight into the development of neurodegenerative diseases and provided supportive evidence to improve diagnosis.

Today, advances in neuroimaging continue to provide invaluable information about the largely unknown mechanisms and order of pathological progression underlying tauopathies. Different imaging modalities can facilitate early and accurate differential diagnosis to ensure proper treatment and are commonly used by both clinicians and researchers.

Structural Imaging

Magnetic resonance imaging (MRI) uses a magnetic field to align the nuclei of protons in the body (for review see [99, 100]). The MR machine then sends radio frequency pulses that stimulate the hydrogen protons, causing them to spin in a different direction from the magnetic field. Once the radio frequency pulse is turned off, the MRI sensors are able to detect the energy released as the protons return to their normal position. This information is sent to a computer and complex mathematical formulas convert the energy to a 3D image. Protons in different tissues spin at different rates, thus the scanner is able to differentiate between tissue types.

Loss of brain volume, primarily due to decreased synaptic density or neuronal loss, is a key feature in several tauopathies. For this reason, structural MRI of the brain

has been used as a targeted technique to observe brain shrinkage [101, 102]. The atrophy observed by MRI can be used to identify focal atrophic patterns specific to one neurodegenerative disease relative to another. There is usually some overlap in atrophy between disease and controls, and between diseases themselves, thus structural MRI is not a conclusive measure in the diagnostic process. Still, the atrophic patterns may be useful in differentiating, predicting, or monitoring disease status. For example, regional brain atrophy begins early in AD and correlates strongly with cognitive decline [103-105]. Assessments using structural MRI have found that atrophy within AD patients begins in the entorhinal cortex, spreads to the hippocampus, parahippocampal gyrus, and amygdala, and then further extends to the parietal and frontal lobes, similar to the pathological findings of NFT deposition in *post-mortem* brains [47, 106-108].

Molecular Imaging

In addition to MRI measures, positron emission tomography (PET) can give important and essential information about molecular changes in the living brain. PET is a nuclear medicine technique that introduces trace amounts of drugs tagged with a radioisotope ("tracers"; for review see [109]). The amount of tracer uptake is detected by a PET camera, enabling qualitative and quantitative assessment of brain function (e.g., glucose metabolism, neurotransmitter activity), proteinopathy burden (e.g., Aβ, tau), microglial activation, and astrocytes.

PET imaging begins with injection of a radioactive tracer ("radiotracer"), usually intravenously. Either upon injection or after a short time of allowing uptake of the injected radiotracer into the target organ such as the brain, the patient is placed in the circular center of the PET detectors. The radiotracer begins to decay, emitting positrons. However, emitted positrons can only travel a small distance before encountering an electron. The meeting of the positron and electron will cause an annihilation event,

generating two 511 keV gamma rays (“photons”) to be emitted at directions 180° from one another. The gamma rays are then detected by two opposing scintillator crystals in the PET scanner. Two annihilation photons that are registered within a short period of time (3-15 nanoseconds) is called a “coincidence.” The coincidence events are collected and stored by the PET scanner and later reconstructed through back-calculation of the origin of the photons to create images. Indirect mapping of functional processes is then assessed from these images for prognostic, diagnostic, and research purposes.

The most commonly used PET tracer, which is an important oncological marker in addition to being used in neurologic studies, is [^{18}F]fluoro-2-deoxy-D-glucose (FDG). [^{18}F]FDG PET is used to detect cerebral metabolic rates of glucose, the brain’s only source of energy. After uptake, [^{18}F]FDG is phosphorylated by hexokinase. The phosphorylated [^{18}F]FDG does not undergo further metabolism and becomes trapped in neurons, allowing for the measurement of the glucose metabolic rate. Cerebral glucose metabolism is decreased in several tauopathies generally due to synaptic dysfunction and neural degeneration. Thus, [^{18}F]FDG serves as a surrogate marker for neural activity and is potentially capable of detecting dysfunction before structural changes occur. [^{18}F]FDG PET has proven to be a useful tool for the differential diagnosis of AD from other dementias and cognitively normal individuals, as well as for prediction of disease course (for review, see [110]).

The introduction of *in vivo* Aβ PET tracers has provided new and invaluable insight into our understanding of the underlying pathophysiological processes of amyloidogenic neurodegenerative disorders. Over the past 15 years, several amyloid tracers have been developed and are available for research use but only three have been approved by the US Food and Drug Administration (FDA) – [^{18}F]florbetapir (AV-45, Amyvid), [^{18}F]florbetaben (BAY94-9172, NeuraCeq), and [^{18}F]flutemetamol (GE067, Vizamyl) – and are available for clinical use [111-113]. The most widely utilized research

tracer is [^{11}C]Pittsburgh Compound B (PIB) and retention of [^{11}C]PIB highly correlates with amyloid pathology *post-mortem* [114]. However, it is not widely used in clinic due to its short half-life of carbon-11 [115].

Extensive effort has been made to develop PET tracers that can help to visualize PHF-tau deposition *in vivo*. Accordingly, several tau ligands have been developed, although none have yet to be completely validated as superior or FDA approved. However, several of these tracers showed low specificity for tau or high white matter retention, leading to inaccurate interpretation. There is currently one tau-specific tracers in phase 2 research, [^{18}F]Flortaucipir (also known as AV-1451 and T807). AV-1451 shows more than a 25-fold selectivity for PHF-tau over Aβ and demonstrates low white matter binding, providing a high grey-white matter contrast [116]. *Post-mortem* studies further validate AV-1451 as a strong binder of PHF-tau, but suggest that the tracer may not be suitable for other tau species [117].

1.5 Biofluid Markers

Biofluid markers offer an alternative quantitative analysis of brain pathology. Proteins found in the brain interstitial fluid can be interchanged with the biofluids cerebrospinal fluid (CSF) and blood through the blood- and CSF-brain barriers. These biofluids contain proteins that may reflect physiological processes and pathological changes. These measures of proteins known to be abnormal in disease provide an estimate of protein concentration that track disease progression over time, and increase diagnostic accuracy, amongst several other contexts of use. The field is rapidly evolving with new, high sensitivity assays in development.

Cerebrospinal Fluid Markers

CSF has the closest proximity to the brain interstitial fluid and thus offers the most direct way to measure biochemical changes that occur in the brain, making CSF an important biomarker of disease.

Research into CSF markers that reflect the pathological processes of disease have been fruitful. CSF measurements of total tau (t-tau), tau phosphorylated at threonine 181 (p-tau), and $A\beta_{1-42}$ were some of the earliest markers investigated [118, 119]. Since then, other candidate markers for neurodegeneration, such as neurofilament light chain (NFL, a marker of axonal neurodegeneration) and neurogranin (a postsynaptic markers expressed in dendritic spines), have been investigated [120].

Alterations in CSF measures of amyloid and tau in tauopathies, especially AD, have been heavily investigated. Individuals with AD express higher CSF levels of t-tau, p-tau, and low levels of $A\beta_{1-42}$ [121, 122]. The high tau levels are thought to be a reflection of neuron death and a resulting release of tau into the interstitial fluid, while the low CSF levels of $A\beta_{1-42}$ are possibly due to aggregation of amyloid into neuritic plaques and thus, reduction in “free” amyloid that is not bound to plaques in the interstitial fluid. Combining amyloid and tau markers into t-tau/$A\beta_{1-42}$ and p-tau/$A\beta_{1-42}$ ratios has been shown to be able to differentiate AD and MCI from controls [122]. The effect of non-AD and familial neurodegenerative diseases on CSF tau levels is less clear [123-125]. Results between studies are highly inconsistent suggesting the use of CSF tau in diseases other than AD may have little diagnostic value per se, but may aid in disease differentiation, particularly from AD.

Blood-based Markers

Contrary to neuroimaging and CSF collection, blood-based biomarkers are minimally invasive and offer a more time- and cost-effective option to detect and track

disease pathology. Additionally, peripheral biomarkers easily allow for repeated collection in a short period of time. The discovery of a peripheral biomarker for tauopathies would substantially alter the field by offering an easily obtainable first-line screening tool that could be used for disease detection, diagnosis, risk assessment, and monitoring response to therapeutics, for example. One of the biggest challenges in using blood-based biomarkers for disease detection is the complex composition of proteins that are constitutively present in the blood. However, there have been new developments in ultra-sensitive assays that are capable of detecting proteins, including tau and NFL, at extremely low concentrations [126, 127]. Plasma levels of tau protein have been shown to be significantly elevated in AD and traumatic brain injury [21, 128]. Furthermore, plasma NFL has also recently been associated with AD and progressive supranuclear palsy [129, 130]. Plasma Aβ has also been investigated in AD but studies have consistently reported no significant difference between disease and controls [131].

1.6 Statement of Purpose

Great heterogeneity is observed in sporadic and familial tauopathies, both clinically and pathologically. While familial dementias have been well clinically defined and a causative mutation identified, characterization of disease progression at the molecular level is needed to better understand the underlying brain changes leading to disease phenotype. For sporadic tauopathies, it is likely that multiple genes with small effect sizes contribute to overall disease risk. Furthermore, there is a need for peripheral, non-invasive biomarkers that can accurately represent brain injury in these neurodegenerative disorders. Accordingly, the goals of this work were as follows:

1. Using PET imaging, identify disease-specific glucose metabolic patterns in primary and secondary familial tauopathies, specifically multiple systems tauopathy with

presenile dementia (MSTD) and Gerstmann–Sträussler–Scheinker (GSS) disease, respectively, to better define the molecular changes in these diseases.

2. Investigate the association of plasma tau and plasma NFL, markers of axonal degeneration, with grey matter density measured on MRI in order to evaluate these blood-based proteins as suitable markers of neurodegeneration in Alzheimer's disease.

3. Develop a tau biological network curated from gene and protein databases and literature review to offer an alternative method to investigate the genetic contribution of tau-related genes to tauopathies.

Chapter 2: Review of [^{18}F]FDG PET in Alzheimer's Disease

2.1 Introduction

Selection of appropriate imaging modalities, in combination with other established biomarkers, can further our knowledge regarding the temporal and spatial patterning of protein deposition and neuronal function in neurodegenerative disorders. This chapter will provide an overview of the major findings from [^{18}F]fluoro-2-deoxy-D-glucose (FDG) positron emission tomography (PET) studies of patients across the spectrum of late-onset Alzheimer's disease (LOAD).

2.2 Metabolic Patterns in AD

Relative to cognitively normal controls (CN), AD patients show glucose hypometabolism in regions of the temporoparietal cortex, medial temporal lobe (MTL), posterior cingulate, and precuneus, with frontal involvement in more advanced AD (Figure 1A). These regions were confirmed in a meta-analysis of 16 FDG PET studies, suggesting they show a robust reduction in glucose metabolism in AD [132]. The earliest metabolic changes in AD are seen in the posterior cingulate cortex [133]. The cerebellum, anterior cingulate, striatum, thalamus, primary sensorimotor and visual cortices are relatively spared until late in the disease. In comparison, early-onset AD (EOAD) shows greater hypometabolism in the parietal and frontal regions compared to LOAD [134]. Asymptomatic familial AD patients with mutations in *APP*, *PSEN1*, or *PSEN2* show similar metabolic patterns to LOAD, providing evidence for the importance of these brain regions in AD [135]. Of note, there is no significant effect of apolipoprotein E (*APOE*) ε4 status on glucose metabolic levels in AD, with no difference in [^{18}F]FDG uptake between AD patients who are *APOE* ε4 carriers relative to non-carriers [136]. The regional hypometabolic patterns observed in AD have been highly reproducible

suggesting that the observed [^{18}F]FDG pattern is specific to AD and therefore could be helpful in diagnosis and differentiation from other dementias.

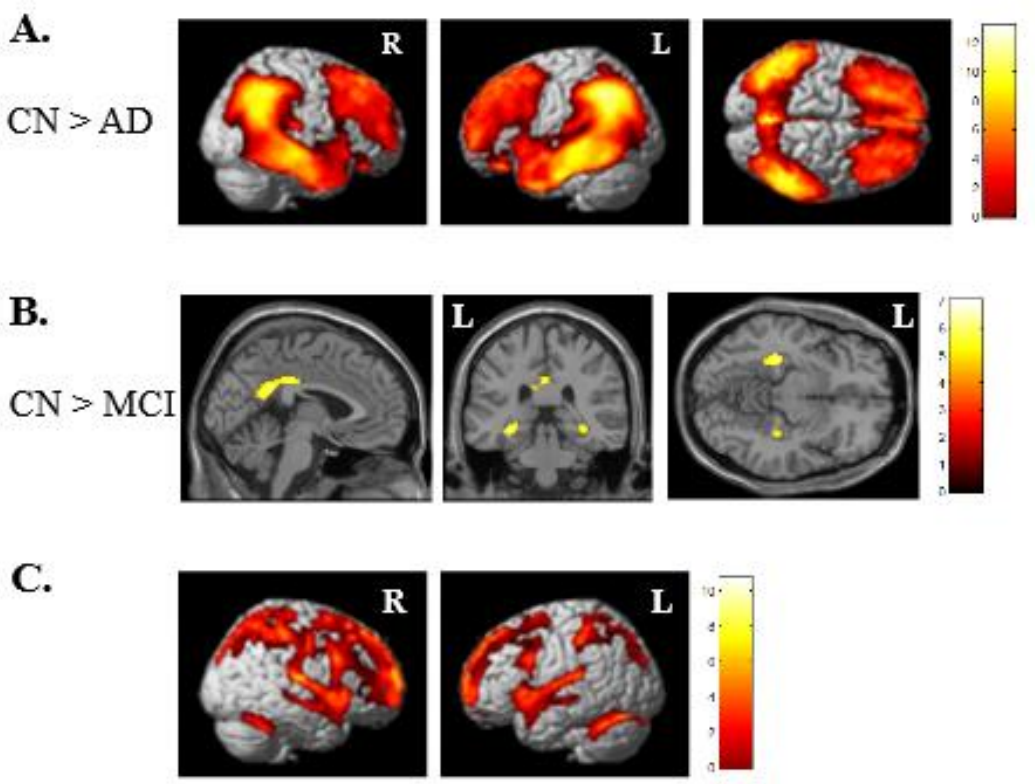

Figure 1. [^{18}F]FDG uptake across the Alzheimer's disease spectrum.

(A) Difference in [^{18}F]FDG PET uptake between Alzheimer's disease (AD) vs cognitively normal controls (CN), and (B) mild cognitive impairment (MCI) vs CN. (C) Glucose metabolic pattern in CN subjects only. Voxel-wise image analysis was done using standard VBM methods in SPM8 with results displayed at $p<0.05$ (FWE corrected) and a minimum cluster size (k) = 100 voxels. R = right; L = left.

2.3 Metabolic Patterns in Mild Cognitive Impairment

Although a heterogeneous pattern is often found, mild cognitive impairment (MCI) participants predominantly show reduced glucose metabolism in the posterior cingulate and hippocampus (Figure 1B) [137]. Additionally, *APOE* ε4 carriers with MCI show lower glucose metabolism in the typical AD-related regions compared to non-carriers [138].

Further, since the same regions that are hypometabolic in AD show hypometabolism in MCI, [^{18}F]FDG may also be useful for predicting MCI progression to AD. For example, longitudinal studies of MCI have suggested that MCI participants who later converted to AD showed a significant reduction in [^{18}F]FDG uptake in AD-specific hypometabolic regions compared to non-converters prior to conversion, supporting [^{18}F]FDG as an effective tool for tracking AD progression. A review by Perani et al. discussed several studies in which quantitative measures allowed for derivation of a cut-off score to discriminate and predict converters from non-converters with sensitivity and specificity greater than 78% [139]. These findings suggest that decreased glucose metabolism in the typical AD-specific regions precedes the onset of AD symptoms and may be a predictor of MCI to AD progression.

2.4 Metabolic Patterns in CN

Neuronal integrity can be somewhat compromised during normal aging (Figure 1C) [140]. In general, a global decrease in glucose metabolism is correlated with increasing age. The most affected regions are the medial and orbital prefrontal, anterior cingulate, and motor cortices. Healthy individuals who are *APOE* ε4 carriers show hypometabolism in the parietotemporal cortex, posterior cingulate, and precuneus, which are also affected in MCI and AD [141]. Interestingly, recent studies have noted that CN participants with a maternal history of AD also show metabolic patterns consistent with

AD [142]. These findings suggest that the regional hypometabolic changes in preclinical AD participants that mirror the hypometabolism seen in AD (although to a lesser extent) may precede the onset of clinical and cognitive symptoms. Indeed, [^{18}F]FDG PET can predict CN conversion to MCI or AD, with CN-converters showing reduced glucose metabolism particularly in the temporal, frontal, and parietal cortices compared to CN-stable [143].

2.5 Associations Between Metabolic Patterns and Neuropsychological Patterns

Glucose metabolism is associated with cognition across the AD spectrum. A positive association between better executive function and increased glucose metabolism in the occipital, temporal, and parietal cortices was observed in AD and MCI [144]. Memory performance also showed an association with glucose metabolism with higher (better) test scores associated with increased [^{18}F]FDG in frontal regions for AD and in the precuneus and posterior cingulate cortex in MCI. Longitudinal studies demonstrated that MCI participants with abnormal hypometabolism had worse neuropsychological test scores and declined at a faster rate than MCI participants with normal glucose metabolism [145]. Furthermore, longitudinal studies of the CN individuals reported that reduced MTL, parietal, and hippocampal glucose metabolism are associated with a faster decline in cognitive function. These observations suggest that changes in glucose utilization mirror the cognitive deterioration that occurs during the progression of AD and further support the use of [^{18}F]FDG in the clinical research and diagnosis of AD.

2.6 Differential Diagnosis

Different neurodegenerative disorders can affect different brain regions producing disease-specific metabolic patterns. Identifying these areas with lower

metabolism can thus aid in differentiating dementias, especially in the early stages. [^{18}F]FDG PET can discriminate AD from controls with high sensitivity and specificity, leading to improved diagnosis. Similarly, studies have also shown that [^{18}F]FDG PET can distinguish AD from frontotemporal lobar degeneration (FTLD) and dementia with Lewy bodies (DLB) with sensitivity as high as 99% and specificity as high as 98%, in addition to other non-AD dementias [139]. DLB shares similar symptoms and hypometabolic brain regions with AD, thus making it difficult for clinicians to accurately distinguish the two. However, it has been noted that DLB patients present with more significant occipital hypometabolism relative to AD patients, enabling differentiation of DLB from AD [146]. FTLD rarely shows the same hypometabolic pattern as AD. In fact, differentiation of FTLD from AD can be done by assessment of frontal and anterior temporal hypometabolism, which is more prevalent and significant in FTLD than AD [147] . However, differentiation of FTLD from AD is better served using amyloid PET [148]. Vascular dementia (VaD) is another common dementia in older adults and can present with clinical symptoms similar to AD. In VaD, lower metabolism is often observed in the deep gray nuclei and cerebellum, which differentiates VaD from AD [149]. Clinically, the use of [^{18}F]FDG PET in differentiating AD from non-AD dementias is important not only for accurate diagnosis, but to ensure the proper treatment.

2.7 Summary

Without a doubt, it is clear that PET imaging has increased our understanding of the pathological and functional changes that occur in the living brain. The specific spatial and temporal patterns observed using [^{18}F]FDG PET imaging enable clinicians and researchers to detect significant brain alterations in AD from prodromal and preclinical stages of the disease. Longitudinal PET studies suggest that glucose utilization begins

to decline before cognitive symptoms occur and continues to decline as disease progresses.

PET, along with other neuroimaging techniques and biomarkers, will enable differential diagnosis among dementias and hopefully early and accurate detection and *pre-mortem* diagnosis of AD. Future studies that combine the longitudinal collection of multi-modal imaging and biomarker data will hopefully provide the information necessary for accurate *pre-mortem* diagnosis of AD.

Chapter 3: Glucose Metabolism in Multiple Systems Tauopathy with Presenile Dementia

3.1 Introduction

Frontotemporal dementia (FTD) is a clinically, genetically, and pathologically heterogeneous neurodegenerative disorder which is considered to be the second leading cause of early onset dementia after Alzheimer's disease [150]. FTD is characterized by marked changes in behavior, personality, executive function, and language.

Approximately 40-50% of patients with FTD report a positive family history of dementia, with 10% of these cases having an autosomal dominant inheritance pattern [151]. Up to 30% of familial FTD cases have been linked to genetic variations in the microtubule associated protein tau (*MAPT*) gene located at 17q21 [152]. These patients typically present with FTD with parkinsonism and with tau inclusions (FTDP-17T). Additional mutations in progranulin (*PGRN*), which is also located at 17q21, have been linked to familial FTD. However, histopathologically, mutations in *PGRN* are not associated with tau inclusions, while *MAPT* mutations are associated with tau pathology [153-155].

A family with multiple systems tauopathy with presenile dementia (MSTD), a form of FTDP-17T, was discovered by our group to have an (a) to (g) transition in *MAPT* intron 10 +3 [9, 14, 156, 157]. In the normal adult human brain, six tau isoforms are expressed from the alternative splicing of *MAPT* exons 2, 3, and 10. The exclusion or inclusion of exon 10 leads to the expression of three (3R) or four (4R) repeat microtubule-binding domains, respectively, at a balanced ratio [16, 158]. The (a) to (g) transition in this family leads to an overproduction of the 4R tau isoform. Clinically, these patients have heterogeneous presentations, but present frequently as behavioral variant FTD (bvFTD) with changes in personality, such as disinhibition and disordered social

conduct, and impaired executive function, memory, and speech [159, 160]. Both clinical imaging and post-mortem assessment show marked neurodegeneration in medial temporal and frontal regions [161].

Previous studies have investigated grey matter (GM) loss and hypometabolism in sporadic bvFTD. Reduced glucose uptake has previously been identified in the frontal and temporal lobes, anterior cingulate cortex, anterior insula, and subcortical regions [162-169]. Additionally, [^{18}F]fluorodeoxyglucose ([^{18}F]FDG) positron emission tomography (PET) studies with other FTDP-17 families showed a reduction in glucose metabolism in temporal cortices, parietal cortices, hippocampi, and the amygdalae, although these samples were quite small [170-172]. Studies have also shown GM loss in the frontotemporal lobe regions, insula, and putamen [162, 171, 173, 174]. However, anatomical changes and glucose metabolism in the brain has yet to be reported in this MSTD family or in a FTDP-17 sample of this size.

The goal of the present study is to investigate changes in glucose metabolism with [^{18}F]FDG PET in MSTD to better define the metabolic features associated with *MAPT* mutations and further characterize this large MSTD family. Magnetic resonance imaging (MRI) was also utilized for comparison with [^{18}F]FDG PET using an expanded sample from Spina et al. (2008) [161]. While the information derived from these two imaging modalities may identify abnormalities in the same structure that are related, there may be a temporal ordering of the onset of abnormalities detected by these complementary techniques. For example, glucose hypometabolism may precede grey matter atrophy as is observed in other familial neurodegenerative disorders [175]. We hypothesized that the *MAPT* intron 10 +3 mutation causes reduced glucose metabolism in carriers within this MSTD family, particularly in the medial temporal and frontal areas that are known to be susceptible to atrophy in bvFTD. We also hypothesized that

clinically-affected mutation carriers would show greater glucose hypometabolism in target areas than carriers who are not yet cognitively impaired.

3.2 Material and Methods

Subjects

Nineteen participants, including eleven *MAPT* intron 10 +3 mutation carriers ((eight symptomatic (SC), three asymptomatic (AC)) and eight non-carriers (NC), underwent neurological, and cognitive assessments, as well as [^{18}F]FDG PET and structural magnetic resonance imaging (MRI) at the Indiana Alzheimer Disease Center (IADC). Demographic information for four of these SCs has previously been reported [161]. Participants were diagnosed with bvFTD using standard criteria [159, 176] from neuropsychological testing, neurological examination, informant interviews, and past medical records.

Genotyping

Genotyping of the *MAPT* intron 10 +3 mutation was performed as previously described [161]. Briefly, genomic DNA was extracted using standard protocols [161] and the purified DNA product from PCR amplification was compared to the known *MAPT* exon 10 sequence previously determined [9].

Magnetic Resonance Imaging Acquisition and Processing

All participants underwent a structural MRI scan within 1.00 ± 1.11 days (range: 1-5 days) of the [^{18}F]FDG PET scan. Seventeen participants, including ten *MAPT* intron 10 +3 mutation carriers (7 symptomatic, 3 asymptomatic) and seven non-carriers, underwent a single T1-weighted SPGR volumetric scan on a 1.5T GE Signa scanner as previously described [161]. Two participants, one affected mutation carrier and one non-

carrier, received a single T1-weighted MPRAGE volumetric scan on a 3T Siemens Trio scanner. Structural MRI scans were processed using voxel based morphometry (VBM) in SPM8 (http://www.fil.ion.ucl.ac.uk/spm/) using previously described techniques [177]. Briefly, scans were co-registered to a T1-weighted template and segmented into GM, white matter, and cerebrospinal fluid compartments using standard templates with bias correction. GM images were unmodulated, normalized to Montreal Neurologic Institute (MNI) space as 1 x 1 x 1 mm voxels, and smoothed with an 8mm full-width half maximum (FWHM) Gaussian kernel. All scans underwent extensive quality control at all processing steps. Only smoothed, normalized GM images generated from the SPGR volumes acquired on the 1.5T GE scanner were used in the VBM analysis, given the differences in data acquisition for 3T scans. Parameters generated from the structural MRI segmentation were also used for [^{18}F]FDG PET processing as described below (see *PET Data Acquisition and Imaging Processing*).

PET Data Acquisition and Image Processing

All participants also underwent a [^{18}F]FDG PET scan, acquired on a Siemens EXACT HR+ scanner. After positioning within the scanner, a 10-minute transmission scan using three internal rod sources was acquired for attenuation correction. A 60-min dynamic acquisition protocol was then initiated with the injection of approximately 10 mCi of [^{18}F]FDG using the following frame sequence: 12 x 5s, 4 x 15s, 2 x 30s, 7 x 60s, 10 x 300s. [^{18}F]FDG scans were reconstructed using the manufacturer's software (CTI Molecular Imaging Inc.; Knoxville, TN) with the filtered back-projection algorithm. Corrections for scatter, randoms, and attenuation were applied.

Reconstructed [^{18}F]FDG scans were processed using standard techniques. Using SPM8, scans were converted from ECAT to NiFTI format, coregistered to the structural MRI scan from the same visit, motion corrected, and normalized to MNI space

using matrices from the same time-point MRI segmentation. A static [^{18}F]FDG image from 30-60 minutes was created from the appropriate frames, intensity normalized using a cerebellar GM reference region to create a standardized uptake value ratio (SUVR) image for each participant, and smoothed with an 8 mm FWHM kernel. The SUVR images were then used for further analysis as described below.

Image Analysis

Within the SPM8 framework, an analysis of covariance (ANCOVA) was performed on normalized MRI GM density and [^{18}F]FDG PET SUVR maps to compare the effect of mutation status (carrier vs. non-carrier) on GM density and [^{18}F]FDG uptake on a voxel-by-voxel basis. Age at scan and sex were used as covariates for the [^{18}F]FDG PET analysis. Age, sex, and total intracranial volume (tICV) were used as covariates for the GM density contrasts. In addition, since five of the NCs and two of the SCs were positive for apolipoprotein (*APOE*) ε4 allele, which has been shown to affect glucose metabolism in late mid-life [178], we computed similar analyses for both [^{18}F]FDG and GM density that also included *APOE* ε4 carrier status as covariate. However, the inclusion of *APOE* ε4 carrier status did not significantly affect the observed results and thus was not included in the final reported results (*data not shown*). An explicit GM mask was applied to both MRI and PET datasets to restrict the search area. Significant findings were displayed using a threshold of $p<0.001$ (uncorrected) for MRI, and a threshold of $p<0.01$ (uncorrected) for [^{18}F]FDG PET; for both analyses, minimum cluster size was (k) = 50 voxels. A composite image using the significant clusters for MRI and [^{18}F]FDG PET was created to determine areas of MRI and PET overlap between mutation carriers and non-carriers. MarsBaR toolbox (version 0.42) in SPM was used to extract mean GM density and mean glucose uptake for the significant medial temporal

lobe (MTL) clusters from MRI and PET analyses, respectively. Note that MRI results for four *MAPT* 10 +3 mutation carriers has been previously reported [161].

Statistical Analysis

While the three diagnostic groups were too small to do voxel-based imaging analysis, we had a special interest in the AC group and wanted to determine if they showed any regional metabolic, GM density, and/or neuropsychological differences from NC and SC participants. An ANCOVA was used to test for the association of continuous demographic variables and neuropsychological test performance with mutation and diagnostic status. Sex was assessed with mutation and diagnostic status using a chi-square test. Age and years of education were used as covariates when evaluating neuropsychological test scores. Z-scores of left and right mean MTL GM density and MTL glucose uptake from the significant MTL clusters identified in previous voxel-wise analyses were calculated for each participant using means and standard deviations from the NC group. The left and right z-scores were then averaged to create a bilateral mean GM density and bilateral mean glucose uptake z-score for each participant. ANCOVA was again used to test the association of diagnostic/mutation group (SC, AC, NC) with MTL GM density and glucose uptake z-scores. Age and sex were used as covariates for the assessment of MTL glucose uptake, while age, sex, and tICV were used as covariates for the evaluation of MTL GM density. Pairwise contrasts between groups were adjusted for multiple comparisons using a Bonferroni correction. Linear regression was used to compare MTL GM density and MTL glucose uptake. All statistical analyses were done in SPSS (version 20.0, Chicago, IL) and all graphs were created using SigmaPlot (version10.0).

3.3 Results

Neuropsychological assessment

Demographics and neuropsychological testing results are displayed in Table 1. Although not statistically significant, symptomatic carriers were on average older and more likely to be male than the other groups. Thus, age and sex were used as covariates in all subsequent neuroimaging analyses. As expected, a significant association between diagnostic/mutation status group and neuropsychological performance was observed on the COWA ($p=0.045$) and the CERAD Word List Immediate Recall ($p=0.006$) and Delayed Recall ($p<0.001$). Upon post-hoc analysis, SCs showed poorer performance on the COWA than NCs ($p=0.044$). In addition, ACs and NCs showed better performance than SCs on the CERAD Word List Immediate Recall (SC vs. AC, $p=0.022$; SC vs. NC, $p=0.012$) and Delayed Recall (SC vs. AC, $p=0.004$; SC vs. NC, $p<0.001$).

Table 1. Demographic and neuropsychological data in MSTD participants.

	SC	AC	NC	p-value
N	8	3	8	
Age (years)	50.1 (5.4)	42.55 (8.7)	43.7 (12.0)	0.313
Sex (M, F)	5, 3	0, 3	2, 6	0.106
Education (years)	12.75 (0.9)	14.3 (2.1)	13.4 (1.3)	0.764
% *APOE* ε4+	25	0	62.5	0.106
MMSE Total Score	23.6 (5.6)	28.3 (0.6)	27 (1.6)	0.189
COWA Total Score*	22.1 (10.6)	33.7 (6.7)	38.86 (10)	0.045
Block Design Total*	23.4 (12.8)	33.3 (10)	34.43 (4.2)	0.235
Word List Imm Total**	11.75 (5.5)	28 (1.4)	21.9 (4.6)	0.006
Word List Del Total**	2.75 (2)	9.5 (0.7)	8.13 (1.6)	<0.001

SC = symptomatic carrier; AC = asymptomatic carrier; NC = non-carrier; M = male; F = female; MMSE = Mini-Mental State Exam; COWA = Controlled Oral Word Association; Word list Imm = CERAD Word List – Immediate Recall; Word List Del = CERAD Word List – Delayed Recall. Mean (Standard Deviation). * Missing one non-carrier. ** Missing one asymptomatic carrier.

MRI

Cerebral atrophy was observed in *MAPT* mutation carriers relative to non-carriers. Specifically, decreased GM density was observed bilaterally in the MTL, including in the parahippocampal gyri, hippocampi, entorhinal cortices, uncus, and amygdala, as well as in the caudate nucleus (Figure 2; voxel-wise threshold of $p<0.001$(uncorrected for multiple comparisons); $k = 50$ voxels)). GM atrophy was also observed in mutation carriers in the precuneus, insula, medial and superior frontal gyri, and the precentral gyrus, in addition to other regions of the frontal, parietal, occipital, and lateral temporal lobes (Figure 2). However, as has been seen in previous bvFTD studies, there were surprisingly few differences between mutation carriers and non-carriers in the prefrontal cortex and cingulate gyrus.

The most striking GM atrophy in mutation carriers was seen bilaterally in the MTL (Figure 2), as has been previously shown [161]. Further analysis of these regions to evaluate distribution of atrophy among diagnostic/mutation groups showed a significant overall difference in GM density z-score (Figure 3, $p<0.001$). Pairwise comparisons showed reduced GM density in both AC and SC relative to NC (NC vs. AC, $p=0.022$; NC vs. SC, $p<0.001$). GM atrophy in AC was intermediate between that of NC and SC, with significantly more atrophy than NC but less atrophy than SC (AC vs SC, $p=0.01$).

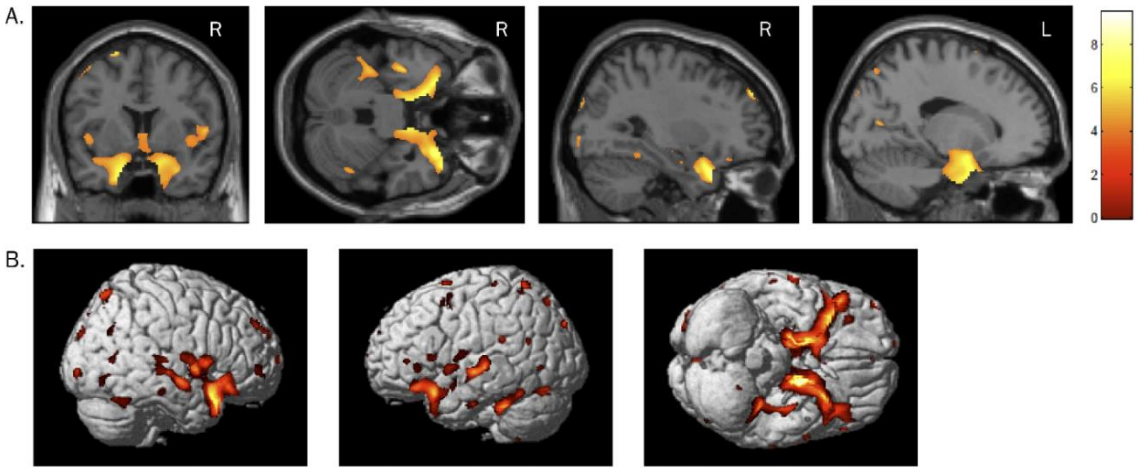

Figure 2. Voxel-wise analysis of the effect of *MAPT* intron 10 +3 mutation status on GM density.

Whole-brain grey matter (GM) density was compared between carriers of the *MAPT* intron 10 +3 mutation and non-carriers. Mutation carriers show GM atrophy relative to non-carriers in regions of the (A) medial temporal lobe and, (B) other cortical and subcortical regions. Differences between mutation carriers and non-carriers are displayed at a voxel-wise threshold of $p<0.001$ (uncorrected for multiple comparisons) and minimum cluster size (k) = 50 voxels. Age, sex, and total intracranial volume were used as covariates.

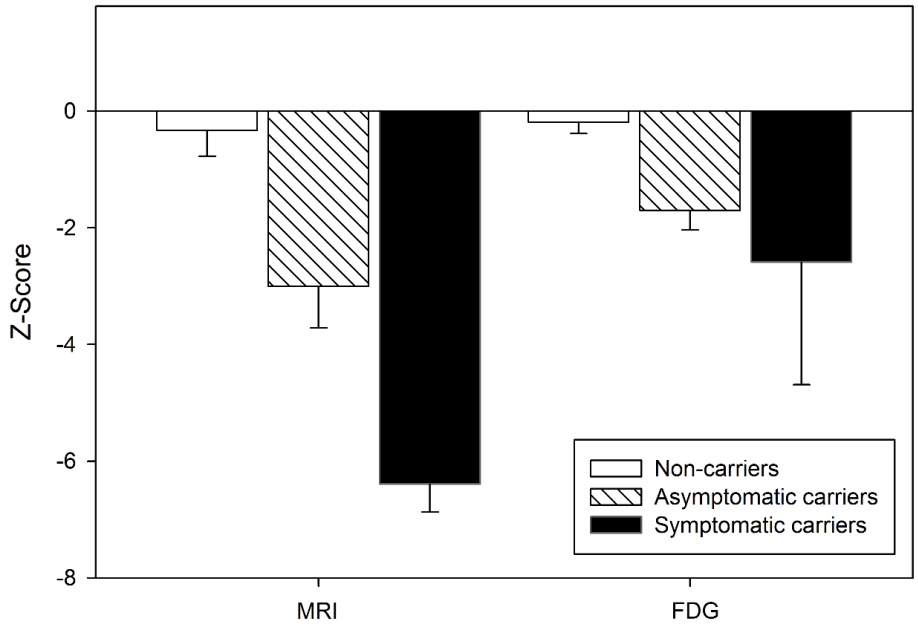

Figure 3. Medial temporal lobe GM density and glucose metabolism in carriers and non-carriers of the *MAPT* intron 10 +3 mutation.

Mean grey matter (GM) density and glucose metabolism were extracted from the medial temporal lobe (MTL) clusters identified in the voxel-wise comparisons (Figures 2 and 4) using MarsBaR. Z-scores were then calculated and the effect of mutation and clinical status on GM atrophy and glucose hypometabolism was evaluated, covaried for age and sex. Total intracranial volume was also included in the analysis of GM atrophy. Significant differences between groups were observed for both GM density ($p<0.001$) and glucose uptake ($p<0.001$). Post-hoc comparisons of GM density showed a significant difference between all group pairs, with symptomatic carriers (SC) showing the greatest MTL atrophy and asymptomatic carriers showing intermediate MTL atrophy between SC and mutation non-carriers (NC; NC vs. AC, $p=0.022$; NC vs. SC, $p<0.001$; AC vs SC, $p=0.01$). Post-hoc comparisons of glucose uptake demonstrated significant greater glucose metabolism in NC relative to both carrier groups (NC vs. AC ($p=0.004$) and NC vs. SC ($p<0.001$)), but no difference between carriers based on clinical status ($p=0.154$).

[^{18}F]FDG PET

Bilateral hypometabolism was observed in mutation carriers relative to non-carriers in regions of the MTL and limbic system, including the parahippocampal gyri, hippocampi, entorhinal cortices, amygdala, uncus, and the anterior cingulate cortex, as well as in the caudate nucleus (Figure 4, Table 2). Some lateralization of hypometabolism in mutation carriers relative to non-carriers was observed with more reductions in glucose metabolism in the right anterolateral temporal lobe than in the left. Other frontal and parietal cortical regions also showed hypometabolism in mutation carriers relative to non-carriers, including in the anterior prefrontal cortex, the medial and superior frontal gyri, and the postcentral gyrus (Figure 4).

Further examination of the difference in glucose metabolism among the three groups in the MTL showed a significant association of diagnostic/mutation status with mean MTL glucose SUVR z-score (Figure 3; $p<0.001$). The asymptomatic carriers again showed mean MTL glucose uptake intermediate between the NC and SC. Comparisons of NC and AC ($p=0.004$) and NC and SC ($p<0.001$) reached statistical significance, whereas the AC and SC carrier groups ($p=0.154$) were not significantly different.

Table 2. Anatomical distribution of reduced glucose metabolism for in *MAPT* intron 10 +3 carriers relative to non-carriers.

			MNI Coordinates			
Location	**BA**	**T-value**	**x**	**y**	**z**	**p-value**
L. Inferior Frontal Gyrus	47	4.58	−26	10	−18	0.000
L. Inferior Parietal Lobule	40	3.11	−58	−32	46	0.004
L. Middle Frontal Gyrus	10	3.38	−26	66	12	0.002
	6	2.92	−46	10	50	0.005
	9	3.03	−52	26	34	0.004
L. Middle Temporal Gyrus	21	3.29	−56	2	−18	0.002
		2.98	−64	−10	−12	0.005
		2.68	−58	−18	−6	0.009
L. Superior Frontal Gyrus	10	2.83	−36	48	32	0.006
	6	3.55	−20	6	70	0.001
		3	−8	28	66	0.004
	8	3.96	−6	44	52	0.001
		3.13	−22	32	56	0.003
L. Superior Parietal Lobule	7	3.34	−28	−58	64	0.002
L. Superior Temporal Gyrus	10	4.77	−14	70	18	0.000
	38	3.85	−22	14	−34	0.001
L. Thalamus		3.22	−8	−32	−4	0.003
L. Uncus	34	4.42	−18	2	−22	0.000
R. Anterior Cingulate	32	3.71	2	46	6	0.001
R. Caudate Body		3.98	16	22	16	0.001
		3.57	14	12	20	0.001
R. Medial Frontal Gyrus	25	5.29	8	6	−22	0.000
R. Middle Frontal Gyrus	8	3.1	40	24	56	0.004
R. Middle Temporal Gyrus	21	3.92	64	−6	−12	0.001
R. Postcentral Gyrus	7	3.16	16	−52	72	0.003
R. Superior Frontal Gyrus	10	4.66	22	68	14	0.000
		4.1	16	62	28	0.000
	6	3.11	14	32	60	0.004
	8	2.94	20	38	52	0.005
R. Superior Parietal Lobule	7	3.47	18	−68	58	0.002
R. Superior Temporal Gyrus*	38	5.99	44	16	−22	0.000
R. Uncus	34	4.57	20	4	−22	0.000

MNI = Montreal Neurologic Institute; BA = Brodmann area; L.= left; R.= right

p-value <0.01, uncorrected

*Significant cluster for p<0.05 at FWE-corrected

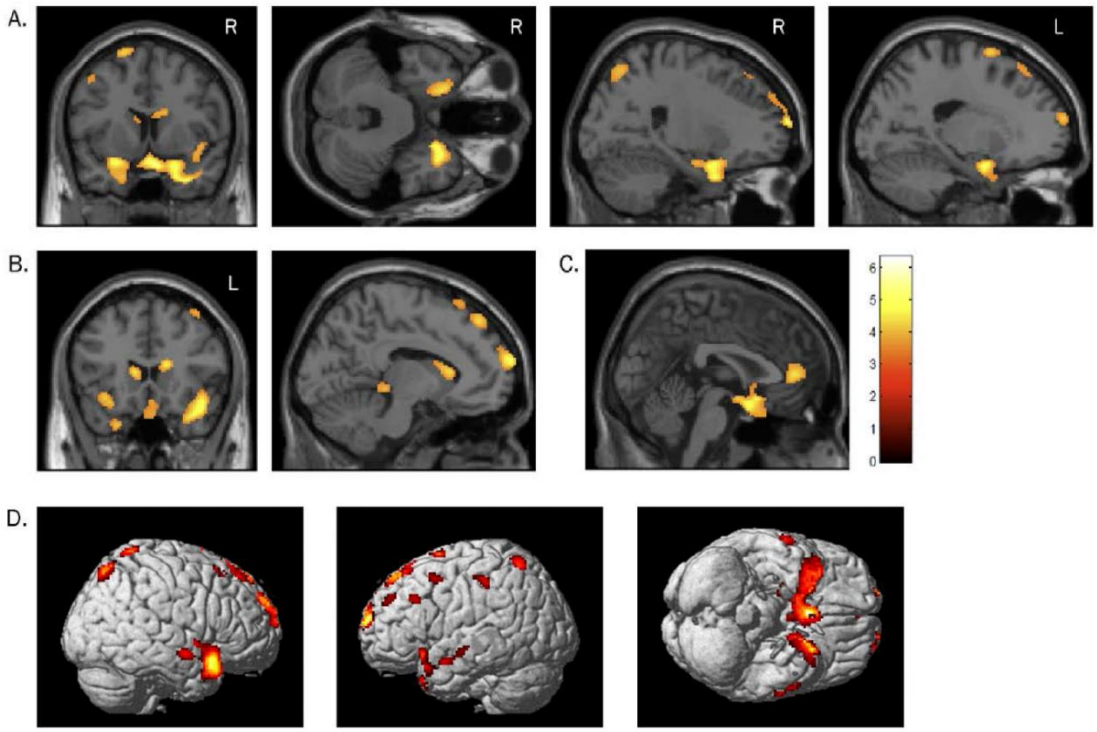

Figure 4. Voxel-wise analysis of the effect of *MAPT* intron 10 +3 mutation status on glucose metabolism.

Whole-brain glucose metabolism was compared between carriers of the *MAPT* intron 10 +3 mutation and non-carriers. Mutation carriers showed hypometabolism relative to non-carriers in the (A) medial temporal lobe (MTL), (B) caudate nucleus, (C) anterior cingulate gyrus, and (D) in frontal, parietal, and temporal cortices. Group differences are displayed at a voxel-wise threshold of $p<0.01$ (uncorrected for multiple comparisons) and minimum cluster size (k) = 50 voxels. Age and sex were used as covariates.

Comparison of MRI and [^{18}F]FDG

In other familial neurodegenerative disorders (i.e. familial Alzheimer's disease), hypometabolism may precede brain atrophy [175]. Therefore, we investigated the relationship between MRI and PET findings in the MSTD sample. There was moderate overlap of the regions showing neurodegeneration and those showing glucose hypometabolism in mutation carriers relative to non-carriers, most especially in the MTL (Figure 5). While significant overlap can be seen in MTL structures such as the uncus, hippocampus, and parahippocampal gyrus, atrophy appeared to be more widespread than hypometabolism in mutation carriers relative to non-carriers. However, other regions, including the anterior cingulate cortex and caudate nucleus, showed very little or no overlap of GM atrophy and reduced glucose metabolism. When left and right MTL atrophy and glucose metabolism measures were directly compared, reduced GM density was highly associated with reduced glucose hypometabolism (left: $r=0.93$, $p<0.001$; right: $r=0.88$, $p<0.001$; Figure 6).

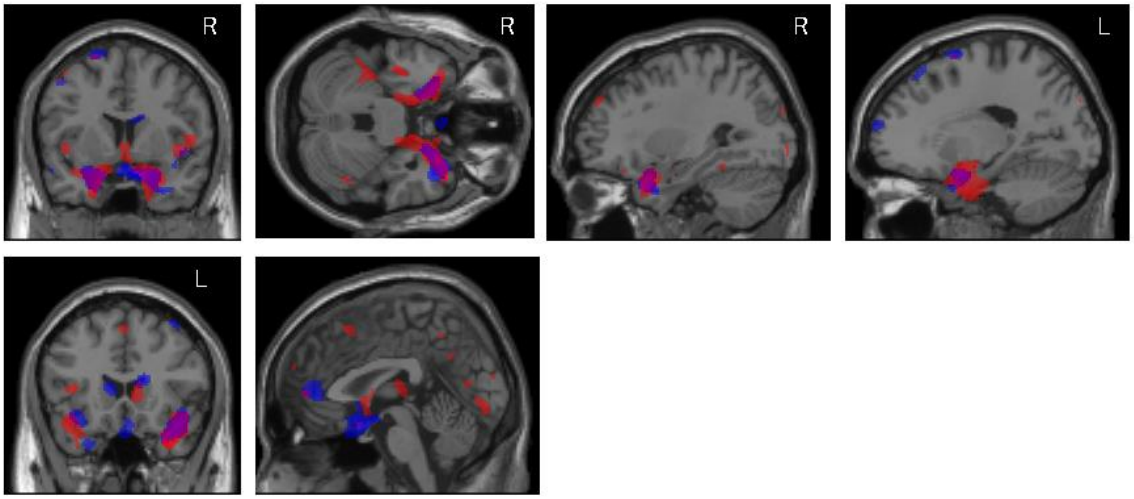

Figure 5. Anatomical overlap of GM atrophy and glucose hypometabolism in *MAPT* intron 10 +3 mutation carriers relative to non-carriers.

The overlap of regions showing significantly reduced GM density (red) and [^{18}F]FDG uptake (blue) for *MAPT* intron 10 +3 carriers relative to non-carriers is presented. Significant overlap is observed in the medial temporal lobe (MTL) and other temporal regions, while little overlap is seen in cortical and striatal regions. Images shown here are displayed at a voxel-wise threshold of $p<0.001$ (uncorrected for multiple comparisons) for GM density and $p<0.01$ (uncorrected for multiple comparisons) for glucose uptake, both with minimum cluster size (k) = 50 voxels. The GM density comparison was covaried for age, sex, and total intracranial volume, while the [^{18}F]FDG PET analysis was covaried for age and sex.

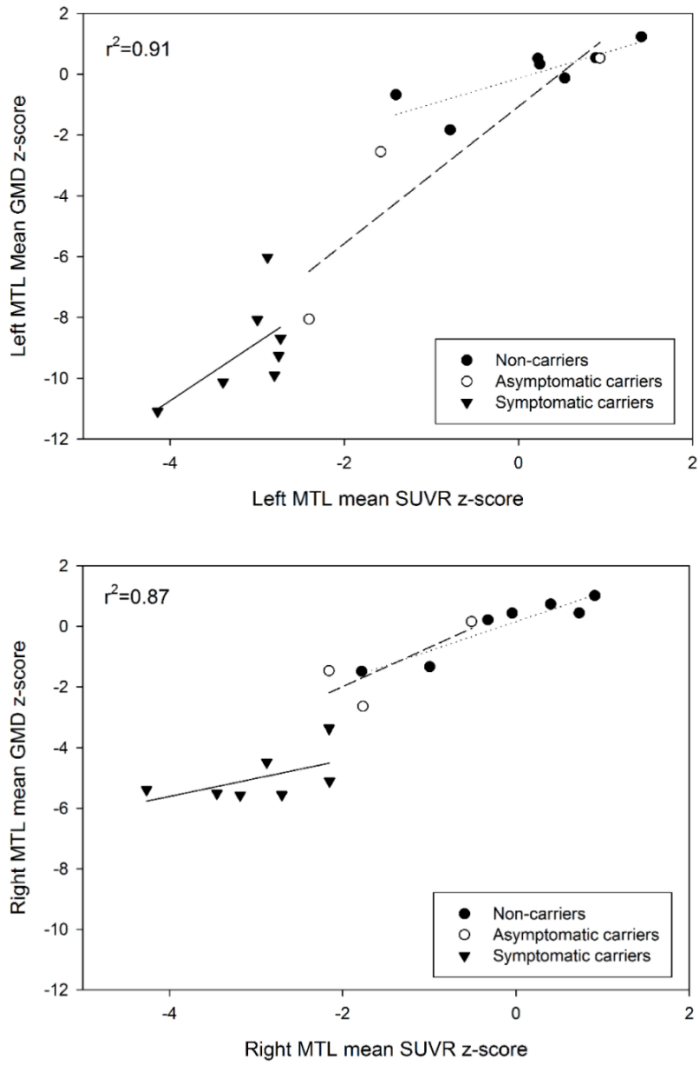

Figure 6. Relationship between medial temporal lobe atrophy and hypometabolism in carriers and non-carriers of the *MAPT* intron 10 +3 mutation.

A significant association between grey matter (GM) density and glucose metabolism in the left and right medial temporal lobe (MTL) was observed across and within groups. Individual data points represent raw GM density and [^{18}F]FDG SUVR values. The reported R-squared value corresponds to the correlation across all participants, covaried for age, sex, and total intracranial volume. Linear fits are shown for individual groups, including non-carriers (dotted line), asymptomatic carriers (dashed line), and symptomatic carriers (solid line).

3.4 Discussion

Although MRI and [^{18}F]FDG PET studies have been reported for sporadic bvFTD [162-167, 170], few studies have investigated changes in glucose metabolism or brain atrophy in FTDP-17T [170, 179]. Our findings show that individuals with the *MAPT* mutation at position +3 of intron 10 have prominent GM atrophy bilaterally in the MTL regions and reduced glucose metabolism in MTL regions and the prefrontal cortex, when compared to non-carriers. Furthermore, asymptomatic mutation carriers showed anatomical and metabolic changes intermediate between the SC and NC participants. We also observed substantial overlap in cortical atrophy and hypometabolism, specifically in MTL regions.

MRI Findings

VBM results for four of the eleven MSTD patients used in this study have been previously reported, and showed extensive GM loss in the hippocampus, parahippocampal gyrus, insular cortex, and to a lesser extent, the anterior cingulate cortex, head of the caudate nucleus, posterolateral orbital cortex, and insular cortex [161]. Results in the expanded sample are similar to the previous findings by Spina et al. with increased statistical power [161]. The prominent atrophy in mutation carriers compared to non-carriers in the MTL is similar to findings from studies of other familial FTD with *MAPT* mutations [171, 173, 174, 179-181]. However, contrary to other bvFTD studies, our results showed very little GM atrophy in the frontal lobes [182]. The MSTD patients did show anterior temporal atrophy, which is consistent with the new diagnostic criteria for bvFTD [160]. The AC group showed a level of atrophy intermediate between the NC and SC groups, with significant differences detected between all groups. This suggests that neurodegeneration occurs prior to clinical decline in mutation carriers, perhaps years before expected clinically significant decline. However, it is of importance

to note that the sample size of the AC group prohibited voxel-based analysis, thus further studies should be done to increase the power of this analysis.

[^{18}F]FDG PET Metabolism

Prior bvFTD studies have demonstrated hypometabolism in frontal and temporal lobes, anterior cingulate cortex, anterior insula, and subcortical regions [162-169]. MSTD mutation carriers showed near symmetrical hypometabolism in the MTL, parietal cortex, and frontal cortex relative to non-carriers. Consistent with the diagnosis for probable bvFTD [160], anterior temporal hypometabolism was observed, affecting the right hemisphere more than the left. Several subcortical structures, many of which belong to the limbic system known to regulate emotion and memory, showed glucose hypometabolism in the *MAPT* intron 10 +3 mutation carriers when compared to non-carriers, consistent with the clinical presentation of these participants. These regions include the cingulate gyrus, uncus, parahippocampal gyri, entorhinal cortex, and amygdala. The most notable reduction in glucose uptake was seen in the MTL, which is similar to other studies in FTDP-17T [170, 171]. Interestingly, glucose uptake in the AC group was between that of the NC and SC groups, suggesting a reduction in glucose metabolism prior to clinical decline. Utility of this [^{18}F]FDG PET predictor biomarker will require future longitudinal follow-up studies. No significant difference in glucose metabolism was observed between AC and SC, which may be a function of the small size of the AC group or may suggest the majority of the metabolic decline occurs prior to significant clinical symptomatology. Larger samples and longitudinal follow-up should be completed to help resolve this issue.

Comparison of Cortical Atrophy and Glucose Metabolism

Cortical atrophy and hypometabolism in the MTL were strongly associated in the present study. The distribution of metabolic changes also overlaps previously described patterns of neurodegeneration in MSTD patients and are consistent with the clinical characteristics of their cognitive dysfunction [161]. The striking similarity between the MRI and [^{18}F]FDG PET results and the high correlation of mean GM density and [^{18}F]FDG uptake in this region also raises a question as to whether the observed hypometabolism is due to a reduction in local GM tissue in the MTL. However, given the marked effect of the MSTD mutation, it seems likely that the functional hypometabolism and structural neurodegenerative changes are occurring concurrently in these patients as two aspects of the underlying disease process. Both MTL glucose uptake and cortical atrophy in the AC group were intermediate between the NC and SC groups. The differences in cortical atrophy were significant between all groups, whereas the AC and SC participants were not significantly different in glucose uptake. In other words, the hypometabolism in ACs before onset of clinical symptomatology is similar to SC, while the change in MTL atrophy is intermediate. These results suggest the possibility that hypometabolism may occur before atrophic changes are detectable, which would support the hypothesis that the change in metabolism is not of direct consequence of atrophy, as ambiguous similar findings have been observed in a previous study of Alzheimer's disease [183]. The lack of observable atrophy in hypometabolic regions in the anterior cingulate cortex and caudate nucleus also support the hypothesis that dysfunctional glucose metabolism may predate atrophy in disease-associated regions. However, these differences between cortical atrophy and glucose metabolism, or lack thereof, could also be due to different variability in the [^{18}F]FDG PET and structural MRI measures, which complicates interpretation.

Study Limitations

As previously indicated, the present study contains limitations. First, the AC group was small, which permitted quantitative ROI analysis but not voxel-based mapping of differences between the three groups. Further studies with a larger samples would provide the power needed to better detect the structural and metabolic differences in asymptomatic mutation carriers and would offer a better assessment of the impact of mutation status and clinical symptoms on the relative rates of cortical atrophy and cognitive dysfunction. Additionally, it is possible that the hypometabolism observed by the mutation-positive group was an effect of the cortical atrophy, as quantitative analysis of the MTL also showed the two variables (metabolism, atrophy) were highly correlated. While mutation status appeared to be causal for both the lower GM density and glucose uptake, once again, the small sample size of the AC group prevented us from having the power to fully determine the topography of differences across groups. Prospective longitudinal studies will be important in order to investigate the temporal relationships between metabolic and structural neuroimaging changes. Other functional imaging modalities could also prove informative with regard to early changes in brain networks, activation dynamics, and regional cerebral blood flow. Future studies with recently developed tau-specific PET tracers are also likely to elucidate the pattern of early changes and may provide better prediction of neurodegeneration and cognitive decline [184, 185]. Overall, these results suggest that neuroimaging, in addition to genetic testing, may provide useful insights into the sequence of disease processes and characterization of the effects of *MAPT* mutation, especially in the prodromal stage of MSTD.

Summary

Cortical atrophy and hypometabolism were observed in MSTD patients, especially in the MTL. These changes in brain structure and function are consistent with the observed cognitive dysfunction in these patients. Furthermore, reduced glucose metabolism and atrophy in the MTL were observed in asymptomatic carriers, suggesting these changes precede clinical onset. Future studies of expanded samples with longitudinal follow-up are needed to replicate the observed results and further elucidate the role of structural and functional brain changes in patients with MSTD.

Chapter 4: PET Signatures in Gerstmann–Sträussler–Scheinker Disease

4.1 Introduction

Gerstmann–Sträussler–Scheinker (GSS) disease is an autosomal-dominant neurodegenerative disorder associated with prion protein (PrP) gene (*PRNP*) mutations [186-188]. Onset occurs most frequently between the fourth and the sixth decades of life, with an average disease duration of five years. GSS is clinically characterized by ataxia, extrapyramidal signs, and cognitive impairment [189, 190]. The neuropathologic diagnosis is based on the presence of unicentric and multicentric APrP plaques in the cerebrum and cerebellum; however, the distribution and severity of PrP deposits vary substantially among GSS phenotypes [191]. A point mutation in *PRNP* at codon 198 (c.593T>C) results in a form of GSS (p.Phe198Ser; F198S) that is neuropathologically characterized by neurofibrillary tangles with paired helical filaments, in addition to PrP amyloid deposition [75, 188, 192, 193]. Patients with valine (V) homozygosity at codon 129 have an onset of disease more than 10 years earlier than those who are heterozygous for methionine (M)/V at codon 129 [192].

Previous [^{18}F]Fluorodeoxyglucose (FDG) positron emission tomography (PET) studies measuring glucose metabolism in GSS are extremely limited and likely to show varying results due to phenotypic heterogeneity of the different *PRNP* mutations [194-197]. Two symptomatic GSS F198S subjects have been previously been examined with [^{18}F]FDG PET. Results of this study suggest reduced [^{18}F]FDG uptake in the striatum, thalamus, and frontal and parietal cortices, as well as the cerebellum, without involvement in the medial temporal lobe [196]. However, studies have yet to examine glucose metabolism in a GSS family of a relatively large size.

Additionally, *in vivo* imaging of amyloid has become a valuable tool for evaluating amyloid plaque burden. [^{11}C]Pittsburgh compound B (PiB) is a PET radioligand with a high affinity for beta-amyloid (Aβ) fibrils [115]. [^{11}C]PiB retention is strongly correlated

with the presence of amyloid deposits made of Aβ protein in the *post-mortem* brain of patients with Alzheimer's disease. [^{11}C]PiB binds with high affinity to the β-sheet structure of Aβ plaques and fails to show retention with other abnormally conformed proteins such as tau of neurofibrillary tangles and α-synuclein of Lewy bodies [114, 115]. However, one case study showed cerebellar [^{11}C]PiB retention in a subject with BRI-amyloid (ABri) deposition, suggesting that [^{11}C]PiB may be capable of binding non-Aβ proteins found in plaques [198].

Like Aβ and ABri, APrP contains a higher-order β-sheet secondary structure. Neuropathological dyes such as the Congo Red derivative (*trans*, *trans*),-1-bromo-2,5-bis-(3-hydroxycarbonyl-4-hydroxy)styrylbenzene (BSB) and the Thioflavin T derivative [4′-(methylamino)phenyl] benzothiazole (BTA-1) bind these three types of amyloid, both *in vitro* and *in vivo* in mouse and human brains [199, 200]. Given that [^{11}C]PiB is a Thioflavin T derivative, we hypothesized that it may also bind to other amyloid proteins in addition to Aβ and ABri. Previous [^{11}C]PiB PET studies have demonstrated that [^{11}C]PiB is not specifically retained in individuals affected by a prion disease; however, the majority of these reports were based on single case studies and a heterogeneous sample of prion diseases [197, 201-204].

The purpose of this study was to evaluate (1) if [^{11}C]PiB PET is capable of detecting APrP in *PRNP* P102L (proline to leucine at codon 102) or F198S (phenylalanine to serine at codon 198) gene carriers, and (2) assess brain glucose metabolism using [^{18}F]FDG PET on a voxel-wise basis in GSS F198S mutation carriers. For the [^{11}C]PiB PET study, we evaluated cross-sectional and longitudinal [^{11}C]PiB PET scans in asymptomatic carriers of either the *PRNP* P102L or the *PRNP* F198S point mutations, relative to non-carriers. Furthermore, in a symptomatic GSS F198S patient, we investigated the neuropathologic changes and correlated these findings with the [^{11}C]PiB PET data that was obtained 46 months prior to death. Determining the ability of

[^{11}C]PiB PET to detect APrP would provide evidence about the suitability of this tracer in trials of novel therapeutics or in early detection of PrP amyloidosis and differentiating them from other prion disease.

To our knowledge, this is the largest study to investigate [^{18}F]FDG uptake in GSS subjects with the F198S mutation. Additionally, this is the first study to investigate the sensitivity of [^{11}C]PiB PET for binding APrP plaques in the P102L and F198S GSS mutation.

4.2 Materials and Methods

Participants

A total of 25 participants with, or at risk for GSS were included in this study. Investigators were initially blinded to the participant's genetic status related to the *PRNP* gene. Investigators were later unblinded after obtaining all neuropsychological and imaging data reported in the present paper. Neuropsychological testing, cognitive assessments, and neuroimaging was completed at the Indiana Alzheimer Disease Center (IADC). In addition, neuropsychological, clinical, and [^{11}C]PiB PET data from eight cognitively healthy non-carriers (NC) from a separate study on aging and dementia at the IADC (the Indiana Memory and Aging Study (IMAS) were included for the amyloid study. All NC and asymptomatic carriers (AC) displayed no clinically relevant cognitive impairment or significant cognitive complaints. All participants or their legally authorized representative provided written informed consent according to the Declaration of Helsinki and all procedures were approved by the Indiana University Institutional Review Board.

Genotyping

Identification of point mutations in the *PRNP* gene was done as previously described [188]. Briefly, genomic DNA was isolated from fresh blood. The complete *PRNP* gene was amplified and direct sequencing performed using the DTCS quick start kit (Beckman Coulter, Fullerton, CA). The products were loaded onto a CEQ 8000 GeXP Genetic Analysis System (Beckman Coulter). DNA sequences were compared with the published *PRNP* sequence (www.ncib.nlm.nih.gov).

Acquisition and Processing of Magnetic Resonance Imaging Data (baseline only)

All participants underwent a structural MRI scan on the same day of the [^{18}F]FDG PET scan except for three NCs (range: 1-12 days). Fifteen participants, including nine GSS-F198S mutation carriers (5 symptomatic, 4 asymptomatic) and six NCs, underwent a single T1-weighted SPGR volumetric scan on a 1.5T GE Signa scanner as previously described [161]. Seven participants (2 SCs, 1 AC, and 4 NCs) received a single T1-weighted MPRAGE volumetric scan on a 3T Siemens Trio scanner. Structural MRI scans were processed using voxel based morphometry (VBM) in SPM8 (http://www.fil.ion.ucl.ac.uk/spm/) using previously described techniques [177]. Briefly, scans were co-registered to a T1-weighted template and segmented into grey matter (GM), white matter (WM), and cerebrospinal fluid (CSF) compartments using standard templates with bias correction. GM images were unmodulated, normalized to Montreal Neurologic Institute (MNI) space as 1 x 1 x 1 mm voxels, and smoothed with an 8mm full-width half maximum (FWHM) Gaussian kernel. All scans underwent extensive quality control at all processing steps. Only smoothed, normalized GM images generated from the SPGR volumes acquired on the 1.5T GE scanner were used in the VBM analysis, given the differences in data acquisition for 3T scans. Parameters generated from the

structural MRI segmentation were also used for [^{18}F]FDG PET processing as described below (see *Acquisition and Processing of [^{18}F]FDG PET Data below*).

Acquisition and Processing of [^{18}F]FDG PET Data

Twenty-two participants also underwent a [^{18}F]FDG PET scan, acquired on a Siemens EXACT HR+ scanner. After positioning within the scanner, a 10-minute transmission scan using three internal rod sources was acquired for attenuation correction. A 60-min dynamic acquisition protocol was then initiated with the injection of approximately 10 mCi of [^{18}F]FDG using the following frame sequence: 12 x 5s, 4 x 15s, 2 x 30s, 7 x 60s, 10 x 300s. [^{18}F]FDG scans were reconstructed using the manufacturer's software (CTI Molecular Imaging Inc.; Knoxville, TN) with the filtered back-projection algorithm. Corrections for scatter, randoms, and attenuation were applied.

Reconstructed [^{18}F]FDG scans were processed using standard techniques. Using SPM8, scans were converted from ECAT to NiFTI format, coregistered to the structural MRI scan from the same visit, motion corrected, and normalized to MNI space using matrices from the same time-point MRI segmentation. A static [^{18}F]FDG image from 30-60 minutes was created from the appropriate frames, intensity normalized using a pons reference region to create a standardized uptake value ratio (SUVR) image for each participant, and smoothed with an 8 mm FWHM kernel. The SUVR images were then used for further analysis as described below (see *Image Analysis* below).

Acquisition and Processing of [^{11}C]PiB PET Data

Fourteen *PRNP* P102L and F198S participants (9 NC, 4 AC, 1 SC) received a baseline [^{11}C]PiB PET scan, acquired on a Siemens EXACT HR+ scanner. Three asymptomatic carriers (2 *PRNP* P102L, 1 *PRNP* F198S) also received a second [^{11}C]PiB

PET scan approximately one year after the initial scan. Prior to each scan, a 10-minute transmission scan using three internal rod sources was acquired for attenuation correction. For the six individuals at risk for GSS (1 NC, 4 AC, 1 SC) injection of [^{11}C]PiB was followed by a 40min uptake period. Dynamic data acquisition protocol was then initiated with the following frame sequence: 6 x 5min. Two participants from the IMAS study received a similar protocol as those at risk for GSS (40min uptake period, dynamic acquisition, frame sequence: 10 x 5min). In the other 6 participants from IMAS (6 NC), data acquisition was initiated with the injection of [^{11}C]PiB and the frame sequence was: 10 x 30sec, 9 x 1min, 2 x 3min, 8 x 5min, 3 x 10min. The average [^{11}C]PiB injected across all participants (those at risk for GSS and IMAS) was 11.17±2.0 mCi. Scans were reconstructed using manufacturer's software (Siemens; Knoxville, TN) for filtered back-projection. Corrections for scatter, randoms, and attenuation were applied.

Reconstructed [^{11}C]PiB scans were processed using standard techniques. Using Statistical Parametric Mapping 8 (SPM8; Welcome Department of Cognitive Neuroscience, London, UK), scans were converted from ECAT to NiFTI format, coregistered to the structural MR) scan from the same visit (3T MPRAGE scan; Siemens Tim Trio), spatially aligned on a frame-by-frame basis, and normalized to MNI space using matrices from segmentation of the same time-point MRI. A static [^{11}C]PiB image from 40-70 minutes was created from the appropriate frames (depending on scan acquisition type (see above)) and was intensity normalized using a pons reference region to create a SUVR image for each participant. SUVR images were smoothed with an 8 mm FWHM Gaussian kernel.

Image Analysis

Using SPM8, an ANCOVA was performed on normalized MRI GM density (1.5T only) and [^{18}F]FDG PET SUVR images (all subjects) to compare the effect of diagnostic status (NC vs. AC vs. SC) on GM density and FDG uptake on a voxel-by-voxel basis. Age at time of scan, sex, and total intracranial volume (tICV) were used as covariates for the MRI analysis. Age at time of scan and sex were used as covariates for the [^{18}F]FDG PET analysis. In addition, since the M/V codon 129 status is known to influence the clinical and pathological phenotypes of the GSS F198S mutation, separate MRI and [^{18}F]FDG PET analyses were also computed using codon 129 status as an additional covariate. An explicit GM mask was applied to both MRI and PET analyses to restrict the search area for statistical analysis. Significant findings were displayed using a threshold of $p<0.001$ (uncorrected) for MRI and a threshold of $p<0.01$ (uncorrected) for [^{18}F]FDG PET; for both analyses, minimum cluster size (k) was 50 voxels. A composite image using the significant clusters for MRI and [^{18}F]FDG PET was created to qualitatively investigate areas of overlap of diagnostic differences in the MRI and PET analyses. The MarsBaR toolbox (version 0.42) in SPM was used to extract mean GM density and mean glucose uptake for the significant clusters from MRI and PET analyses, respectively.

Visualization of the average group [^{11}C]PiB images served as a primary qualitative assessment. Mean baseline [^{11}C]PiB SUVR images and mean normalized baseline structural MR images for each diagnostic/mutation status group were created using SPM8. To visualize [^{11}C]PiB retention by group, mean [^{11}C]PiB SUVR images was overlaid onto the respective group mean MR images in MRIcron (http://www.mccauslandcenter.sc.edu/mricro/mricron/). For each participant, mean [^{11}C]PiB SUVR values were extracted from a global cortical GM region of interest (ROI) and a whole cerebellum ROI defined from the AAL atlas and extracted using MarsBaR

[205]. SUVR values from each ROI were compared between diagnostic/mutation status groups as described below (Statistical Analysis). In the three AC subjects with follow-up scans, the extracted mean [^{11}C]PiB SUVR values from the ROIs at both time-points were graphed to complement qualitative visual observations.

Statistical Analysis

A chi-square test was used to assess the differences in sex and *PRNP*-129M/V status by diagnosis/mutation group. Continuous demographic variables and baseline neuropsychological test performance were evaluated using an ANCOVA model to examine the differences between NC and mutation carriers. Age and years of education were used as covariates when evaluating neuropsychological test scores. An ANCOVA model was also used to test for association of mutation status (carrier vs. non-carrier) with mean [^{11}C]PiB or mean [^{18}F]FDG SUVR values from the global cortical GM and cerebellar ROIs, covaried for age and sex. Although the small sample number precluded statistical analysis, the mean [^{18}F]FDG SUVR values from the significant regions from identified in the comparison of glucose metabolism in NCs relative to SCs (NCs>SCs), and *PRNP*-129M/V status were graphed. The relationship between mean [^{18}F]FDG SUVR and mean GM density from the significant regions from identified in the comparison of glucose metabolism in NCs relative to SCs (NCs>SCs) and memory and motor function was assessed using a partial Pearson correlation using age, sex, and tICV as covariates. For the Groove Pegboard Test, number of peg drops was added as an additional covariate. Z-scores for GMD and SUVR from significant regions of interest identified in the previous analysis were calculated for each participants using means and standard deviations from the NC group. A linear regression was used to determine the relationship between GMD and SUVR. Age, sex, and tICV were used as covariates. Bonferroni correction was used to adjust for multiple comparisons between groups. All

statistical analyses employed SPSS (version 24.0, Chicago, IL) and graphs were created with SigmaPlot (version 10.0).

Neuropathologic Assessment

The symptomatic individual (*PRNP* F198S) expired 46 months after the [^{11}C]PiB scan. Tissue was harvested at Indiana University School of Medicine. The fresh brain was hemisected along the mid-sagittal plane. The left hemibrain was fixed in formalin and the right hemibrain was sliced, frozen, and stored at −70 °C.

Following fixation in a 10 % formalin solution, brain tissue samples were dehydrated in graded alcohols, cleared in xylene, and embedded in paraffin. Eight-micrometer-thick sections from multiple brain areas were stained with the histological and immunohistochemical methods described below. Hematoxylin and eosin (H&E) and luxol fast blue with hematoxylin & eosin (LFB-H&E) were used to survey gray and white matter for neuronal losses, gliosis, vascular pathology, and other possible pathologic lesions. Thioflavin S method was used to visualize amyloid deposits and neurofibrillary tangles. Neurodegenerative pathology was analyzed using antibodies raised against amyloid β (Aβ) (21F12), tau (AT8), and prion protein (PrP; 3F4).

The signal from polyclonal antibodies was visualized using avidin–biotin, with goat anti-rabbit immunoglobulin as the secondary antibody, followed by horseradish peroxidase-conjugated streptavidin and the chromogens diaminobenzidine or tetramethylbenzidine. The signal from monoclonal antibodies was detected using avidin–biotin, with goat anti-mouse immunoglobulin as the secondary antibody, followed by alkaline phosphatase-conjugated streptavidin and the chromogen diaminobenzidine or tetramethylbenzidine. Immunohistochemical sections were counterstained with hematoxylin.

A semi-quantitative analysis of anatomical brain regions was carried out using a Leica DMLB microscope (Leica Wetzlar, Germany) from the following regions: superior frontal gyrus, middle frontal gyrus, anterior cingulate cortex, posterior cingulate cortex, superior and middle temporal gyri, superior parietal lobule, insular cortex, occipital cortex, amygdala, hippocampus, subiculum, parahippocampus, caudate nucleus, putamen, globus pallidus, thalamus, cerebellar hemisphere, dentate nucleus, substantia nigra, locus coeruleus, basis pontis, and inferior olivary nucleus. The severity of neuropathologic changes were evaluated using a subjective scale: none = 0, mild = 1 (+), moderate = 2 (++), and severe = 3 (+++).

4.3 Results

Neuropsychological Assessment

The demographics, genetic status, and neuropsychological testing results at baseline for the [^{18}F]FDG PET and [^{11}C]PIB PET are displayed in Table 3 and Table 4, respectively. Two participants with the F198S mutation (1 AC, 1 SC) were used for both studies. Although not statistically significant, more female than male participants were available for these studies across all groups.

For the [^{18}F]FDG PET study, no significant difference between groups was observed for sex, years of education, or the COWA test. Although not statistically significant, SCs were on average older than the NC and AC groups. As expected, all F198S mutation carriers had at least one valine at codon 129 of *PRNP*. A significant difference between groups was observed for the Mini-Mental State Exam (MMSE, $p=0.026$), Clinical Dementia Rating – Sum of Boxes (CDR-SB, $p<0.001$), and the Groove Pegboard Test, a high level motor processing task. Specifically, the NCs and ACs showed better cognition (higher MMSE; NC vs SC, $p = 0.029$; AC vs SC, $p = 0.016$),

lower clinical dementia rating (lower CDR-SB; NC vs SC, $p<0.001$; AC vs SC, $p<0.001$), and worse manual motor performance than the SCs (dominant hand: NC vs SC, $p = 0.009$; AC vs SC, $p = 0.043$; non-dominant hand: NC vs SC, $p = 0.0093$; AC vs SC, $p = 0.027$).

For the amyloid study, significant differences were observed for age and education between NC and mutation carriers. As expected, the SC showed lower cognition and significantly impaired manual motor performance compared to ACs and NCs.

Table 3. Baseline demographic, neuropsychological, and motor performance data for the [^{18}F]FDG PET study in GSS F198S.

	NC	AC	SC	p-value
N	10	4	8	
Age (years)	40.5 (15.3)	30.5 (8.7)	47.9 (5.7)	0.72
Sex (Male, Female)	7, 3	1, 3	3, 5	0.212
Education (Years)	14.3 (2.8)	14 (1.8)	12.9 (1.5)	0.401
Codon 129 status (MM, MV, VV)	2, 7, 1	0, 2, 2	0, 2, 6	0.064
MMSE	28.7 (1.3)	29.5 (1)	26.8 (1.8)	0.026
CDR-SB	0	0	0.56 (0.32)	<0.001
COWA*	40.3 (10.8)	45.3 (3.9)	33.5 (14)	0.673
Groove Pegboard (Dom. Hand)**	69.8 (13)	63.8 (7.4)	110.6 (28.6)	0.008
Groove Pegboard (Nondom. Hand)**	74.9 (15.6)	68 (11)	131.4 (36.4)	0.003

NC = non-carriers; AC = asymptomatic carriers; SC = symptomatic carriers; M = methionine; V = valine; MMSE = Mini Mental State Examination; CDR-SB = Clinical Dementia Rating – Sum of Boxes; COWA = Controlled Oral Word Association test; Dom. = dominant; Nondom. = non-dominant. *Missing two symptomatic carriers. **Missing one symptomatic carrier. Mean (Standard Deviation).

Table 4. Baseline demographic, neuropsychological, and motor performance data for the [^{11}C]PIB PET study in GSS F198S and P102L.

	NC	AC	SC	p-value
N	9	4	1	
Age (Years)	66.1 (4.2)	44.3 (11.7)	41	<0.001
Sex (Male, Female)	3, 6	1, 3	0, 1	0.312
Education (years)	16.7 (1.7)	14 (1.4)	13	<0.001
Mutation Status (F198S, P102L)	0, 0	1, 3	1, 0	n.a.
MMSE*	28.9 (1.0)**	29.5 (0.6)	27	0.364
CDR-SB	0.1 (0.2)	0 (0.0)	6	0.933
COWA*	45.7 (8.0)***	44 (6.1)	22	0.968
Finger Tapping (Dom)	n.a.	49.5 (8.8)	26	n.a.
Finger Tapping (Non-Dom)	n.a.	43.3 (8.8)	24	n.a.
Grooved Pegboard (Dom)	n.a.	70.3 (8.1)	154	n.a.
Grooved Pegboard (Non-Dom)	n.a.	80.3 (17.0)	149	n.a.

NC = non-carrier; AC = asymptomatic carrier; SC = symptomatic carrier; MMSE = Mini-Mental State Examination; CDR-SB = Clinical Dementia Rating-Sum of Boxes; COWA = Controlled Oral Word Association; n.a. = not available; Dom = dominant hand; Non-Dom = non-dominant hand). *Covaried for age, sex, and education. **Missing one non-carrier value; ***Missing three non-carrier values. Mean (standard deviation).

[^{18}F]FDG PET

The SC group showed hypometabolism in the cerebellum (right > left), bilaterally in the putamen and claustrum, and the left caudate head relative to NCs (Figure 7A-C). Other affected areas included the right substantia nigra, right red nucleus, and right thalamus, and others (Table 5). A similar hypometabolic pattern was observed in the cerebellum (right > left), left caudate head, right thalamus, and bilaterally in the putamen in SCs relative to ACs (Figure 7D-F).

Unexpectedly, the AC group exhibited hypermetabolism rather than hypometabolism in the left caudate head, left putamen, left claustrum, and left superior temporal gyrus relative to NCs (Figure 7G-I). When *PRNP*-129M/V status was included as a covariate, similar results were observed in all analyses (*data not shown*). For all analyses, no significant clusters were observed in the opposite directions (SC>NC/AC, NC>AC).

Due to the small sample size, a whole-brain voxel analysis could not be completed to determine the association of *PRNP*-129M/V status with glucose metabolism in these subjects. Instead, mean glucose uptake for the large significant clusters identified in the previous analysis in the bilateral cerebellum, right putamen, and left caudate were extracted in order to examine the effect of the *PRNP*-129 genotype on glucose uptake across diagnostic groups. Glucose metabolism in the left caudate head and right putamen of the AC group was increased in *PRNP*-129VV individuals relative to NC *PRNP*-129MV persons and showed a slight increase over NC *PRNP*-129MM persons in the NC group (Figure 8A-B).). AC *PRNP*-129VV individuals did not show increased glucose metabolism in the cerebellum (Figure 8C). SC *PRNP*-129VV participants show reduced [^{18}F]FDG uptake in the caudate and cerebellum relative to SC *PRNP*-129MV persons (Figure 8A-C).

Next, we assessed if glucose metabolism in the caudate and putamen was associated with impaired memory and motor function, two predominant phenotypes

associated with the F198S mutation. [^{18}F]FDG uptake in the left caudate and right putamen was associated with motor function ($r = -0.53$, $p = 0.029$; Figure 9) with lower [^{18}F]FDG uptake associated with poorer motor function. However, the association was not significant when controlling for diagnosis or *PRNP*-129M/V status. No significant association was observed between [^{18}F]FDG uptake in the striatal ROIs and memory performance ($r = 0.41$, $p = 0.09$).

In order to evaluate the anatomical overlap between atrophic and metabolic group differences, a composite image of GM atrophy and hypometabolism of SCs relative to NCs was created. Significant overlap of the atrophic and metabolic patterns (NCs>SCs) was observed in the putamen (Figure 10). No other overlap was observed. Further evaluation of the right putamen revealed that GM atrophy exceeded hypometabolism in the SC group (Figure 10B). Also, the AC groups showed increased hypermetabolism, as described above, but no increases in GM in these regions (Figure 10B). The atrophy and glucose uptake measurement of the right putamen were directly compared and showed a higher association (Figure 10C; $r = 0.82$; $p < 0.001$).

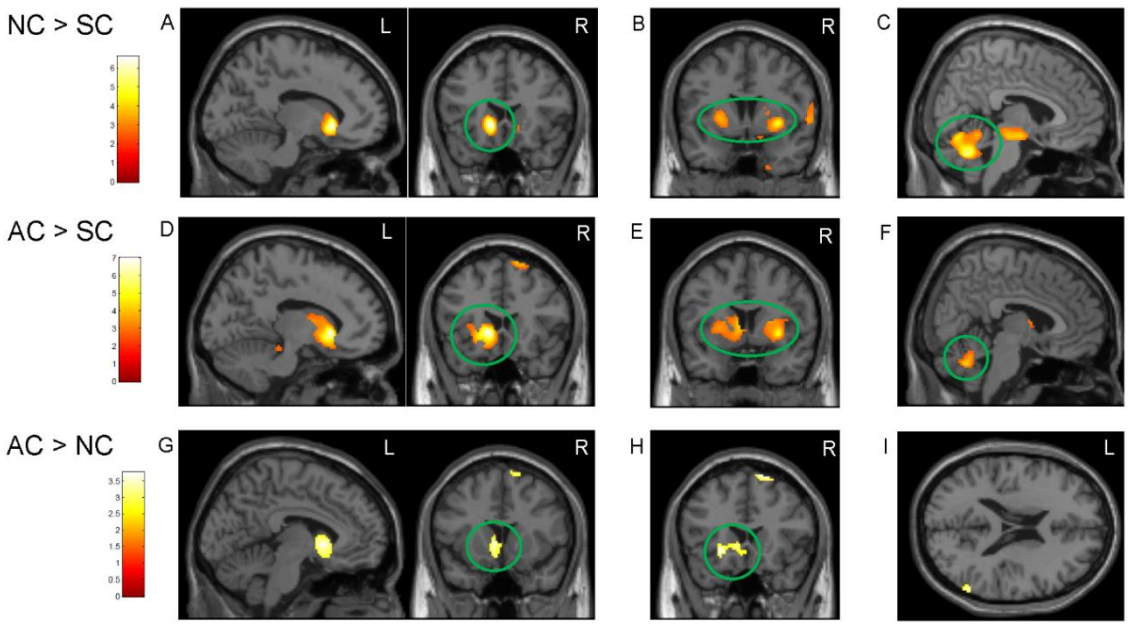

Figure 7. Hypometabolic regions in GSS F198S carriers and non-carriers.

Symptomatic carriers (SC) showed reduced [^{18}F]FDG uptake in the (A) left caudate head, (B) putamen, and (C) cerebellum. Relative to asymptomatic carriers (AC), SCs showed reduced [^{18}F]FDG uptake in the (D) caudate head, (E) putamen, and (F) cerebellum. ACs showed increased [^{18}F]FDG uptake in the (G) left caudate head, (H) left putamen, and (I) the right superior temporal gyrus (BA22/39) relative to NCs. Group differences were are displayed at a voxel-wise threshold of $p < 0.01$ (uncorrected for multiple comparisons) and at a minimum cluster size (k) = 50 voxels. Age and sex were used as covariates.

Table 5. Anatomical distribution of reduced glucose metabolism in symptomatic GSS F198S carriers relative to non-carriers.

			MNI coordinates			
Location	BA	T-value	x	y	z	p-value
L. Caudate Head		6.59*	−12	20	−4	0.000
L. Putamen		4.68	−32	−6	0	0.000
		3.88	−22	10	2	0.001
R. Caudate Head		2.71	14	20	−6	0.007
R. Claustrum		4.78	32	4	0	0.000
R. Anterior Cerebellum (Culmen)		5.52	6	−60	−30	0.000
		4.35	6	−70	−14	0.000
		3.7	4	−50	−12	0.001
		3.47	20	−40	−20	0.001
R. Putamen		3.32	20	10	12	0.002
R. Substantia Nigra		4.56	8	−20	−12	0.000
R. Superior Temporal Gyrus	22	4.46	60	8	0	0.000
R. Thalamus		4.09	8	−10	−14	0.000
		2.68	2	−10	−2	0.008
R. Thalamus or R. Parahippocampal gyrus		4.14	14	−36	2	0.000

BA = Brodmann area; L. = left; R. = right

p-value < 0.01, uncorrected; *Significant cluster for p < 0.05 at FWE-corrected

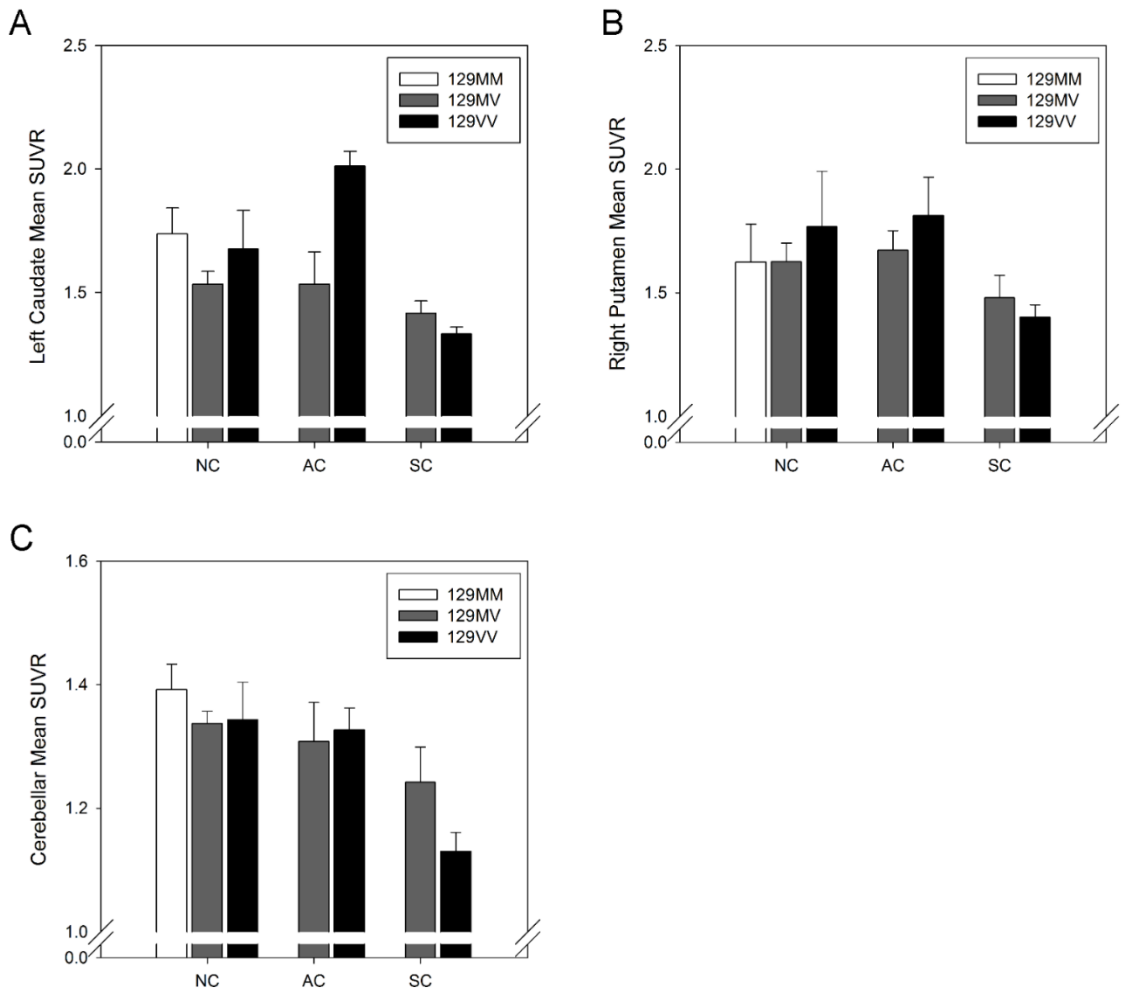

Figure 8. Quantitation of the *PRNP*-M129V haplotype effect on glucose hypometabolism in symptomatic and asymptomatic GSS F198S mutation carriers and non-carriers.

In the left caudate (A) and right putamen (B) of the asymptomatic carrier (AC) group, *PRNP*-129VV participants show more hypermetabolism relative to *PRNP*-129MV. In all ROIs (A-C) for the symptomatic carrier (SC) group, *PRNP*-129VV participants show reduced [^{18}F]FDG uptake relative to *PRNP*-129MV participants.

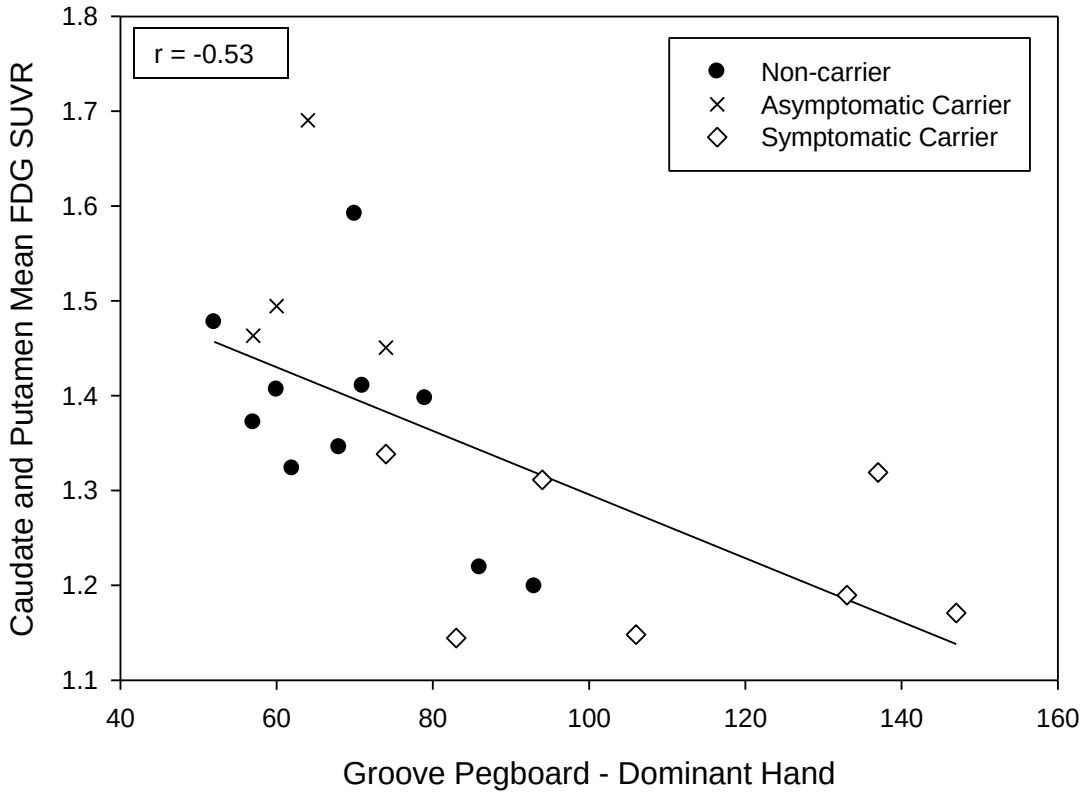

Figure 9. Motor function is correlated with [^{18}F]FDG uptake in the caudate and putamen.

(A) Worse motor function, as measured by the groove pegboard test, was associated with lower [^{18}F]FDG uptake in the striatum (caudate and putamen).

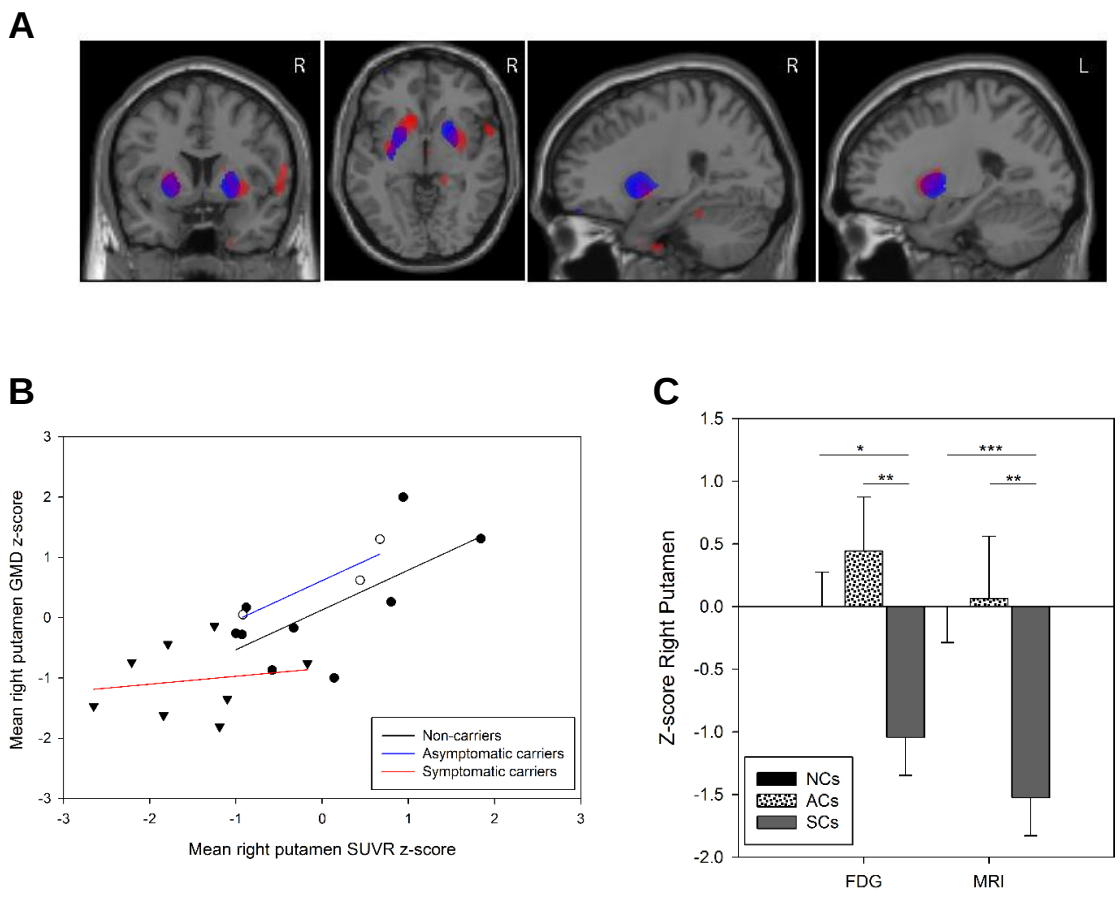

Figure 10. Grey matter and glucose hypometabolism in symptomatic GSS F198S mutation carriers and non-carriers.

(A) Anatomical overlap (purple) of grey matter (GM) atrophy (blue) and glucose hypometabolism (red) in symptomatic GSS F198S symptomatic carriers relative to non-carriers (NC) was observed in the striatum. (B) Mean GM density and [^{18}F]FDG SUVR values from the right putamen were significant associated with each other, covaried for age, sex, and total intracranial volume (r_p = 0.82, p<0.001). Linear fits are shown for each diagnostic group: non-carrier (NC), solid line; asymptomatic carrier (AC), dashed line; symptomatic carrier (SC), dotted line. The association was primarily driven by the NC and AC groups.

[^{11}C]PIB PET

No apparent visual differences in baseline [^{11}C]PiB PET uptake were observed between the NCs, the ACs, and the SC individual, suggesting minimal [^{11}C]PiB binding in ACs and even in the symptomatic individual (Figure 11A-C). MRI of the symptomatic carrier revealed a mild degree of atrophy of the cerebellar cortex. Quantitative regional analysis did not reveal any significant difference in [^{11}C]PiB retention in either global cortical GM or cerebellum between mutation carriers (SC or ACs) and NCs (Figure 11D). Qualitative observation of the baseline and longitudinal follow-up scans for the 3 ACs did not show any appreciable increase in [^{11}C]PiB signal over time (Figure 12A-C). This observation was supported by minimal longitudinal change in mean [^{11}C]PiB SUVR in cortical GM and cerebellum ROIs (Figure 12D).

Moderate (++) to severe (+++) neuronal loss was observed in the superior frontal and cingulate gyri, putamen, caudate nucleus, superior and middle temporal gyri, hippocampus, subiculum, entorhinal cortex, superior parietal lobule, calcarine cortex, cerebellum, midbrain, and spinal cord (anterior horn cells; *data not shown*). In addition, moderate (++) axonal and myelin loss was observed in the superior frontal and cingulate gyri, caudate nucleus and putamen, superior parietal lobule, superior and inferior temporal gyri, occipital lobe, cerebellar white matter, and spinal cord (dorsal spinocerebellar tract, anterior spinocerebellar tract, lateral corticospinal tract, posterior columns; *data not shown*).

Pathologic prion protein (PrP) (Figure 13A, C) and Thioflavin S positive (Figure 13E) unicentric and multicentric plaques (severe, +++) were observed in the superior frontal and cingulate gyri, putamen, caudate nucleus, superior and middle temporal gyri, hippocampus, entorhinal cortex, superior parietal lobule, calcarine cortex, cerebellum, and midbrain.

Tau-immunopositive neurofibrillary tangles (+++) (Figure 13B, D) and neuropil threads (+++) (Figure 13B, D) were observed in the superior frontal and cingulate gyri, entorhinal cortex, amygdala, substantia innominata, superior and middle temporal gyrus, thalamus, superior parietal lobule, middle frontal gyrus, posterior cingulate gyrus, precuneus, inferior parietal lobule, and substantia nigra. Figure 13 is from frontal cortex but is representative of the cerebral cortex. PrP and tau pathologies were more prominent in the deeper layers of the cerebral cortex. In the cerebellum, there was a severe (+++) loss of neuronal perikarya which was associated with numerous (+++) PrP-immunopositive plaques. The white matter showed extensive (+++) axonal loss. Plaques were observed throughout all layers of the cerebellar cortex (Figure 14A-C). No Aβ immunopositive deposits were seen.

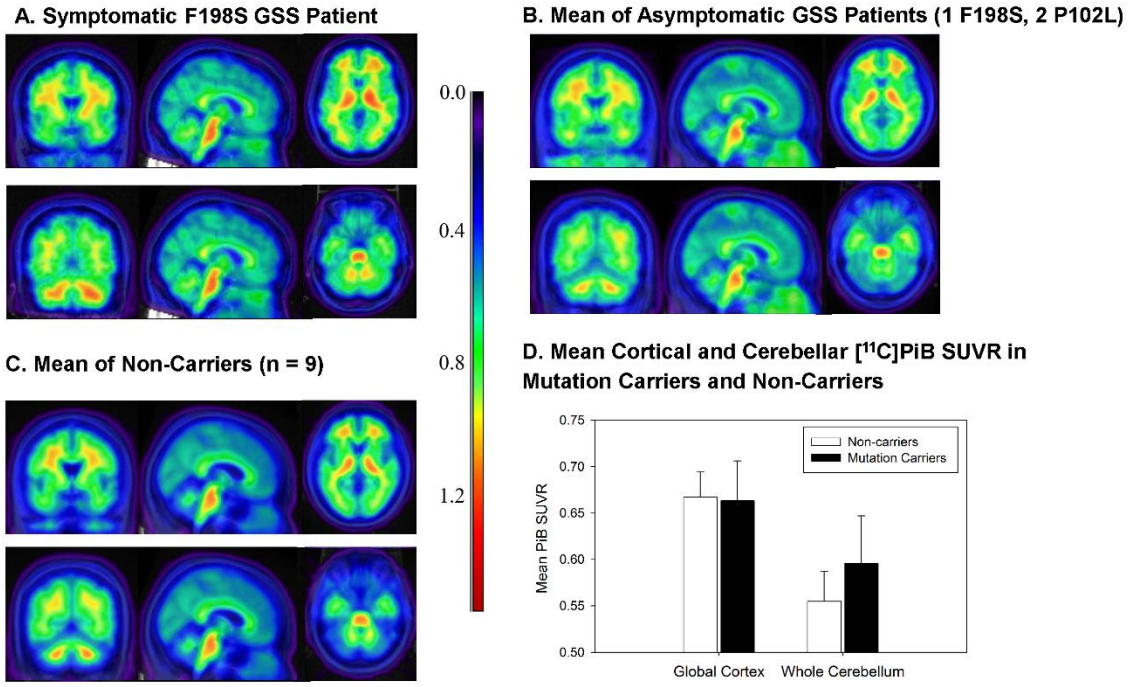

Figure 11. Baseline [^{11}C]PiB PET in F198S and P102L carriers and non-carriers.

[^{11}C]PiB SUVR images for (A) a symptomatic carrier, (B) asymptomatic carriers (n=4), and (C) non-carriers (n=9). Note that B and C are the average image across participants within each group, while A is a single participant. No notable visual differences in [^{11}C]PiB SUVR images were observed between the symptomatic carrier, asymptomatic carriers, and non-carriers. (D) [^{11}C]PiB SUVR levels in the global cortical grey matter and the whole cerebellum in non-carriers and mutation carriers are displayed. No significant difference was observed in global cortex and whole cerebellum [^{11}C]PiB SUVR between non-carriers and mutation carriers.

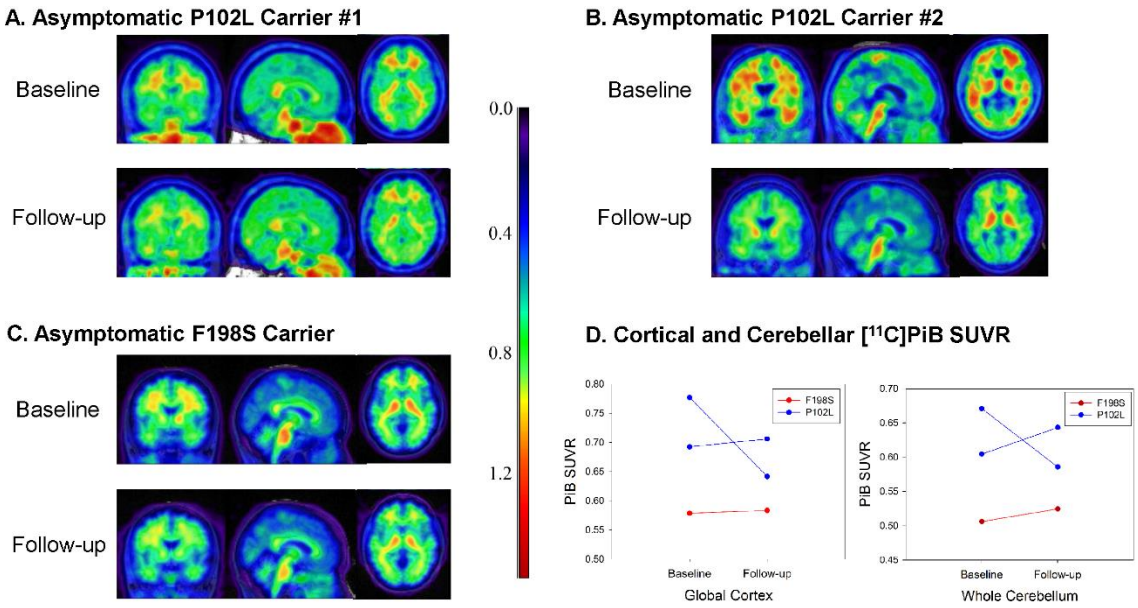

Figure 12. Baseline [^{11}C]PiB PET in F198S and P102L asymptomatic carriers.

Baseline (left) and follow-up (right) [^{11}C]PiB SUVR images for 3 asymptomatic carriers (2 P102L (A, B), 1 F198S (C)). No appreciable increase in [^{11}C]PiB from the baseline to the follow-up scan was observed in any of the participants. (D) Quantitation of mean [^{11}C]PiB SUVR in the cortical grey matter and whole cerebellum supported this qualitative observation.

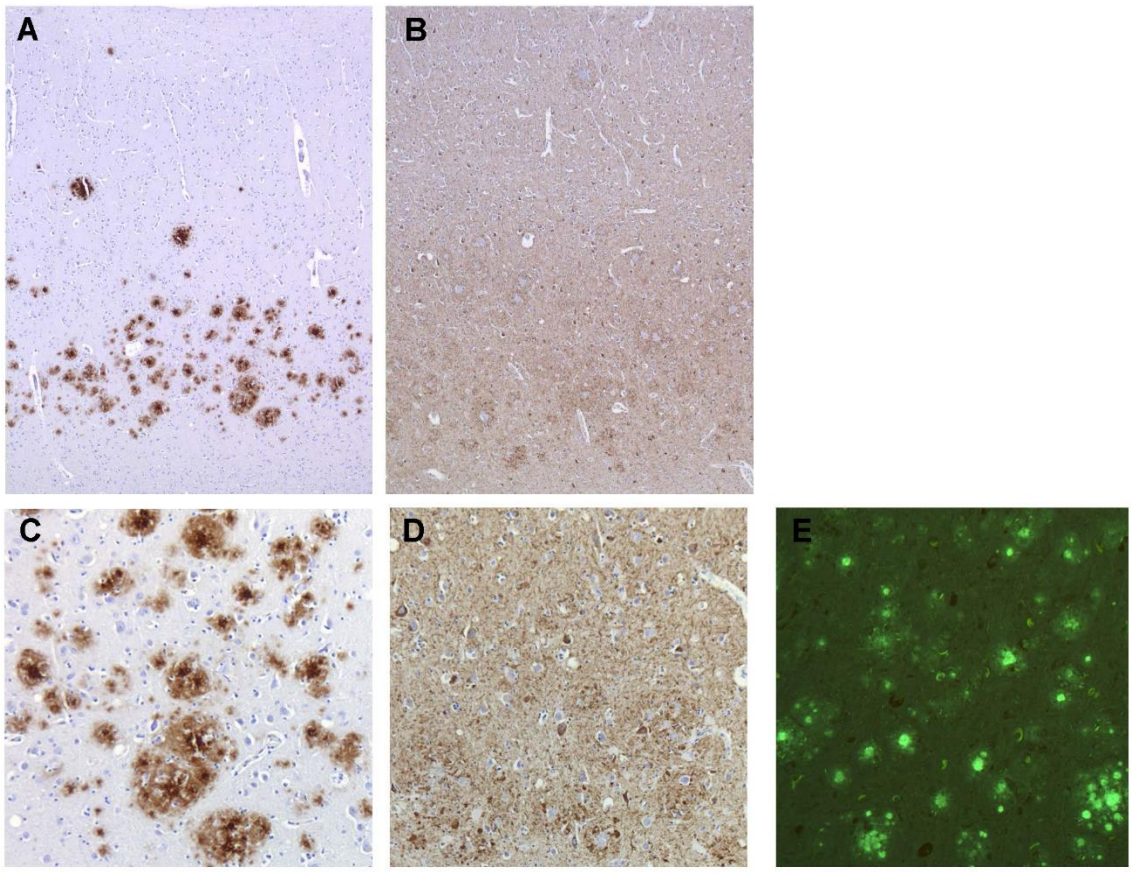

Figure 13. Extracellular PrP deposits and intracellular tau aggregates shown by immunohistochemistry and Thioflavin S in the frontal cortex of the *PRNP* F198S carrier.

3F4 immunohistochemistry reveals unicentric and multicentric PrP immunopositive plaques (A, C). AT8 immunohistochemistry reveals tau-immunopositive neurons and neuropil threads (B, D). Plaques and neurofibrillary tangles are fluorescent with Thioflavin S. PrP deposits and tau aggregates are shown at two different magnifications (A, B = 50X total magnification and C-E = 100X total magnification).

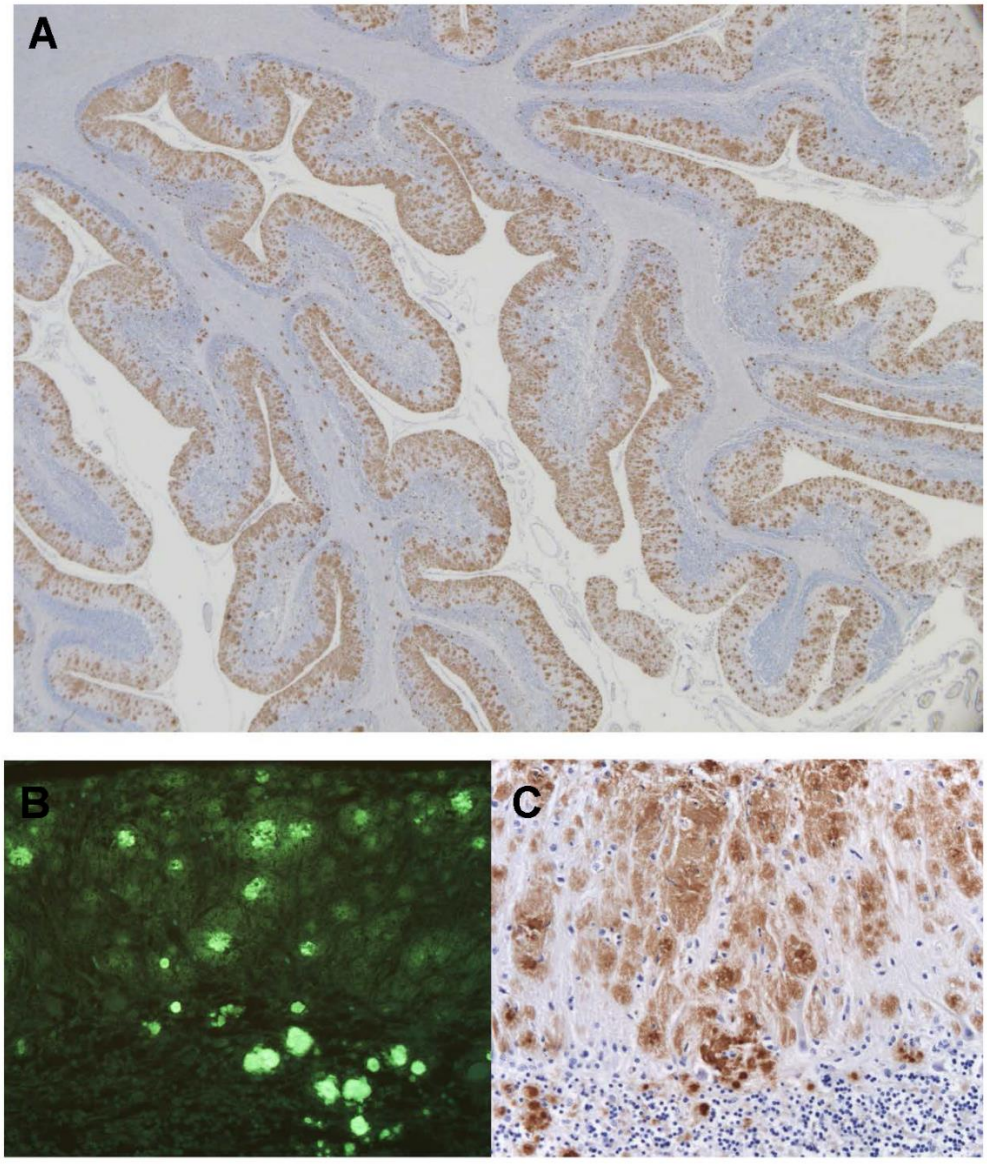

Figure 14. Extracellular PrP deposits shown by immunohistochemistry and Thioflavin S in the cerebellum of the *PRNP* F198S carrier.

3F4 immunohistochemistry reveals unicentric and multicentric PrP immunopositive plaques throughout the cerebellar cortex (A, C). Plaques are fluorescent with Thioflavin S (B). PrP deposits are shown at two different magnifications (A = 10X total magnification and B = 100X total magnification). Thioflavin S fluorescent plaques are shown at 100X total magnification.

4.4 Discussion

The aim of this study was to (1) assess the glucose metabolism patterns in GSS subjects with the F198S mutation, and (2) determine the feasibility of using [^{11}C]PiB PET to detect APrP deposits in individuals at risk for developing GSS, who are carriers of the *PRNP* P102L or F198S mutations. To our knowledge, this is the largest study to investigate [^{18}F]FDG uptake in GSS subjects with the F198S mutation and the largest PET study investigating [^{11}C]PiB in individuals at risk for GSS, and the first to evaluate [^{11}C]PiB in GSS subjects with the F198S mutation. Furthermore, this is the first study evaluating individuals at risk for a hereditary prion disease longitudinally using [^{11}C]PiB PET.

[^{18}F]FDG PET Findings

We observed hypometabolism in the left caudate head and bilaterally in the putamen and cerebellum in SCs relative to both the NC and AC groups. However, atrophy in the putamen largely overlapped with the metabolic pattern in SCs relative to NCs. Hypermetabolism was observed in AC group relative to the NC group in the left caudate head, putamen, claustrum, and superior temporal gyrus. Additionally, *PRNP*-129VV participants showed reduced [^{18}F]FDG uptake relative to *PRNP*-129MV carriers. Reduced metabolism in the caudate and putamen was also associated with poorer motor function. Abnormal glucose metabolism in these regions may underlie the cognitive and motor dysfunction observed in individuals with the F198S mutation and supports previous reports suggesting that *PRNP*-129VV participants have an earlier disease onset.

Increased glucose uptake in the left caudate head and putamen in the ACs relative to NCs may be suggestive of an increased metabolic demand or a

compensatory mechanism due to degeneration of neurons, which occurs early in the disease process. Considering that the hypermetabolism precedes symptom onset and is observed in the same regions that show hypometabolism in SCs suggests that we may be capable of detecting functional brain changes early in the disease course. Hypermetabolism has also been observed in healthy, cognitively normal individuals in regions known to later have high amyloid-beta deposition [206, 207]. Future studies to determine if this hypermetabolism is dependent on APrP or tau deposition in GSS F198S carriers are warranted.

The reduced glucose metabolism observed in the dorsal striatal and cerebellar regions in SCs relative to ACs and NCs was associated with impaired motor function. Further, the glucose hypometabolism is observed in anatomical regions with previously described to have significant deposition of PrP-amyloid and/or tau in subjects with the F198S mutation [191]. These findings are also supported by other PET studies investigating other GSS mutations and familial prion diseases [194-197, 208]. Striatal hypometabolism in SCs has also been observed in other tauopathies associated with Parkinsonism, including progressive supranuclear palsy (PSP) and corticobasal degeneration (CBD) [209]. Neuroimaging studies in familial tauopathies are uncommon considering the rarity of these diseases, but one familial PSP study found bilateral striatal hypometabolism in SCs relative to controls [210]. Thus, our findings are similar to those found in other tauopathies, including those with parkinsonism. However, in this study, a significant associated between GM atrophy and hypometabolism in the putamen was observed suggesting that the metabolic activity observed in this region may be partially due to neuronal loss in the SC group.

Although the sample size was too small to conduct a statistical analysis, glucose metabolism was lower in *PRNP*-129VV SCs in striatal and cerebellar regions, further supporting the notion that these subjects have a more aggressive disease presentation.

PRNP-129VV AC F198S carriers showed higher metabolism in the caudate and putamen, suggesting that this hypermetabolism may be antecedent to symptom onset as the *PRNP*-VV AC individuals are likely to be closer to the earlier age of onset seen in these individuals. However, this trend was not observed in the cerebellum, a region devoid of tau deposition in F198S mutation carriers [211]. One hypothesis may be that the hypermetabolism observed in caudate and putamen may be mediated by tau pathology, as tau and hypermetabolism are both observed in the striatum but not in the cerebellum.

A small number of F198S mutation carriers had follow-up scans. The rate of glucose uptake remained relatively stable over time which is similar to the AC F198S participant reported in Kepe et al. (2010) [196] Moreover, these findings are in agreeance with *post-mortem* findings in which moderate atrophy is observed in the cortex and moderate-to-severe atrophy is observed in the cerebellum [211]. These findings suggest that changes in glucose utilization and atrophy may be the primary drivers of dysfunction in this family.

[^{11}C]PiB PET Findings

[^{11}C]PiB PET imaging is highly informative for the *in vivo* early detection of deposits of fibrillar Aβ and possibly for the differential diagnosis of Alzheimer's disease versus other dementias. Our results show that there was no appreciable [^{11}C]PiB retention in one symptomatic and four asymptomatic mutation carriers [212]. Considering the fact that the asymptomatic mutation carriers were close to the age of disease onset of their parents, it is conceivable that APrP might have been already present in some of the AC individuals and particularly in the *PRNP* F198 symptomatic case.

The findings in our sample are consistent with other reports that also show no [^{11}C]PiB retention in participants with a *PRNP* mutation. Most of these studies investigated [^{11}C]PiB PET in a single subject, with one study reporting a slightly larger sample size [201]. Our data extend these preliminary findings in a larger cohort of participants. However, other studies have suggested that alternative amyloid tracers, including [^{18}F]FDDNP and [^{11}C]BF-227, show some sensitivity for GSS APrP, opening up the possibility that the various amyloid radioligands have unique binding properties with respect to amyloid type [196, 204].

The apparent lack of [^{11}C]PiB retention was not likely due to an absence of APrP in the *PRNP* mutation carriers studied. No [^{11}C]PiB retention was observed in the symptomatic individual, who had significant APrP deposition in cortical and cerebellar regions, as shown in the neuropathologic specimen obtained 46 months after the PET study. The impairment in neuropsychological and motor performance of this patient at the time of the PET scan also suggested a significant dysfunction of cortical, cerebellar, and striatal function likely due to APrP deposition. Further, in cases carrying the F198S mutation APrP deposition begins prior to significant clinical symptoms (BG unpublished observations), suggesting that the older F198S AC in this study may also have had APrP deposits that were not detected by [^{11}C]PiB PET. In addition, in some cases Aβ is observed around the APrP plaques [213, 214]. However, we were unable to detect this *in vivo* using [^{11}C]PiB PET despite its known sensitivity for Aβ. MRI data of the SC obtained at the time of the [^{11}C]PiB PET imaging (data not shown), revealed atrophy of the cerebellar cortex, a finding supporting the view that extensive PrP amyloid deposits were already present 46 months before death. Given the lack of appreciable specific signal in the symptomatic GSS patient, we suggest that [^{11}C]PiB may not bind to APrP nor is there enough Aβ deposition to be detected by [^{11}C]PiB PET. The apparent lack of ability of [^{11}C]PiB to detect APrP plaques in GSS could be due to several factors,

including altered tracer distribution and metabolism in this sample. However, the most likely possibility is that the APrP plaques possess a different conformational structure from the Aβ plaques, which may not be conducive to [^{11}C]PiB binding despite their sensitivity to thioflavin on neuropathologic assessment.

Study Limitations

The limitation presented in these studies included small sample size. This precluded statistical analysis for the effect of the *PRNP*-129M/V status on glucose metabolism and the sample of symptomatic carriers who are known to have extensive neuropathological APrP deposits. Future studies using a larger sample of affected individuals would be desirable, as these participants would have significant amounts of the APrP deposits and would allow us to better investigate the effect of *PRNP*-129M/V status. Additionally, due to the small sample size, we were unable to run separate analyses for the MRI study so both 1.5T with 3T scans were combined into one group. We also did not use a standard partial volume correction method to account for possible atrophy. In addition, evaluation of other amyloid tracers alone, or in combination with [^{11}C]PiB may potentially provide valuable insight into the timing and distribution of APrP deposition in this population, as well as the relative sensitivity of different amyloid tracers for detection of the various forms of amyloid. Finally, PET studies with recently developed tau radiotracers in individuals affected by GSS associated with the *PRNP* F198S, which are known to have neurofibrillary tangles, in combination with amyloid tracers - could be useful for the *in vivo* analysis of pathophysiological processes underlying disease symptoms and for tracking of disease progression.

Summary

Multi-modal neuroimaging can offer insight into brain structure and function underlying the phenotypes of disease. We identified striatal and cerebellar hypometabolism in symptomatic GSS F198S subjects, with the striatal regions also showing hypermetabolism in asymptomatic carriers of the F198S mutation. Homozygosity for valine at *PRNP*-129 was associated with lower metabolism in the SC group but higher metabolism in the AC group. These findings suggest that dysfunctional metabolism in the striatum and cerebellum may underlie the cognitive and motor dysfunction seen in GSS participants with the *PRNP* F198S mutation. Overall these findings suggest that glucose metabolism measured using [^{18}F]FDG PET is a potential tool for early prognostication of future clinical decline in individuals with the GSS F198S mutation. Additionally, we found no evidence for significant [^{11}C]PiB retention in participants carrying the *PRNP* P102L or F198S mutations, regardless of diagnostic status. Our findings agree with previous reports and suggest that [^{11}C]PiB may be clinically useful for ruling out AD in people at risk for GSS, but would provide no utility for detecting APrP pathology in these patients.

Chapter 5: Neuroimaging Correlates of Peripheral Markers of Neuronal Injury

5.1 Introduction

Understanding the underlying pathological processes of Alzheimer's disease (AD) and developing reliable biomarkers are critical to identify the causes and pathogenesis of AD. Both *in vivo* and *post-mortem* studies have shown that pathological tau is correlated with neurodegeneration, disease severity, and cognitive impairment [87]. Likewise, *in vivo* central measures of tau in cerebrospinal fluid (CSF) also correlate with *post-mortem* tau pathology and are increased in AD patients relative to those in a prodromal stage of AD referred to as mild cognitive impairment (MCI) and cognitively normal controls (CN), aiding prediction of disease progression [215, 216]. However, CSF collection is regarded as invasive, leading researchers to search for alternative methods to monitor MCI and AD such as blood biomarkers.

A recent meta-analysis reported plasma tau as the only blood-based biomarker to delineate AD from controls [217]. Fortunately, a new ultrasensitive technique, the single molecule array (Simoa) platform, was developed capable of detecting tau at low concentrations in plasma [127]. Similar to CSF, plasma tau concentrations were found to be significantly higher in AD relative to MCI and CN. Although not significantly different, plasma tau was also higher in MCI compared to CN [128, 218, 219]. However, a large overlap was observed between the MCI and CN groups suggesting plasma tau may not be suitable as a diagnostic marker. Further, the correlation between plasma tau and CSF tau and hippocampal volume was weak or non-existent [128, 218, 219]. Mattsson et al. (2016) did show evidence that plasma tau was associated with a greater longitudinal decline in hippocampal volume and Dage et al. (2016) showed that high levels of plasma tau were associated with lower cortical thickness in AD-specific brain regions [128, 218]. These results suggest plasma tau may be correlated with atrophy of AD-specific regions as the disease progresses.

Neurofilament light chain (NFL) is a scaffolding protein of myelinated axons. Similar to CSF and plasma levels of tau, a microtubule-associated protein that is a main pathological hallmark of Alzheimer's disease (AD), CSF and plasma levels of NFL have been shown to increase after neural injury in several neurodegenerative disorders such as AD, Progressive Supranuclear Palsy, and Frontotemporal Dementia [18, 43, 130, 220]. Very recently, Mattsson et al. (2017) released the first large study investigating plasma NFL in AD [129]. Plasma NFL was significantly increased in AD and in β-amyloid positive mild cognitive impairment (MCI) subjects. Additionally, plasma NFL level was correlated with the level of CSF NFL, suggesting it may be a good peripheral marker of central NFL levels. Plasma NFL was also associated with a decline in hippocampal volume and cortical thickness in AD-specific brain regions over time. This group had also reported similar findings with plasma tau; however, no correlation was observed between plasma and CSF levels of tau [128]. When directly compared, plasma NFL also performed better then plasma tau at discriminating AD from controls. However, plasma NFL concentrations largely overlapped across diagnostic groups and is also increased in other neurodegenerative disorders. Thus, they suggested that plasma NFL, like plasma tau, cannot alone be used as a diagnostic marker. Even so, the findings reported by Mattsson et al. suggest that NFL may be another target protein for peripheral measurement of neural injury and may show be more robust than tau.

The goal of this study was to look at two markers of axonal degeneration, tau and NFL, in association with neurodegeneration by MRI. We also aimed to determine if plasma and CSF concentrations of tau and NFL were related to atrophy in similar brain regions. We hypothesize that plasma tau and NFL will be inversely correlated with grey matter density (GMD), a measure of grey matter atrophy as seen in the previous reports of plasma tau, plasma NFL, and measures of atrophy [221]. Secondly, we hypothesize

that plasma total-tau (t-tau) and CSF t-tau, and plasma NFL and CSF NFL will be related to similar regions of atrophy.

5.2 Materials and Methods

Alzheimer's Disease Neuroimaging Initiative (ADNI)

Data used in the preparation of this article were obtained from the Alzheimer's Disease Neuroimaging Initiative (ADNI) database (adni.loni.usc.edu). The ADNI was launched in 2003 as a public-private partnership, led by Principal Investigator Michael W. Weiner, MD. The primary goal of ADNI has been to test whether serial magnetic resonance imaging (MRI), positron emission tomography (PET), other biological markers, and clinical and neuropsychological assessment can be combined to measure the progression of mild cognitive impairment (MCI) and Alzheimer's disease (AD). Written informed consent was obtained from all participants according to the Declaration of Helsinki.

Plasma Tau Collection and Quality Control

Peripheral plasma tau concentrations were measured for 581 non-Hispanic Caucasian participants using the Single Molecule array (Simoa) technique with the Human Total Tau assay (Human Total Tau 2.0 kit, Quanterix Corp, Boston, MA, USA). This assay and the plasma tau characteristics for ADNI have been previously described [127, 128]. In brief, the assay uses two monoclonal antibodies which bind to the N-terminus and mid-region of tau, and measures both normal and phosphorylated tau protein. Values are given as pg/mL. A total of 38 samples had plasma concentration below the Limit of Detection (LOD) or below the Lower Limit of Quantification (LLOQ) and were removed from further analysis. An additional four samples had missing values. To reduce the possible effect of extreme outliers on statistical analysis, the mean and

standard deviation (SD) of plasma tau were calculated; participants with a value more than three SDs above or below the mean value were regarded as outliers and removed from further analysis. This resulted in the removal of eight participants. Only participants with a MRI scan were included, leaving 508 participants for the plasma tau study (166 CN, 174 MCI, 168 AD).

Plasma NFL Collection and Quality Control

Plasma NFL concentrations were measured for 560 non-Hispanic Caucasian participants using an NFL assay (UmanDiagnostics) and transferred to the Simoa platform using a home brew kit (Simoa Homebrew Assay Development Kit; Quanterix Corp., Boston, MA, USA) as previously described [129, 222]. No samples were below the limit of detection and all samples were within the limit of quantification. All subjects with valid plasma NFL samples were used in order to extend the findings reported in Mattson et al. (2017) [18].

CSF Collection and Quality Control

CSF analytes ($A\beta_{1-42}$, t-tau and p-tau_{181p}) were measured using the multiplex xMAP Luminex platform (Luminex Corp, Austin, TX) with Innogenetics (INNO-BIA AlzBio3; Ghent, Belgium; for research use-only reagents) immunoassay kit-based reagents. To reduce the possible effect of outliers on statistical analysis, the mean and standard deviation of CSF analytes were calculated and participants with at least one analyte value more than three SD below or above the mean value of each of CSF variable were regarded outliers and removed from the analysis. This resulted in 341 valid CSF samples. For the MRI-CSF study, only participants with a CSF value for both t-tau and p-tau were included in the CSF study leaving 331 participants available (91

CN, 158 MCI, 82 AD). Participants were classified as amyloid positive (Aβ+) if CSF $A\beta_{1-42}$ <192pg/mL.

CSF NFL was measured using an ELISA (NF-light ELISA kit, UmanDiagnostics AB, Umea, Sweden) as previously described [220, 223]. We removed eight Aβ-negative (Aβ-) participants with AD from analysis. In total, 367 participants had CSF NFL samples available for analysis (104 CN, 180 MCI, 83 AD).

MRI Scan Processing

All participants had baseline 1.5T magnetization-prepared rapid gradient-echo (MPRAGE) images downloaded from the ADNI LONI site (http://adni.loni.usc.edu/). Scan processing with voxel-based morphometry (VBM) in Statistical Parametric Mapping 8 (SPM8; Wellcome Trust Centre for Neuroimaging, http://www.fil.ion.ucl.ac.uk/spm/software/spm8/) and quality control were done as previously described [177]. Briefly, scans were co-registered to a T1-weighted template and segmented into different tissue classes (GM; white matter, WM; CSF). GM maps were normalized to MNI (Montreal Neurologic Institute) space without modulation as 1 x 1 x 1 mm voxels and smoothed with an 8 mm Gaussian kernel to create GM density (GMD) images for further analysis. GMD is the average concentration of grey matter around the voxel thus, a reduction of GMD serves as a proxy of atrophy [221].

Image Analysis

Voxel-wise linear regression models in SPM8 were used to evaluate the relationship between central (CSF) and peripheral (plasma) measures of tau and NFL with GMD. Age, sex, education, *APOE* status (ε4 carrier or ε4 non-carrier), and total intracranial volume were included as covariates in the regression models. Analyses were done with and without diagnosis as an additional covariate. An explicit GM mask was

applied to the MRI scans to restrict the search area for the statistical analysis. Significant results were displayed at a voxel-wise $p < 0.05$ (family-wise error (FWE) correction for multiple comparisons) and with a minimum cluster size (k) of 100 voxels. If no brain regions survived correction for multiple comparisons, then a slightly less stringent voxel-wise p-value of 0.001 (uncorrected for multiple comparisons) was used. To determine if there were any overlapping brain regions significantly correlated to plasma and CSF analytes of tau or NFL, a composite image was created in SPM8. Anatomical regions were defined by using the x-y-z coordinates for the most significant voxel within each cluster. These coordinates were entered into the Talairach daemon (http://www.talairach.org/daemon.html) to receive the anatomical names for the GM regions closest to that coordinate [4].

Statistical Analysis

SPSS V24.0 was used for all statistical analyses. CSF t-tau, p-tau, NFL, and plasma NFL values were log transformed in order to achieve normal distribution. Plasma tau values were normally distributed and thus absolute values were used for analysis; results were unchanged when transformed plasma values were used. The association of sex, *APOE* ε4 status, and Aβ positivity with diagnostic group was assessed using a Pearson chi-squared test. ANOVA was used to assess the relationship of age, education, Mini-Mental State Exam (MMSE), Clinical Dementia Rating Scale – Sum of Boxes (CDR-SB), plasma tau, and CSF analytes with diagnostic status. Post-hoc pairwise differences among diagnostic groups were assessed using a Bonferroni correction for multiple comparisons. The MarsBaR toolbox in SPM8 was used to extract mean GMD from significant clusters from the voxel-wise results for further characterization of the results [224].

Regional Analysis

In order to determine whether replication of the Dage et al. (2016) plasma tau findings was observed, we analyzed the ADNI data using a similar method as was described in the manuscript [218]. Briefly, MRI scans from all participants were processed using Freesurfer version 5.1 to extract mean cortical thickness from the bilateral entorhinal cortex, inferior temporal gyri, middle temporal gyri, and fusiform [225, 226]. These cortical thickness estimates were averaged to create an AD signature cortical thickness measure, as in Dage et al. (2016) [218]. Abnormal cortical thickness was defined as a mean thickness below the 90th percentile of the AD participants as previously described [218, 227], resulting in an abnormal cortical thickness cut-off of <2.77 mm. As in Dage et al. (2016), we sought to investigate the association between plasma tau and the probability of having abnormal cortical thickness, as defined above, in MCI and CN participants (n=339), as well as in the full sample. A logistic regression was used to estimate this association both unadjusted (model 1) and adjusted for age, sex, education, and *APOE* ε4 status (model 2), as was done by Dage et al (2016) [218].

5.3 Results

Demographic and Clinical Characteristics

There was a near equal number of participants in each diagnostic group for both the plasma tau and NFL studies (Table 6). Significant differences among diagnostic groups were observed for all demographic and clinical characteristics examined except for age. As expected, for both the plasma NFL and tau study, the AD group had the highest percentage of *APOE* ε4 carriers, followed by the MCI group. Significant differences in the mean MMSE and CDR-SB among the diagnostic groups, with the AD group showing the most impairment and the MCI group showing intermediate impairment between AD and CN ($p < 0.001$ for both the plasma tau and plasma NFL

study). Plasma tau, plasma NFL, CSF t-tau, CSF p-tau and CSF NFL were significantly different between groups, with the AD group showing significantly higher concentrations compared to MCI and CN. The number of Aβ+ participants was also significantly different among diagnostic groups ($p < 0.001$).

Similar to previous reports, the mean plasma tau concentrations in the MCI and CN groups were nearly equal. There was no significant difference in demographic and clinical characteristics for the 35 ADNI participants whose samples were excluded compared to those included in the present study (Table 7). However, as expected the plasma tau was significantly different between the included/excluded groups since the excluded plasma tau samples all had a value <1. Plasma tau levels between diagnostic groups for the excluded samples was not statistically different ($p=0.202$).

Plasma Tau Association with Cortical Thickness

A recent report by Dage et al. (2016) found that high levels of plasma tau were associated with lower cortical thickness in the entorhinal, inferior temporal, middle temporal, and fusiform of MCI and controls [218]. However, we did not find a significant association of plasma tau levels with abnormal cortical thickness in either the unadjusted or adjusted models (Table 8).

Table 6. Demographic and clinical characteristics for the plasma tau and NFL studies.

	Plasma Tau Study				Plasma NFL Study			
	CN	**MCI**	**AD**	**p-value**	**CN**	**MCI**	**AD**	**p-value**
N	166	174	168	-	184	188	175	
Age (years)	75.2 (5.1)	74.1 (7.6)	75.3 (7.3)	0.789	75.3 (4.9)	74.1 (7.5)	74.7 (7.3)	0.26
Sex (M, F)	95, 71	115, 59	87, 81	*0.025*	104, 80	124, 64	89, 86	0.013
Education (years)	16.1 (2.7)	15.8 (3)	14.8 (3.1)	<0.001	16 (2.7)	15.8 (3)	14.7 (3.1)	<0.001
% *APOE* ε4+	27.1%	54%	67.9%	<0.001	27.2%	53.2%	68.6%	<0.001
MMSE	29.1 (1)	26.9 (1.8)	23.2 (2)	<0.001	29.1 (1)	26.9 (1.8)	23.2 (2)	<0.001
CDR-SB	0 (0.1)	1.6 (0.9)	4.3 (1.6)	<0.001	0 (0.1)	1.6 (0.9)	4.3 (1.6)	<0.001
% Amyloid+*	35.2%	73.9%	93.8%	<0.001	34.8%	74.1%	100%	<0.001
CSF t-tau pg/mL**	65.7 (24.7)	97.6 (48.6)	121.2 (52.4)	<0.001	-	-	-	-
CSF p-tau pg/mL**	22.3 (10.5)	34.3 (16.2)	41.5 (18.5)	<0.001	-	-	-	-
Plasma tau pg/mL	2.7 (1)	2.8 (1.2)	3.1 (1.3)	0.002	-	-	-	-
Plasma NFL pg/mL	**-**	-	-	-	35 (21.8)	42.2 (28.6)	51.1 (27)	<0.001
CSF NFL pg/mL***	**-**	-	-	-	1090.4 (425.8)	1489.6 (884.6)	1694.5 (843.1)	<0.001

CN = cognitively normal; MCI = mild cognitive impairment; AD = Alzheimer's disease; M = male; F = female; *APOE* = apolipoprotein; MMSE = mini-mental state exam; CDR-SB = clinical dementia rating-sum of boxes; CSF = cerebrospinal fluid. Mean (standard deviation). *n = 91 CN, 157 MCI, 81 AD for plasma tau study; n = 92 CN, 162 MCI, 80 AD for plasma NFL study. **n = 91 CN, 158 MCI, 82 AD. ***n = 104 CN, 180 MCI, 83 AD.

Table 7. Demographic and clinical characteristics for the 35 excluded ADNI samples from the plasma tau study.

	CN_Exc	CN_Inc	p-value	MCI_Exc	MCI_Inc	p-value	AD_Exc	AD_Inc	p-value
N	14	166	-	11	174	-	10	168	-
Age (years)	75.9 (2.5)	75.2 (5.1)	0.65	75.4 (6.4)	74.1 (7.6)	0.6	70.7 (5.8)	75.3 (7.3)	0.06
Sex (M, F)	6, 8	95, 71	0.23	7, 4	115, 59	0.87	4, 6	87, 81	0.47
APOE ε4 (% ε4 positive)	28.6%	27%	0.91	27%	54%	0.09	60%	68%	0.61
MMSE	29.1 (.9)	29.1 (1)	0.89	26.9 (2.4)	26.9 (1.8)	0.99	23.6 (1.5)	23.2 (2)	0.59
CDR-SB	0.07 (0.2)	0 (0.1)	0.3	1.4 (0.8)	1.6 (0.9)	0.51	4.4 (1.2)	4.3 (1.6)	0.9
Plasma tau pg/mL	0.5 (0.2)	2.7 (1)	*<0.001*	0.5 (0.3)	2.8 (1.2)	*<0.002*	0.7 (0.2)	3.1 (1.3)	*<0.001*
CSF t-tau pg/mL*	77.5 (43.2)	65.7 (24.7)	0.19	91.5 (37.1)	97.6 (48.6)	0.64	94.9 (66.7)	121.2 (52.4)	0.19
CSF p-tau pg/mL*	28.1 (17.9)	22.3 (10.5)	0.24	28.6 (12.6)	34.3 (16.2)	0.23	33.5 (21.3)	41.5 (18.5)	0.26
Amyloid (-/+)**	6, 5	59, 32	0.58	4, 7	41, 116	0.43	1, 5	5, 76	0.29

CN = cognitively normal; MCI = mild cognitive impairment; AD = Alzheimer's disease; Exc = excluded from current study; Inc = Included in current study; M = male; F = female; *APOE* = apolipoprotein; MMSE = mini-mental state exam; CDR-SB = clinical dementia rating-sum of boxes; CSF = cerebrospinal fluid. Amyloid + if CSF Aβ ≤ 192 pg/mL. Mean (standard deviation). Significant p-values < 0.05 are italicized. *CN_Exc = 11; CN_Inc = 91; MCI_Exc = 11; MCI_Inc = 158; AD_Exc = 6; AD_Inc = 8. **Missing 1 MCI_Inc and 1 AD_Inc.

Table 8. Association of plasma tau levels with cortical thickness in AD-specific brain regions.

	abnormal cortical thickness (<2.77)	Model 1			Model 2		
		N	**OR (95% CI)**	**p-value**	**N**	**OR (95% CI)**	**p-value**
CN+MCI	**Continuous**	339	0.95 (0.78 - 1.16)	0.62	339	0.94 (0.77 – 1.15)	0.55
	Quartiles						
	1	339	reference		339	reference	
	2		0.79 (0.44 - 1.42)	0.43		0.72 (0.39 – 1.32)	0.29
	3		0.89 (0.5 - 1.6)	0.69		0.86 (0.47 - 1.57)	0.61
	4		0.93 (0.51 - 1.73)	0.83		0.88 (0.47 - 1.67)	0.7
CN+MCI+AD	**Continuous**	507	1.12 (0.96 - 1.31)	0.16		1.1 (0.93 - 1.3)	0.27
	Quartiles						
	1	507	reference		507	reference	
	2		1 (0.61 - 1.66)	0.98		0.87 (0.52 - 1.47)	0.61
	3		0.96 (0.58 - 1.59)	0.88		0.85 (0.5 - 1.43)	0.53
	4		1.49 (0.89 – 2.5)	0.13		1.36 (0.79- 2.32)	0.27

CN = cognitively normal; MCI = mild cognitive impairment; AD = Alzheimer's disease; OR = odds ratio; CI = confidence interval. Model 1 is unadjusted. Model 2 is adjusted for age, sex, education, and *APOE* ε4 status. The cortical thickness measure is an average of the entorhinal, fusiform, inferior temporal, and middle temporal regions of interest.

Voxel-based MRI Analysis

Across all participants, a significant association between higher plasma tau and lower GMD in several brain regions was observed, including in the middle, inferior, and superior temporal gyrus, parahippocampus, hippocampus, fusiform, uncus, precuneus, thalamus, caudate, putamen, and middle and inferior frontal gyrus (Figure 15A-D, voxel-wise $p<0.001$ (uncorrected), $k=100$ voxels). As would be expected, AD participants had lower mean GMD in the larger clusters identified (parahippocampus and striatum; Figure16A). When controlling for diagnosis, a significant association between plasma tau and GMD was still observed in the right thalamus and bilaterally in the striatum (Figure 15C-D). No voxels, either with or without diagnosis as a covariate, survived correction for type I error rate. No significant clusters were observed in the positive/unexpected direction (*data not shown*).

High plasma NFL was associated with low GMD in the frontal, temporal, insular, and occipital cortices (Figure 17, voxel-wise $p<0.05$ (FWE corrected), $k=100$ voxels). When diagnosis was added a covariate, the association of high plasma NFL with low GMD was more localized to the medial temporal lobe (MTL), including in the hippocampus and parahippocampus, as well as in the superior frontal gyrus and insula (Figure 17B). When the hippocampal cluster was extracted, AD subjects showed significantly lower GMD compared to both Aβ+ and Aβ- MCI and CN subjects (Figure 17C). Aβ+ MCI subjects also had significantly lower GMD in this region relative to Aβ+ and Aβ- CN participants (Figure 17C). Similar results were observed with the parahippocampus, superior frontal gyrus, and insula (*data not shown*). No significant clusters were observed in the opposite direction (high plasma NFL associated with higher GMD).

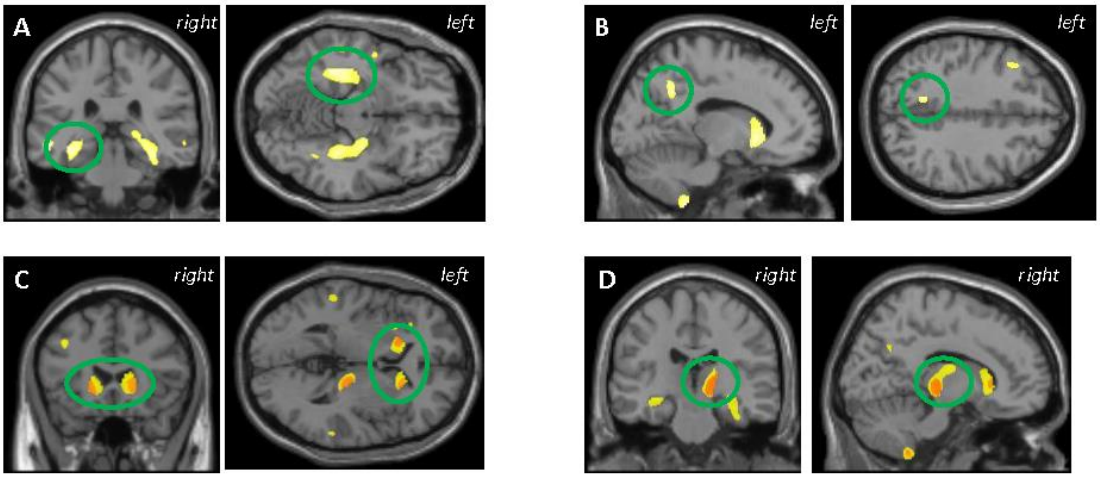

Figure 15. VBM analysis of MRI and plasma tau in all participants.

High plasma tau is correlated with low grey matter (GM) density in the (A) parahippocampus, (B) precuneus, (C) striatum, and (D) thalamus. C and D represent the anatomic overlap (orange) of regions of GM atrophy associated with increased plasma tau using only age, sex, *APOE* ε4 status, and total intracranial volume as covariates (yellow) and with the addition of diagnosis as a covariate (red). Results are displayed at $p<0.001$ (uncorrected) and at a threshold (k) of 100 voxels.

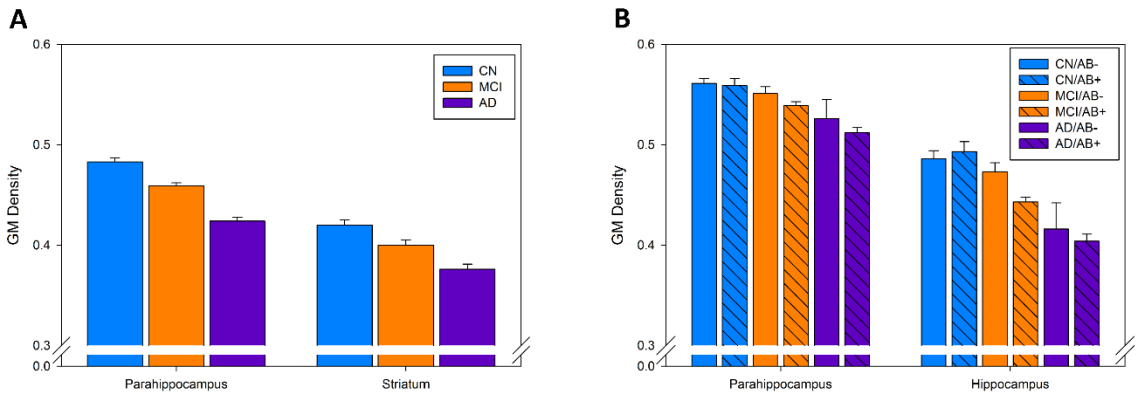

Figure 16. Mean grey matter density in all participants of the plasma tau study.

Selected regions significant in the voxel-wise analysis across (A) diagnostic and (B) amyloid status. Covariates included in both models include age, sex, *APOE* ε4 status, and total intracranial volume. Bars are mean ± standard error. CN = cognitively normal; MCI = mild cognitive impairment; AD = Alzheimer's disease; AB- = amyloid-beta negative; AB+ = amyloid-beta positive.

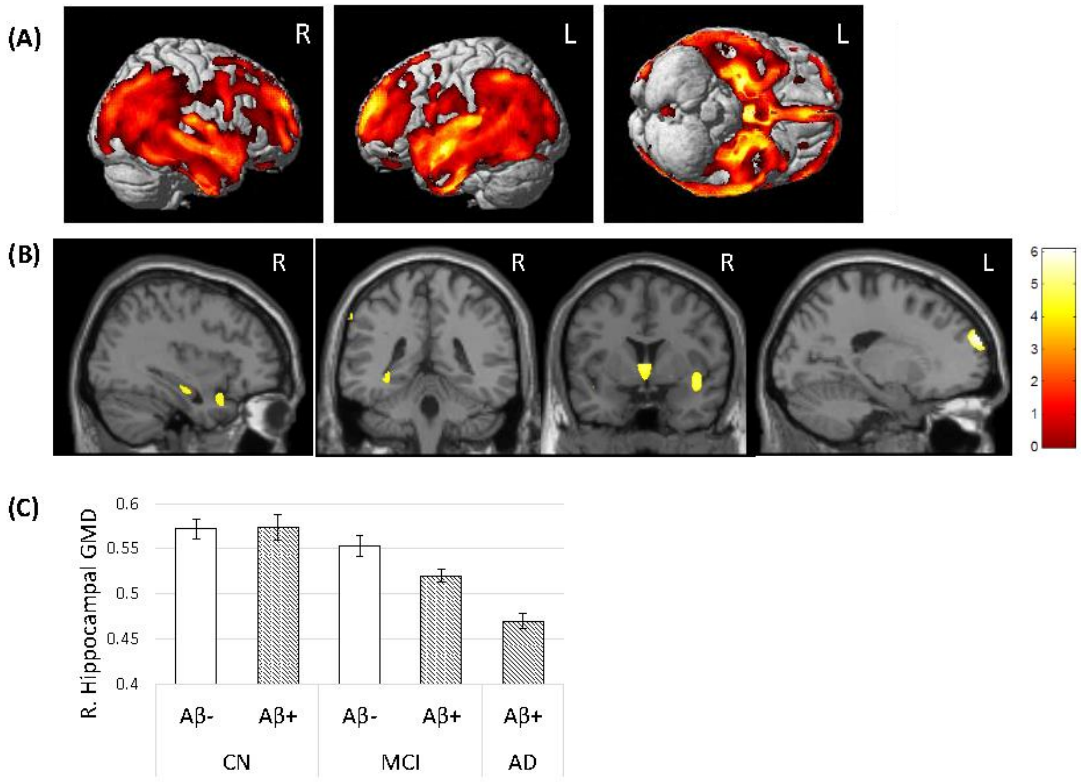

Figure 17. VBM analysis of MRI and plasma NFL in all participants.

(A) High plasma NFL was associated with low GMD largely in the frontal, temporal, insular, and occipital cortices, covaried for age, sex, education, *APOE* ε4 carrier status, and total intracranial volume (ICV). (B) When diagnosis was also included as a covariate, high plasma NFL was associated with low GMD in more focal regions, including hippocampus, parahippocampus, insula, and superior frontal gyrus. (C) GMD in the right hippocampal cluster in (B) was significantly different between groups based on diagnosis and Aβ status (positive/negative; striped bars indicate Aβ-positive), with AD patients and Aβ-positive MCI showing the lowest GMD in this region. Results in (A) and (B) are displayed at $p<0.05$ (FWE corrected) and a minimum cluster size (k) of 100 voxels. No significant clusters were observed in the opposite direction (high plasma NFL associated with more GMD).

Amyloid-positive Participants

There was no significant association between plasma tau and GMD in the Aβ- participants, however higher plasma tau was significantly correlated with lower GMD in the Aβ+ participants in the fusiform, hippocampus, parahippocampus, precuneus, and premotor cortex (Figure 18A-D, voxel-wise $p<0.001$ (uncorrected), $k=100$ voxels), as well as the frontal and parietal lobes, pre- and post-central gyri, and the globus pallidus. Notably, in the MTL cluster for MCI and AD, Aβ+ participants showed lower mean GMD compared to Aβ- participants (Figure 16B). After diagnosis was added as a covariate, many of the same regions of low GMD remained significantly correlated with higher plasma tau including in the precuneus, parahippocampus, and premotor cortex (Figure 18B-D). No voxels, either with or without diagnosis as a covariate, survived correction for type I error rate. No significant clusters were observed in the positive/unexpected direction (*data not shown*).

Similar to plasma tau, no significant association between plasma NFL and GMD was observed in Aβ- participants only. In Aβ+ participants, higher plasma NFL levels was associated with reduced GMD in the angular gyrus, supramarginal gyrus, dorsolateral prefrontal cortex, anterior prefrontal cortex, pre- and postcentral gyrus, middle temporal cortex, caudate, hippocampus, and parahippocampus (Figure 19A, voxel-wise $p<0.05$ (FWE corrected), $k=100$ voxels). When controlling for diagnosis, lower GMD in the right superior frontal gyrus and left precentral gyrus were associated with high plasma NFL (Figure 19B). Results were unchanged when *APOE* ε4 status was excluded as a covariate (*data not shown*). No significant clusters were observed in the opposite direction.

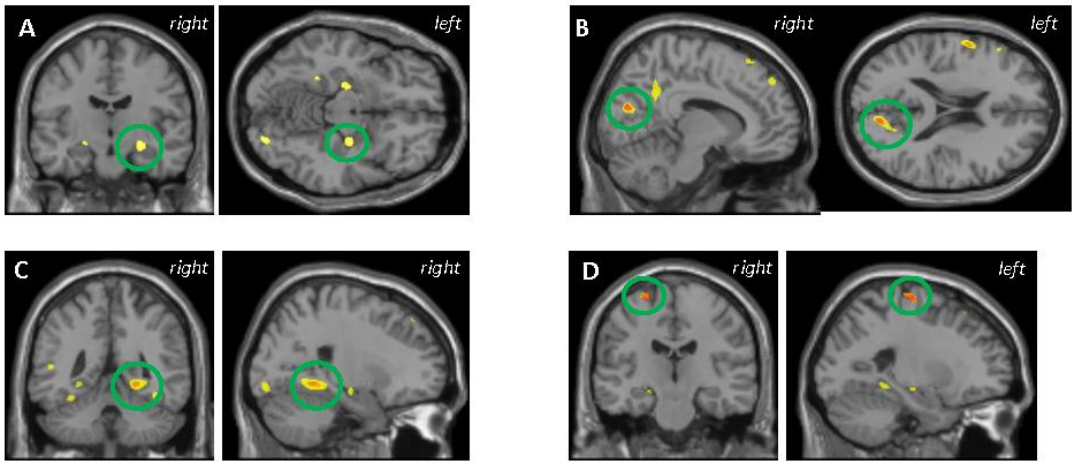

Figure 18. VBM analysis of MRI and plasma tau in amyloid positive participants.

High plasma tau is correlated with low grey matter (GM) density in the (A) hippocampus, (B) precuneus, (C) parahippocampus, and (D) BA 6 premotor cortex. B-D also represent the anatomic overlap (orange) of regions of GM atrophy associated with increased plasma tau using only age, sex, *APOE* ε4 status, and total intracranial volume as covariates (yellow) and with the addition of diagnosis as a covariate (red). Results are displayed at $p<0.001$ (uncorrected) and at a threshold (k) of 100 voxels.

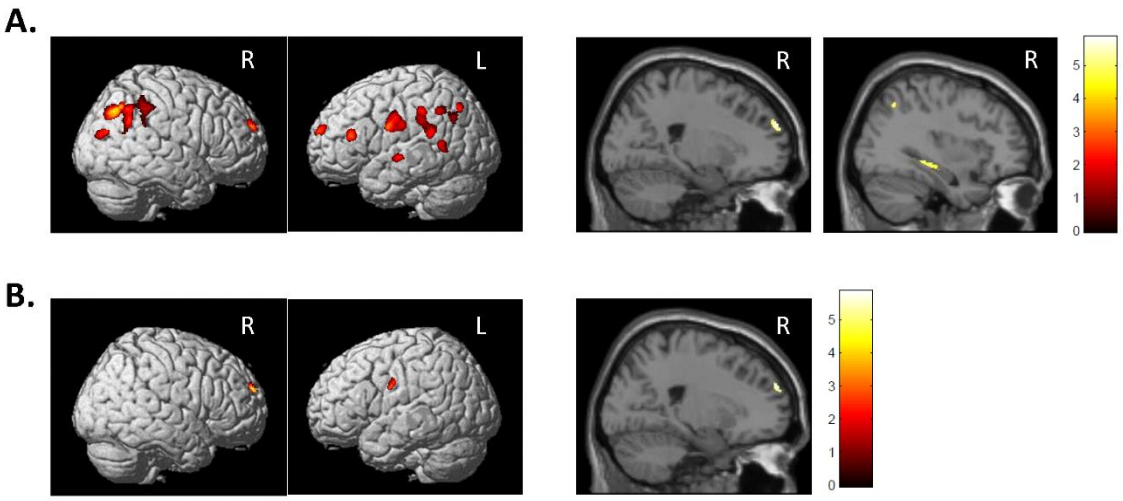

Figure 19. VBM analysis of MRI and plasma NFL in amyloid positive participants.

(A) In Aβ-positive participants only, high plasma NFL was associated with low GMD in the temporal and parietal cortices, superior frontal gyrus, and hippocampus, covaried for age, sex, education, *APOE* ε4 carrier status, and total intracranial volume (ICV). (B) When diagnosis was included as an additional covariate, high plasma NFL was associated with low GMD in the right superior frontal gyrus and the left precentral gyrus. Results are displayed at $p<0.05$ (FWE corrected) and minimum cluster size (k) of 100 voxels. No significant clusters were observed in the opposite direction (high plasma NFL associated with more GMD).

CSF-Plasma Tau Comparison

Central (CSF) and peripheral (plasma) tau were significantly associated, although were not highly correlated in this subsample of participants ($r = 0.232$, $p<0.001$). Peripheral measures of tau protein were of total-tau only, thus, we sought to compare the regional atrophy associated with plasma tau to that associated with CSF t-tau only. At $p < 0.05$ (FWE corrected), higher CSF t-tau was associated with lower GMD in the precuneus, temporal gyrus, and fusiform gyrus in all participants (Figure 20). However, the uncorrected results were used for comparison with the plasma tau results, as this threshold was used in the plasma tau analyses described above. Central and peripheral measures of tau protein were associated with GMD in some overlapping, but largely different brain regions. Across all participants, the temporal pole, fusiform, and angular gyrus were brain regions in which both higher CSF t-tau and plasma tau were associated with lower GMD (Figure 21). As several reports have previously shown, higher CSF t-tau was associated with lower GMD in cortical structures known to be affected in persons with AD. However, as above, in the present study plasma tau was predominantly associated with subcortical structures. Within the Aβ+ participants, no significant overlap was observed between the association of GMD with plasma tau and the association of GMD with CSF t-tau (*data not shown*).

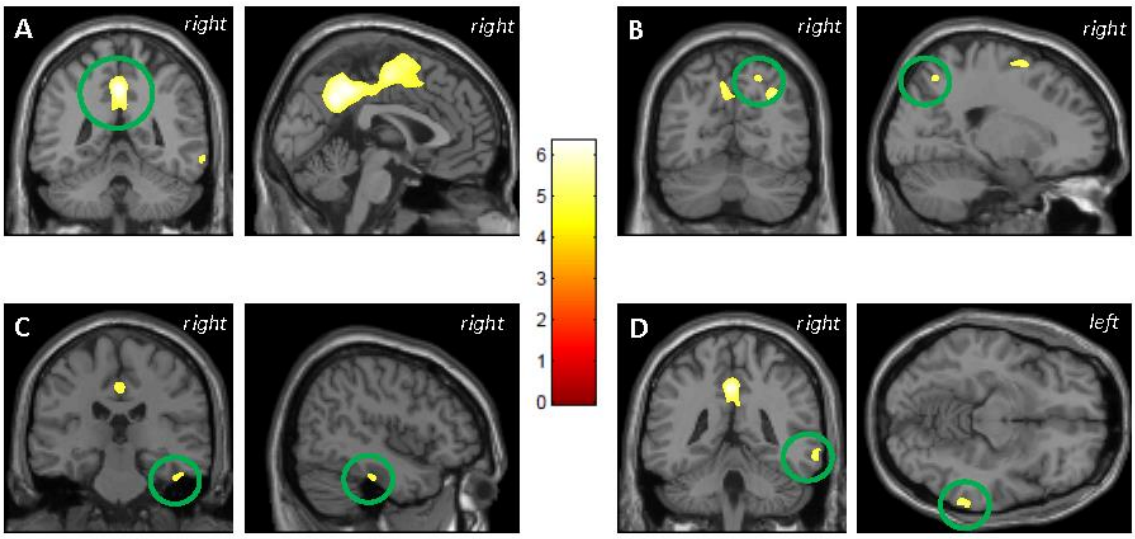

Figure 20. VBM analysis of MRI and CSF total-tau in all participants.

High CSF total-tau is correlated with low grey matter density in the (A-B) precuneus, (C) fusiform, and (D) BA21. Covariates included in the regression analysis were age, sex, *APOE* ε4 status, and total intracranial volume. Results are displayed at $p<0.05$ (FWE corrected) and at a threshold (k) of 100 voxels.

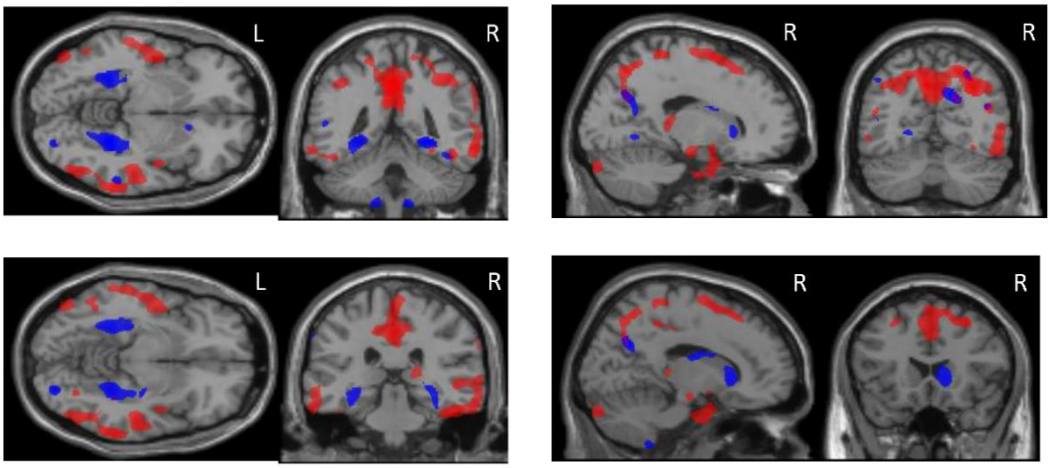

Figure 21. Anatomical overlap of grey matter density with plasma tau and CSF total-tau.

Low grey matter density was associated with high plasma tau (blue) and high CSF t-tau (red) in some overlapping region (purple). Covariates included were age, sex, *APOE* ε4 status, total intracranial volume. Results are displayed at $p<0.001$ (uncorrected) and at a threshold (k) of 100 voxels.

CSF-Plasma NFL Comparison

Similar to the findings in Mattson et al., central (CSF) and peripheral (plasma) concentrations of NFL were highly correlated in this subsample of participants ($r = 0.62$, $p<0.001$). Across all participants, significant overlap was observed in the anatomical location of the associations between high levels of CSF NFL and low GMD and between high levels of plasma NFL and low GMD. Specifically, the overlap in association was largely observed in MTL regions (Figure 22A). When diagnosis was added as a covariate, overlap was only observed in the superior temporal cortex (BA22, Figure 22B). In only the Aβ+ participants, a small amount of overlap was observed in the anterior temporal cortex (*data not shown*). When diagnosis was added as a covariate, no overlap was observed between the association of GMD with plasma NFL and the association of GMD with CSF NFL (*data not shown*).

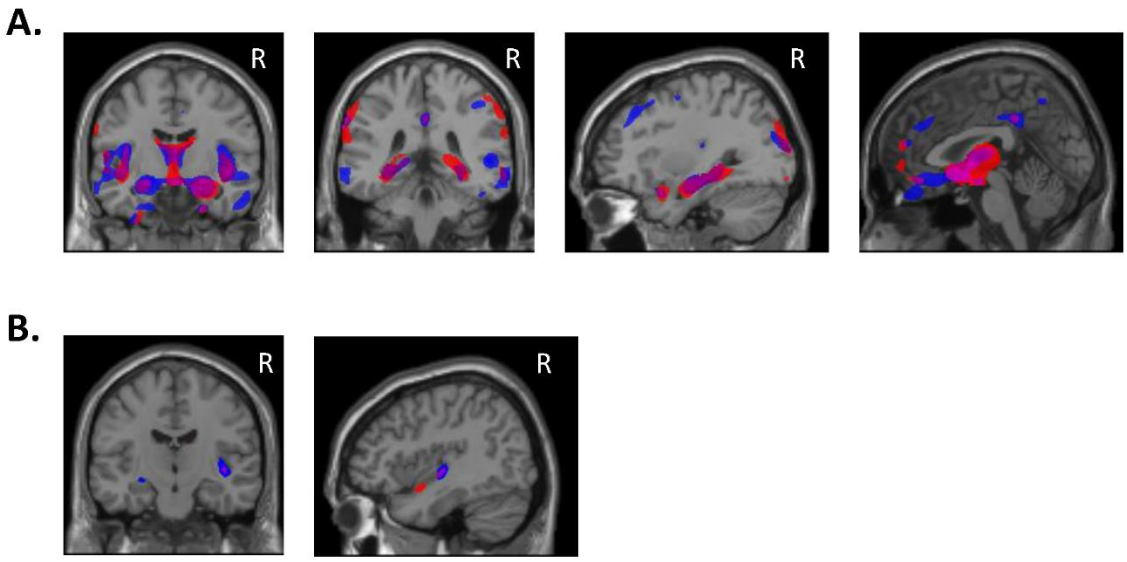

Figure 22. Anatomical overlap of grey matter density with plasma NFL and CSF NFL in all participants.

Low grey matter density was associated with high plasma NFL (red) and high CSF NFL (blue) in largely overlapping regions (purple). Covariates included were age, sex, *APOE* ε4, total intracranial volume. Analyses were run (A) with diagnosis, and (B) without diagnosis as an additional covariate. Results are displayed at $p < 0.05$ (FWE-corrected) and at a threshold (k) of 100 voxels.

5.4 Discussion

Plasma tau and NFL in AD quantified using the Simoa technique has only recently been investigated. The findings from these studies have been similar, with plasma tau and NFL significantly higher in AD compared to MCI and controls, but no significant difference between MCI and controls [128, 129, 218, 219]. However, there was high overlap in plasma tau and plasma NFL levels between these diagnostic groups which suggested they will not be a suitable biomarker for AD. Mattsson et al. (2016 and 2017) also showed that higher plasma tau and NFL were associated with worsening cognition, atrophy, and hypometabolism over time suggesting evaluation of plasma tau may provide insight into brain changes over time [128, 129]. The main goal of this study was to determine how two markers of axonal neurodegeneration, tau and NFL, associated with neurodegeneration on a voxel-wise basis. Additionally, we investigated how peripheral and central measures of tau and NFL correlated with GMD. Both plasma tau and NFL were associated with cortical atrophy in a population at risk for AD or already manifesting signs of clinical AD.

Plasma Tau Findings

We found high levels of plasma tau was correlated with low GMD in several AD-specific brain regions, including the MTL and precuneus, as well as in the thalamus and striatum. Further investigation into only Aβ+ participants also revealed an association between higher plasma tau concentrations and lower GMD in MTL structures, the precuneus, and the premotor cortex. In Aβ- participants, no significant association between plasma tau and GMD was observed for any analysis. These findings suggest that plasma tau may reflect neurodegeneration in both AD-specific regions and more generally. Additionally, we failed to replicate the correlation of atrophy as measured by cortical thickness described by Dage et al. (2016) [218].

The MTL is one of the first brain regions that shows tau pathology and the earliest to degenerate in AD patients [86]. Thus, our observation that high plasma tau is associated with cortical atrophy in several MTL structures including the parahippocampus and hippocampus across all participants and in Aβ+ participants suggests that this peripheral measure of tau may be reflective of CSF and brain tau pathology as well as brain atrophy. Although a different method was used to investigate the brain integrity, our findings are similar to but not replicative of that of Dage et al. (2016) who showed higher plasma tau was associated with lower cortical thickness in the entorhinal, inferior temporal, middle temporal, and fusiform [218]. The mean plasma tau levels for MCI and CN were nearly equivalent in this study which could account for our failure to replicate. We also observed a correlation between higher plasma tau and lower GMD in the precuneus. A functional decline in the precuneus occurs early in the course of AD. Specifically, the precuneus along with the hippocampus are both core components of the default mode network, an important functional resting-state network that is impaired early in AD [228]. Thus, the atrophy in the precuneus associated with plasma tau could be reflective of structural deterioration in the default mode network early in AD.

Even more striking was the inverse association of plasma tau with GMD in the thalamus and the striatum across all participants, especially given that these areas are affected later in the disease course. These were the only brain regions that were also independent of diagnosis, suggesting that plasma tau may reflect neurodegeneration unrelated to AD diagnosis, possibly due to normal aging. Studies evaluating plasma tau in other tauopathies may shed light on this hypothesis. Additionally, cholinergic neurons project to thalamic nuclei and high levels of acetylcholine are found in the striatum [229, 230]. Tau protein may play a role in that loss of cholinergic neurons through a mechanism involving the interaction of extracellular tau with M1/M3 muscarinic receptors

present in the cholinergic neurons [231, 232]. This interaction between tau and muscarinic receptors may be a way, although not the only one, to explain the spreading of tau pathology occurring in AD. This interaction was mediated by soluble tau suggesting its association in the healthy brain, binding leads to an increase in calcium and thus cell death. Alternatively, in the Aβ+ participants, the association of plasma tau and GMD in the parahippocampus and precuneus was independent of diagnosis. These findings suggest that plasma tau may be reflecting neurodegeneration specific to AD pathology.

Our initial hypothesis was that plasma tau and CSF t-tau would be related to similar regions of atrophy, especially if the two tau measures were truly reflective of AD neurodegeneration. Unexpectedly, plasma tau and CSF t-tau had very little overlap, with plasma tau mapping more to subcortical structures and CSF t-tau mapping more to cortical structures. Additionally, the CSF and plasma tau concentrations were not highly correlated, although significantly associated, suggesting the significance may be driven by the large sample size. Only small regions of overlap were observed in the temporal pole, fusiform, and angular gyrus. These results suggest that CSF and plasma measures of tau protein may reflect related but somewhat different pathological substrates of AD. This could be due to differences in the assays, tau isoforms detected by the assays, or in the variability of the measurements. There may also be differences in how tau, released from neurons, is cleared from brain interstitial fluid to CSF and plasma. Additionally, peripheral tau may be influenced by systemic tau since tau is expressed in regions outside of the brain, for example in the breast, skeletal muscle, testis, and colon. Further work is needed to further elucidate the differences between plasma and CSF tau.

We have shown that plasma tau may be a non-specific marker for neurodegeneration. However, plasma tau may still be relevant to AD since we observed

associations of higher plasma tau with AD-specific brain atrophy in Aβ+ participants but not in Aβ- participants. Future replication and longitudinal studies will be important to fully elucidate the contribution of plasma tau as a possible biomarker in AD and other tauopathies.

Plasma NFL Findings

. High concentrations of plasma NFL were associated with low GMD in MTL regions and the insula, independent of diagnosis and after correction for multiple comparisons. No significant association between plasma NFL and GMD was observed in Aβ- participants; however, Aβ+ participants showed an association between high plasma NFL concentrations and low GMD in the hippocampus, although these findings were not independent of diagnosis. Plasma and CSF NFL concentrations also showed overlapping associations with GMD in the MTL. Our findings support plasma NFL as a peripheral biomarker associated with brain neurodegeneration.

NFL is encoded by the neurofilament light chain polypeptide (*NEFL*) gene. NFL co-assembles with neurofilament medium (NFM) and neurofilament heavy (NFH) chain proteins to form intermediate filaments that run the length of the axon. Mutations in the NFL, NFM, and NFH genes have been found in Charcot-Marie-Tooth disease, Parkinson's disease, and Amyotrophic Lateral Sclerosis, respectively [233-235]. While NFL is mainly expressed in large-caliber myelinated axons, it has been found in neurites of the CNS and other tissues such as endocrine, kidney, muscle, testis, and spleen [236]. Knockout NFL mice develop normally, similar to tau knockout mice, but a 20-fold reduction in NFM and NFH were reported along with a decrease in the number of myelinated axons [237]. Additionally, transgenic mice expressing APP/PS1 (AD mouse model) mutations with the NFL knockout showed increased Aβ deposition, dystrophic neurites, microgliosis, and synapse vulnerability [238]. These studies suggest that NFL

is important for neural integrity and potentially how abnormal functioning might lead to disease.

Post-mortem immunohistochemical analysis has shown increased NFL in the hippocampus of AD patients relative to controls [239]. Our voxel-wise analysis of plasma NFL with GMD support these findings, as well as the findings by Mattsson et al. (2017) [129]. Mattsson et al. (2017) reported high plasma NFL was associated with a decline in hippocampal volume over time. Although our analysis was cross-sectional, our voxel-wise analysis showed high plasma NFL was associated with reduced hippocampal GMD. This association may represent a pattern of normal aging considering these findings are independent of diagnosis. While studies investigating plasma NFL in older, cognitively healthy adults have yet to be reported, a study showed CSF NFL predicted higher hippocampal atrophy in cognitively normal, older adults [240]. Since plasma and CSF NFL are highly correlated, it is likely that this association would also be observed with plasma. However, no association of plasma NFL in the CN group was observed in our study (*data not shown*). Instead, hippocampal GMD was lowest in AD, followed by MCI Aβ+ participants suggesting that plasma NFL may reflect disease-associated neurodegeneration.

An inverse correlation between high plasma NFL and low GMD in the hippocampus in Aβ+ subjects was also observed, although this association was not independent of diagnostic status. Our results also indicate that *APOE* ε4 status did not have a significant effect on atrophy in this group. Those who are Aβ+ are at higher risk for AD further supporting that plasma NFL may be capable of detecting neural injury in a disease-specific group. Plasma NFL was not significantly associated with neurodegeneration in the Aβ- subjects, even when a less-stringent, uncorrected p-value was used (*data not shown*). These findings support the notion that neuronal injury is not

associated with plasma levels in early stages, perhaps because it is not extensive in the preclinical stage [241].

Plasma and CSF levels of NFL are highly correlated and associated with AD, Parkinson disease, progressive supranuclear palsy, and degeneration mediated by HIV-infection, suggesting plasma NFL may be a suitable non-invasive biomarker for neural injury [126, 129, 130, 242]. Our initial hypothesis was that plasma NFL and CSF NFL would be related to similar regions of atrophy, especially since the two measures of NFL were highly correlated. As expected, high central and peripheral concentrations of NFL were associated with low GMD in largely overlapping brain regions, particularly in the MTL. These results suggest that CSF and plasma measures of NFL protein may be reflecting related pathological substrates of axonal degeneration. As discussed earlier in this section, NFL is expressed in the peripheral nervous system and non-neural tissues [236]. The concentration of NFL in plasma and CSF were highly correlated in this cohort and were associated with neurodegeneration in largely overlapping regions, suggesting that these two markers of NFL are likely reflecting injury specific to the central nervous system.

Mattsson et al. (2017) also reported plasma tau was a weaker biomarker for axonal degeneration compared to plasma NFL [129]. Recently, our group reported the association of plasma tau with neurodegeneration on MRI [243]. We observed an observation between higher plasma tau and low GMD in predominantly subcortical structures of the brain. This anatomical distribution was strikingly different from comparison of CSF tau and GM, which mapped mainly to cortical structures (Supplemental Figure). While we did not directly compare the plasma NFL with plasma tau in the current study, we did a visual comparison of the two markers and their association with GMD. While both plasma NFL and tau were inversely correlated with GMD, several differences were noted. First, the association between plasma NFL and

GMD survived correction for Type I error (FWE correction for multiple comparison) while the plasma tau analysis did not. The robust association of plasma NFL with GMD suggests that it may be a better peripheral marker for neurodegeneration than plasma tau. Furthermore, the concentration of plasma and CSF NFL are highly correlated and, plasma and CSF NFL were associated with atrophy in overlapping brain regions, while the plasma and CSF tau showed vastly different associations with GMD. These findings further suggests that plasma NFL may be a more suitable peripheral marker for brain neurodegeneration, as it likely measures a similar pathological substrate as CSF NFL.

Study Limitations

One study limitation is the lack of a commensurate replicate data set. This tau and NFL quantification method is relatively new and hopefully independent data sets will become available. Additionally, accumulated p-tau is the main hallmark in AD and other tauopathies but there is not yet a technique for measuring p-tau in plasma, thus yielding a second limitation to this study. New techniques to assess p-tau in plasma could be extremely beneficial. A third limitation is that our data is cross-sectional only. Longitudinal plasma tau and NFL data would provide us the information needed to better assess changes in plasma tau over time and the association between changing plasma tau measures and rate of neurodegeneration. Next, we excluded participants with plasma tau values below the lower limit of quantification, although the results were not significantly different when these participants were included (*data not shown*). Lastly, the plasma NFL study had more participants relative to the plasma tau study, thus we did not do a direct analytical comparison but a visual comparison of the two markers and their association with neurodegeneration.

Summary

In conclusion, high concentrations of plasma tau and plasma NFL were associated with lower GMD. However, plasma NFL had a more robust association with neurodegeneration and may by a better peripheral marker for neural injury. Taking into account these findings and those described by Mattsson et al. (2016, 2017), we believe plasma tau and plasma NFL may be useful as a screening tool for detecting early AD-related neurodegeneration, rather than as a diagnostic tool per say [128, 129].

Chapter 6: The Tau Biological Network

6.1 Introduction

With the marked heterogeneity observed in sporadic tauopathies, no single candidate gene or protein is likely the ultimate cause of disease. Developing new approaches to determine the genetic contribution to complex diseases have been a major area of study. GWAS, polygenic risk score, gene expression analysis, and whole-exome or whole-genome sequencing are some of the tools currently used to better understand genetics and disease [244-246]. However, current approaches often fail to take into account the interaction between different molecules and genes; thus, another analytical approach is needed. One approach to overcome these issues involves investigating the physical and functional interactions of molecules and evaluating the effect of these interactions on risk for complex diseases, such as Alzheimer's disease (AD). Genes, their protein products, and the interactions they have with other molecules is called a "biological network" [247, 248]. The interactions in the biological network can be protein-protein, gene-gene, gene-protein, protein-DNA, or protein-RNA. The aberrant function of one or more molecules in the biological network could potentially lead to abnormal function of a molecule up- or downstream of that signal.

Biological networks can be curated using different methodologies, both *a posteriori* and *a priori*. For example, information for networks can be obtained *a posteriori* from assays such as yeast two-hybrid, which is used to detect protein-protein interactions, or microarray gene expression data used to detect functional relationships between gene transcripts [249, 250]. Additionally, statistical and computational methods can be utilized to predict or infer gene networks from existing data [251]. Another way to construct a biological network is to use *a priori* knowledge from network databases or reported associations in the literature to build a network of interest [252].

Several networks are currently defined such as co-expression, gene regulatory, signaling, or metabolic networks. Our goal was to develop a special network, one focused on the biology of the tau protein, the major pathogenic protein in tauopathies. Tau can undergo several modifications through interactions with a complex network of proteins ("the tau biological network"). As discussed in Chapter 1, although we do not know the exact cause of cause tau aggregation, dysfunction related to these modifications are likely to cause conformational changes, hyperphosphorylation and other post-translational modifications, and aggregation, ultimately culminating in tau pathology. One example of a functional interaction of molecules in the tau biological network is seen between O-GlcNAc and phosphorylation. O-GlcNAc glycosylation of tau occurs when O-GlcNAc is attached to phosphorylation sites on tau, competing with phosphate groups. Indeed, an inverse correlation has been observed between O-GlcNAc glycosylation and phosphorylation, with O-GlcNAc glycosylation reduced in AD *post-mortem* brain samples [253]. Increased O-GlcNAc could potentially inhibit tau hyperphosphorylation and reduce tau aggregation. However, the reason for the reduction in O-GlcNAc glycosylation in AD is unknown. Investigation of genetic variation surrounding the gene that codes for O-GlcNAc and its interacting partners may provide clues as to the underlying causes of the reduction observed in AD brain.

Genetic variations that alter coding and expression of proteins within the tau biological network may have a significant impact on the pathological processing of tau and thus, are an important and under-explored area of study. Further investigation into the tau biological network may provide insights into molecular mechanisms and pathways that may contribute to AD and other tauopathies. Thus, our goal is to develop a tau biological network from proteins and genes involved in the various processes governing tau processing and function as described in Chapter 1.

6.2 Curating the Tau Biological Network

We took an *a priori* approach to curate the tau biological network. First, genes and proteins associated with the search term "*MAPT*" or "tau protein" were collected from the following databases: GeneMania, BioGrid, IMP Princeton, STRING, and Gene Ontology [254-258]. Next, we did a PubMed search using the search terms "*MAPT*", "tau", and "neurofibrillary tangles" in combination with one or more category/subcategory listed in Table 9. Identified genes include those with physical and/or functional interactions with *MAPT* or the tau protein, in addition to genes identified by GWAS, candidate gene, or association studies. Genes associated with *MAPT* or tau were organized by category and subcategory, along with one or more literature reference(s) supporting the association. An example of this organizational scheme is shown in Table 10. Some genes belonged to more than one category, resulting in inclusion of multiple listed categories (Table 10).

Table 9. Search terms for curating the tau biological network.

Category	Subcategory
DNA/RNA and protein processing	translation
	alternative splicing
	gene expression
	post-translational modifications
	other
trafficking/sorting	axonal transport
	golgi appartus
	endoplasmic reticulum
	secretion
	clathrin
	endocytosis
	endosome
	other
clearance and degradation	proteasome
	autophagy
	blood-brain barrier
	CSF absorption
	ISF bulk flow
	microglia
	other
mediator of tau toxicity	mitochondria
	Aβ toxicity
	calcium influx
	other
cellular functions	vesicle trafficking
	neuronal polarity
	microtubule stability
	other

Table 10. A brief example of the tau biological network results.

Gene	Gene Name	Chr	category	subcategory	2nd category	PubMed ID	GWAS
BIN1	bridging integrator 1	2	Trafficking/sorting	clathrin	mediator of tau toxicity	23399914	Y
PICALM	phosphatidylinositol binding clathrin assembly protein	11	Trafficking/sorting	clathrin		25241929	Y
DRP1	dynamin-related protein 1	12	Mediator of tau toxicity	mitochondria		28173111	
PIN1	NIMA-interacting 1	19	Mediator of tau toxicity	other		10391244	
GSK3B	glycogen synthase kinase 3 beta	3	Processing	PTM		14690523	
OGT	O-GlcNAc transferase	X	Processing	PTM		27126545	
TREM2	triggering receptor expression on myeloid cells 2	6	Clearance/degradation	microglia		26364736	
TRIM46	tripartite motif-containing 46	1	Cellular function	neuronal polarity		26671463	

Gene = gene symbol; Chr = chromosome number; GWAS = genome wide association study; PTM = post-translational modification; Y = yes.

6.3 Utilization of the Tau Network

A biological network centered on tau, or any disease-associated protein, has a plethora of research potential. One of the major benefits of a tau biological network is to improve our understanding of the role of genetics in modulating abnormal tau processing and aggregation, especially in sporadic tauopathies. As discussed in Chapter 1, we still have much to learn regarding the physiological and pathophysiological functions of tau. Further investigation into genetic and protein interactions that produce an increase in pathological tau could aid in predicting disease risk. Further, a better understanding of the underpinnings regarding physiological tau could provide insight into alternative pathways or signaling cascades that may be altered in disease.

Additionally, genetic variation within the tau network could be evaluated for association with disease phenotypes such as cognition or neuroimaging or fluid biomarkers. The genetic variation-phenotype association can be investigated using the entire network, similar to a set-based analysis, or using an epistatic association analysis. Results from these analyses may help explain the genotype-phenotype connection in complex diseases, such as AD, since it is likely that that multiple genes with small effect sizes contribute to overall disease risk, perhaps even in a synergistic way. Furthermore, having access to a tau network could aid in the identification of new molecular pathways associated with disease. Ultimately, fully investigating and understanding the tau biological pathway could lead to a more reliable biomarker for diagnosis, identification of potential novel drug targets for a better treatment, and could help explain to similarities and differences between tauopathies.

Another possible outcome from research utilizing a tau network is identification of disease-related subnetworks. Analyzing proteins that interact with tau to enhance phosphorylation, for example, could identify a previously unknown molecule that effects tau phosphorylation state. Any identified molecule could have a direct impact or be from

a neighboring network indicative of a more complex pathway affecting tau phosphorylation. This type of analysis could also help with further classification of diseases involving tau. For example, a set of genetic interactions in the network may be associated with disease state or a specific disease phenotype in a subset of patients. This could help in development of a personalized treatment for AD and other tauopathies.

There are limitations in using a hand-curated network. First, lists that are hand-curated are rarely exhaustive. In addition, since the network is based on previously identified associations, some of the included/excluded molecules could come from assays that were false positives/negatives. Regardless, it is unlikely that any methodology used for building a network will be completely inclusive. However, the composition of a tau biological network provides a starting point for new investigation into the genetic contributions to various tauopathies.

Chapter 7: Summary and Future Directions

Tauopathies encompass a number of familial and sporadic neurodegenerative diseases associated with tau pathology. In this report, we used PET imaging to identify disease-specific metabolic patterns for two forms of familial tauopathy. Additionally, we investigated the association of plasma tau and NFL, two axonal degeneration markers, with neurodegeneration on MRI. Finally, we hand-curated a tau biological network to investigate the genetic contribution to tauopathies.

7.1 Glucose Metabolism in Alzheimer's Disease

Extensive work has been done investigating the metabolic pattern in AD and how [^{18}F]FDG uptake is associated with AD-associated phenotypes. Chapter 2 provides a brief overview of the current state of the knowledge regarding [^{18}F]FDG PET across the AD spectrum. In general, hypometabolism is observed in AD in the temporoparietal cortex, medial temporal lobe (MTL), posterior cingulate, and precuneus, with frontal involvement in more advanced AD. MCI subjects usually show hypometabolism in similar regions to AD, although to a lesser extent, suggesting that [^{18}F]FDG PET may be useful for the tracking the progression of disease. Indeed, several studies have shown reduced [^{18}F]FDG uptake in AD-specific regions in MCI converters relative to MCI non-converters. This AD-specific pattern of hypometabolism also helps differentiate AD from clinically similar neurodegenerative diseases. Hypometabolism observed in cognitively normal individuals is usually associated with advancing age. Changes in glucose utilization were also found to mirror the cognitive decline occurring during disease progression, which further supports the use of [^{18}F]FDG PET in the clinical diagnosis of AD and in research.

7.2 Glucose Metabolic Patterns in Multiple Systems Tauopathy with Presenile Dementia

Chapter 3 investigates glucose metabolism in participants with multiple systems tauopathy with presenile dementia (MSTD), a form of frontotemporal dementia with parkinsonism-17 with tau inclusions (FTDP-17T), caused by an (a) to (g) transition at position +3 of intron 10 of the microtubule associated protein tau (*MAPT*) gene. The mutation causes overexpression of 4 repeat (4R) tau isoforms with increased 4R/3R ratio leading to neurodegeneration. Clinically, these patients primarily present with behavioral variant frontotemporal dementia (bvFTD), showing disinhibition, disordered social comportment, and impaired executive function, memory, and speech. While altered glucose metabolism has been reported in subjects with sporadic bvFTD, it has yet to be investigated in an FTDP-17 sample of this size. In this study, eleven mutation carriers and eight non-carriers in the MSTD family were imaged using [^{18}F]FDG PET. Eight of the *MAPT* intron 10 +3 mutation carriers met diagnostic criteria for bvFTD (symptomatic carrier), while three *MAPT* intron 10 +3 carriers were not cognitively impaired (asymptomatic carrier) at the time of the [^{18}F]FDG PET scan. Images were assessed on a voxel-wise basis for the effect of mutation carrier status. Compared to non-carriers, *MAPT* intron 10 +3 mutation carriers showed lower [^{18}F]FDG uptake bilaterally in the MTL and parietal and frontal cortices. Anatomical changes measured from magnetic resonance imaging (MRI) were predominantly seen bilaterally in the MTL areas and substantially overlapped with the regions identified as hypometabolic. Further, these atrophic and metabolic changes overlap previously described patterns of neurodegeneration in MSTD patients and are consistent with the characteristics of their cognitive dysfunction. Furthermore, asymptomatic carriers showed hypometabolism and atrophy in the MTL suggesting these changes precede clinical onset. This is similar to that observed in MCI and AD as discussed in Chapter 2. However, these findings are in contrast to those observed with the GSS F198S mutation, which show hypermetabolism

in disease-specific regions in asymptomatic carriers, as described in section 4.3. Overall, these results suggest that neuroimaging can describe the neuropathology associated with this *MAPT* mutation.

Future Directions

One area of interest is further determining the different functional and structural changes in the asymptomatic carrier group relative to the symptomatic and non-carrier participants and track their progression over time. For the current study, only three asymptomatic carriers were available for analysis, precluding voxel-based analysis. Increasing the sample size and collecting longitudinal MRI and [^{18}F]FDG PET imaging in this family may help resolve this question and allow for a better investigation of the temporal relationships of structural and functional changes in MSTD. Furthermore, investigation of this family with tau PET is warranted to track the progression of tau pathology *in vivo* as discussed in section 1.4. This information could also be used to compare the difference in the progression of tau pathology during the disease course of different classes in tauopathies, including MSTD. Finally, it would also be interesting to determine if metabolic changes in the brain are associated with clinical presentations of disease, such as differences between those who present with cognitive or behavioral changes only versus those who also have motor abnormalities.

7.3 Amyloid and Glucose Metabolism in Gerstmann–Sträussler–Scheinker Disease

Chapter 4 assesses brain glucose metabolism and amyloid deposition in a prion protein disease. First, we investigated glucose metabolism in Gerstmann–Sträussler–Scheinker Disease (GSS) subjects with the F198S mutation. GSS F198S is a familial neurodegenerative disorder characterized clinically by ataxia, parkinsonism, and dementia, and neuropathologically by deposition of amyloid plaques composed of prion

protein (PrP) and neurofibrillary tangles composed of hyperphosphorylated tau protein. Twelve GSS F198S mutation carriers and ten non-carriers were imaged using [^{18}F]FDG PET. Images were then assessed on a voxel-wise basis for the effect of clinical diagnosis and mutation carrier status. At the time of the scan, eight GSS F198S mutation carriers were symptomatic (symptomatic carriers (SC)), showing signs of motor and cognitive impairment or dementia, and four GSS F198S mutation carriers were asymptomatic (asymptomatic carriers (AC)). SCs showed lower glucose metabolism in the left caudate head and bilaterally in the putamen compared to ACs and non-carriers (NCs), and bilaterally in the cerebellum compared to NCs. ACs showed hypermetabolism in the left caudate head and putamen compared to NCs suggestive of increase in energy demands or compensation for dying neurons. Considering the hypermetabolism occurs prior to clinical symptoms and in the same brain regions which later show hypometabolism suggests that we may be capable of detecting functional brain changes early in the disease course. However, this is different than what was observed in AD and the MSTD family. Considering both AD and GSS are secondary tauopathies with biochemically and structurally indistinguishable neurofibrillary tangles, with amyloid being the primary pathology, these increased glucose metabolism before clinical onset may indicate a more dynamic relationship between amyloid pathology, the brain region affected, and age. Overall, these findings suggest that hypometabolism in the cerebellar and striatal regions may partially underlie motor and cognitive dysfunction in GSS F198S patients. This may be preceded by hypermetabolism, which could serve as an early prognostic marker.

This chapter also evaluated if [^{11}C]Pittsburgh Compound B (PiB) PET is capable of detecting APrP in *PRNP* gene carriers. Six individuals at risk for GSS and eight controls underwent [^{11}C]PiB PET scans using standard methods. Approximately one year after the initial scan, each of the three asymptomatic carriers (two with *PRNP*

P102L mutation, one with *PRNP* F198S mutation) underwent a second [^{11}C]PiB PET scan. Three P102L carriers, one F198S carrier, and one non-carrier of the F198S mutation were cognitively normal, while one F198S carrier was cognitively impaired at the time of the study. No [^{11}C]PiB uptake was observed in any subject at baseline or at follow-up. Neuropathologic study of the symptomatic individual revealed PrP-immunopositive plaques and tau-immunopositive neurofibrillary tangles in cerebral cortex, subcortical nuclei, and brainstem. PrP deposits were also numerous in the cerebellar cortex. This finding suggests that [^{11}C]PiB PET is not suitable for *in vivo* assessment of APrP plaques in patients with GSS.

Future Directions

As described in section 1.4, radiotracers for pathological tau have been successfully used in tauopathies and cognitively normal adults. Considering tau tangles in GSS F198S are biochemically and structurally indistinguishable from those seen in AD, it would be interesting to observe tau deposition *in vivo* in this kindred. I would particularly be interested in observing the association of *in vivo* tau pathology with disease progression, cognitive status, and motor function. Additionally, investigating the structural and functional connectivity using diffusion tensor imaging and resting-state functional MRI could provide clues as to how aberrant connectivity is related to the GSS F198S mutation. It would also be interesting to determine if the hypermetabolism in the AC group was dependent on amyloid or tau deposition in the same regions. However, one challenge with these studies is recruiting an increased number of participants, as the number of living members of the family are limited. Another future direction would be to sequence the *MAPT* gene in the GSS F198S subjects to investigate the impact of *MAPT* genetic variation on neuroimaging phenotypes and determine if there are any

similarities of *MAPT* variation contributing to clinical outcome measurements in participants with GSS and other tauopathies.

7.4 Association of Tau and Neurofilament Light Chain with Grey Matter Density

Chapter 5 examines how two peripheral markers of axonal degeneration, plasma tau and neurofilament light (NFL), were correlated to grey matter density (GMD) on MRI on a voxel-by-voxel basis in healthy, cognitively normal elderly adults (CN) and participants with mild cognitive impairment (MCI) or Alzheimer's disease (AD). The association of plasma tau and plasma NFL with GMD were also compared with the association of central (cerebrospinal fluid, CSF) measures of tau and NFL with GMD. Baseline MRI scans, plasma and CSF tau, and plasma and CSF NFL were evaluated to determine their association with GMD. High levels of both plasma tau and NFL were associated with low GMD across all participants.

For plasma tau, high concentrations were negatively correlated with GMD in the medial temporal lobe (MTL), precuneus, thalamus, and striatum. The associations with thalamus and striatum were independent of diagnosis suggesting that plasma tau may reflect neurodegeneration unrelated to AD diagnosis, possibly due to normal aging. Furthermore, these findings suggest that the association between plasma tau and low GMD in the MTL and precuneus may be a diagnostic effect. Alternatively, in the Aβ+ participants, the association of plasma tau and GMD in the parahippocampus and precuneus was independent of diagnosis. Plasma tau may reflect AD-specific neurodegeneration in a specific population. The association of AD-specific brain regions in a population at high risk for AD (Aβ+ subjects) also supports the use of combining multiple biomarkers to identify higher risk patients for disease. When compared to CSF total-tau, plasma tau showed a notably different associated brain atrophy pattern, with only small overlapping regions in the fusiform gyrus. Plasma tau mapped predominantly

to subcortical regions, while CSF total-tau mapped mainly to cortical regions. These results demonstrate that central and peripheral measures of tau protein may reflect different pathologies. Additionally, peripheral tau may be influenced by systemic tau outside the brain, such as that in the liver or testis. Overall, plasma tau may serve as a non-specific marker for neurodegeneration but is still relevant to AD considering low GMD was associated with plasma tau in Aβ+ participants and not in Aβ- participants.

For plasma NFL, an inverse correlation was observed between plasma NFL and GMD. High plasma NFL was associated with widespread, lower GMD in the frontal, temporal, insular, and occipital cortices. When diagnosis was added a covariate, high plasma NFL was still correlated with lower GMD in the hippocampus, parahippocampus, insula, and superior frontal gyrus suggesting concentrations of plasma NFL may be sensitive to neurodegeneration in AD-specific regions. Across Aβ+ subjects, high plasma NFL was associated with low GMD in the hippocampus and superior frontal gyrus when diagnosis was not entered as a covariate. When diagnosis was added as a covariate, the signal remained in the superior frontal gyrus and inferior parietal lobe. However, no significant clusters were observed in the Aβ- subjects or in the CN group alone suggesting that the neurodegeneration associated with NFL levels may not be measurable in the preclinical stage of disease. Plasma and CSF NFL were highly correlated. When we compared the associations of plasma NFL and CSF NFL with neurodegeneration, the two markers almost completely overlapped in their association with GMD. Large overlap was mainly observed in the MTL and insula. These results support the quantitative analysis that central and peripheral concentrations of NFL protein are closely correlated and may be reflecting similar pathological substrates of disease. Overall, our findings support plasma NFL as a peripheral biomarker associated with neurodegenerative disease.

In general, plasma NFL appeared to be a more specific marker for neurodegeneration than plasma tau. First, since CSF is considered a more accurate reflection of the biochemical composition of the brain, a good peripheral biomarker would show high association between CSF and plasma measurements, especially if we expect peripheral protein markers to accurately reflect brain injury. Reports by Mattsson et al. (2016, 2017) and in our subset of subjects, CSF and plasma NFL were highly correlated while CSF and plasma tau were not [129]. This was corroborated by our voxel-wise findings on MRI in which plasma and CSF NFL were associated with neurodegeneration in overlapping regions. Alternatively, plasma and CSF tau showed markedly different patterns of association with structural integrity. Finally, the plasma and CSF NFL findings survived FWE correction for type I error and the plasma and CSF tau findings did not, suggesting that plasma NFL has a stronger association with atrophy than plasma tau. Ultimately, these findings suggest that central (CSF) and peripheral (plasma) measures of NFL are measuring the same species of NFL result from brain neurodegeneration, and thus, may be a good biomarker for disease. Future studies are needed to confirm this theory.

Future Directions

Considering that plasma and CSF tau were associated with different patterns of neurodegeneration, further work is needed to further elucidate the differences between these measures of tau. Future replication and longitudinal studies will be important to fully elucidate the contribution of plasma tau as a possible biomarker in AD and other tauopathies. It would also be interesting to determine if plasma tau and plasma NFL may be useful together to predict future cognitive decline and increased longitudinal atrophy, and if the two protein markers are similarly or differently associated with cerebral plaque and neurofibrillary tangle deposition. Additionally, future studies in which plasma tau and

plasma NFL could be used in combination with other biomarkers to predict conversion or in a staged approach would be of interest. Since the plasma tau and plasma NFL assays are a relatively non-invasive and inexpensive test that could potentially be done in primary care rather than specialist settings, this technique could serve as a first-line screening tool to detect changes in asymptomatic older individuals and select individuals for more expensive or invasive (e.g. imaging, CSF) tests to more specifically identify AD-based pathology. Another avenue to explore is the use of the tau biological network (described in Chapter 6 and section 7.5) to see if new biomarkers interact with any genes within the network and determine how these associations might be related to tau pathology.

7.5 Building a Tau Biological Network

In Chapter 6, the methodology and use of a hand-curated tau biological network from gene and protein databases and a literature search was described. Aggregation of the microtubule associated protein tau is a major component of neurodegenerative tauopathies. Reports of genetic associations between the tau gene (*MAPT*) and neurodegenerative disease are inconsistent, therefore more research is needed to clarify the contribution of *MAPT* to sporadic tauopathies. Tau can undergo several modifications through interactions with a complex network of proteins. Genetic variation in genes encoding proteins in the tau biological network are hypothesized to significantly influence: (1) the mechanism and rate of tau accumulation in disease and (2) alternative splicing of *MAPT*. Abnormal accumulation of tau may be modulated by other proteins that interact to enhance or suppress its normal function. Manual curation of a list of genes with *a priori* knowledge of their possible association with the production of pathological tau may provide insight into molecular mechanisms and pathways governing aberrant tau aggregation. Integrating and analyzing genes with a physical or

functional impact on tau could present new hypotheses to explore regarding the etiology of complex diseases or factors that may be influencing disease phenotype.

Thus far we have identified over 150 genes that are related to tau or *MAPT* processing, trafficking, sorting, clearance, degradation, mediator of toxicity, and cellular functions were identified. Overall, development and utilization of the tau biological network will improve our understanding of the role of genetics in modulating abnormal tau processing and aggregation in disease, facilitating early diagnosis, novel drug development, and personalized treatment.

Future Directions

The development of a tau biological network creates a number of opportunities for studying the genetic contribution of complex diseases. First, I would like to explore a gene-set analysis and investigate epistatic interactions using the tau network. Specifically, I would like to determine if genetic variation within the network is associated with deleterious or protective effect with disease-related phenotypes such as tau pathology. Second, I would like to pursue the creation of a tau polygenic risk score. Creating a score to summarize the genetic effects of markers associated with tau processing, function, and stability could provide a unique way to investigate the genetic contribution to tauopathies. Additionally, network information could be used to investigate the relationship of tau pathology with other factors in disease such as inflammation or neurodegeneration in non-neuronal cells in the brain (astrocytes, oligodendrocytes, microglia).

7.6 Conclusion

Herein, we discuss the role of neuroimaging, genetics, and biomarkers in better understanding the underlying brain changes in tauopathies. First, glucose metabolism is

reduced in tauopathies, with hypometabolic patterns in brain regions that underlie the cognitive and/or motor function of disease. Some differences in glucose utilization may even be observed before clinical onset. Second, plasma NFL may more accurately represent neurodegeneration in the brain relative to plasma tau, making it a potential non-invasive and inexpensive peripheral biomarker for disease. Lastly, curation of a tau biological network may identify proteins that play an important role in the pathogenesis of tau pathology and disease. Thus, using a combination of techniques to help model the emergence and progression of tau pathology and its physiology and behavior will help us to gain a better understanding of the importance of different patterns of tau pathology in a number of different tauopathies. Ultimately, these combinations may help us to develop more sensitive biomarkers for early detection, identify novel targets for effective drug development, and provide accurate and sensitive diagnosis and disease tracking including using personalized diagnostics and therapeutics.

References

1. Weingarten, M.D., et al., *A protein factor essential for microtubule assembly.* Proc Natl Acad Sci U S A, 1975. **72**(5): p. 1858-62.
2. Binder, L.I., A. Frankfurter, and L.I. Rebhun, *The distribution of tau in the mammalian central nervous system.* J Cell Biol, 1985. **101**(4): p. 1371-8.
3. Cleveland, D.W., S.Y. Hwo, and M.W. Kirschner, *Physical and chemical properties of purified tau factor and the role of tau in microtubule assembly.* J Mol Biol, 1977. **116**(2): p. 227-47.
4. Grundke-Iqbal, I., et al., *Abnormal phosphorylation of the microtubule-associated protein tau (tau) in Alzheimer cytoskeletal pathology.* Proc Natl Acad Sci U S A, 1986. **83**(13): p. 4913-7.
5. Kosik, K.S., C.L. Joachim, and D.J. Selkoe, *Microtubule-associated protein tau (tau) is a major antigenic component of paired helical filaments in Alzheimer disease.* Proc Natl Acad Sci U S A, 1986. **83**(11): p. 4044-8.
6. Wood, J.G., et al., *Neurofibrillary tangles of Alzheimer disease share antigenic determinants with the axonal microtubule-associated protein tau (tau).* Proc Natl Acad Sci U S A, 1986. **83**(11): p. 4040-3.
7. Kidd, M., *Paired helical filaments in electron microscopy of Alzheimer's disease.* Nature, 1963. **197**: p. 192-3.
8. Goedert, M., et al., *Cloning and sequencing of the cDNA encoding a core protein of the paired helical filament of Alzheimer disease: identification as the microtubule-associated protein tau.* Proc Natl Acad Sci U S A, 1988. **85**(11): p. 4051-5.
9. Spillantini, M.G., et al., *Mutation in the tau gene in familial multiple system tauopathy with presenile dementia.* Proc Natl Acad Sci U S A, 1998. **95**(13): p. 7737-41.

10. Hutton, M., et al., *Association of missense and 5'-splice-site mutations in tau with the inherited dementia FTDP-17.* Nature, 1998. **393**(6686): p. 702-5.
11. Heutink, P., et al., *Hereditary frontotemporal dementia is linked to chromosome 17q21-q22: a genetic and clinicopathological study of three Dutch families.* Ann Neurol, 1997. **41**(2): p. 150-9.
12. Wilhelmsen, K.C., et al., *Localization of disinhibition-dementia-parkinsonism-amyotrophy complex to 17q21-22.* Am J Hum Genet, 1994. **55**(6): p. 1159-65.
13. Foster, N.L., et al., *Frontotemporal dementia and parkinsonism linked to chromosome 17: a consensus conference. Conference Participants.* Ann Neurol, 1997. **41**(6): p. 706-15.
14. Spillantini, M.G., et al., *Familial multiple system tauopathy with presenile dementia: a disease with abundant neuronal and glial tau filaments.* Proc Natl Acad Sci U S A, 1997. **94**(8): p. 4113-8.
15. Andreadis, A., W.M. Brown, and K.S. Kosik, *Structure and novel exons of the human tau gene.* Biochemistry, 1992. **31**(43): p. 10626-33.
16. Goedert, M., et al., *Cloning and sequencing of the cDNA encoding an isoform of microtubule-associated protein tau containing four tandem repeats: differential expression of tau protein mRNAs in human brain.* EMBO J, 1989. **8**(2): p. 393-9.
17. Goedert, M., M.G. Spillantini, and R.A. Crowther, *Cloning of a big tau microtubule-associated protein characteristic of the peripheral nervous system.* Proc Natl Acad Sci U S A, 1992. **89**(5): p. 1983-7.
18. Couchie, D., et al., *Primary structure of high molecular weight tau present in the peripheral nervous system.* Proc Natl Acad Sci U S A, 1992. **89**(10): p. 4378-81.
19. Kouri, N., et al., *Novel mutation in MAPT exon 13 (p.N410H) causes corticobasal degeneration.* Acta Neuropathol, 2014. **127**(2): p. 271-82.

20. Poorkaj, P., et al., *An R5L tau mutation in a subject with a progressive supranuclear palsy phenotype.* Ann Neurol, 2002. **52**(4): p. 511-6.

21. Stefansson, H., et al., *A common inversion under selection in Europeans.* Nat Genet, 2005. **37**(2): p. 129-37.

22. Baker, M., et al., *Association of an extended haplotype in the tau gene with progressive supranuclear palsy.* Hum Mol Genet, 1999. **8**(4): p. 711-5.

23. Houlden, H., et al., *Corticobasal degeneration and progressive supranuclear palsy share a common tau haplotype.* Neurology, 2001. **56**(12): p. 1702-6.

24. Zabetian, C.P., et al., *Association analysis of MAPT H1 haplotype and subhaplotypes in Parkinson's disease.* Ann Neurol, 2007. **62**(2): p. 137-44.

25. von Bergen, M., et al., *Assembly of tau protein into Alzheimer paired helical filaments depends on a local sequence motif ((306)VQIVYK(311)) forming beta structure.* Proc Natl Acad Sci U S A, 2000. **97**(10): p. 5129-34.

26. Drechsel, D.N., et al., *Modulation of the dynamic instability of tubulin assembly by the microtubule-associated protein tau.* Mol Biol Cell, 1992. **3**(10): p. 1141-54.

27. Papasozomenos, S.C. and L.I. Binder, *Phosphorylation determines two distinct species of Tau in the central nervous system.* Cell Motil Cytoskeleton, 1987. **8**(3): p. 210-26.

28. Brady, R.M., R.P. Zinkowski, and L.I. Binder, *Presence of tau in isolated nuclei from human brain.* Neurobiol Aging, 1995. **16**(3): p. 479-86.

29. Malmqvist, T., K. Anthony, and J.M. Gallo, *Tau mRNA is present in axonal RNA granules and is associated with elongation factor 1A.* Brain Res, 2014. **1584**: p. 22-7.

30. Aronov, S., et al., *Axonal tau mRNA localization coincides with tau protein in living neuronal cells and depends on axonal targeting signal.* J Neurosci, 2001. **21**(17): p. 6577-87.

31. Morita, T. and K. Sobue, *Specification of neuronal polarity regulated by local translation of CRMP2 and Tau via the mTOR-p70S6K pathway.* J Biol Chem, 2009. **284**(40): p. 27734-45.

32. Hirokawa, N., et al., *Selective stabilization of tau in axons and microtubule-associated protein 2C in cell bodies and dendrites contributes to polarized localization of cytoskeletal proteins in mature neurons.* J Cell Biol, 1996. **132**(4): p. 667-79.

33. Li, X., et al., *Novel diffusion barrier for axonal retention of Tau in neurons and its failure in neurodegeneration.* EMBO J, 2011. **30**(23): p. 4825-37.

34. Johnson, G.V. and W.H. Stoothoff, *Tau phosphorylation in neuronal cell function and dysfunction.* J Cell Sci, 2004. **117**(Pt 24): p. 5721-9.

35. Watanabe, A., et al., *In vivo phosphorylation sites in fetal and adult rat tau.* J Biol Chem, 1993. **268**(34): p. 25712-7.

36. Lovestone, S., et al., *Alzheimer's disease-like phosphorylation of the microtubule-associated protein tau by glycogen synthase kinase-3 in transfected mammalian cells.* Curr Biol, 1994. **4**(12): p. 1077-86.

37. Baumann, K., et al., *Abnormal Alzheimer-like phosphorylation of tau-protein by cyclin-dependent kinases cdk2 and cdk5.* FEBS Lett, 1993. **336**(3): p. 417-24.

38. Correas, I., J. Diaz-Nido, and J. Avila, *Microtubule-associated protein tau is phosphorylated by protein kinase C on its tubulin binding domain.* J Biol Chem, 1992. **267**(22): p. 15721-8.

39. Litersky, J.M., et al., *Tau protein is phosphorylated by cyclic AMP-dependent protein kinase and calcium/calmodulin-dependent protein kinase II within its microtubule-binding domains at Ser-262 and Ser-356.* Biochem J, 1996. **316 (Pt 2)**: p. 655-60.

40. Liu, F., et al., *Contributions of protein phosphatases PP1, PP2A, PP2B and PP5 to the regulation of tau phosphorylation.* Eur J Neurosci, 2005. **22**(8): p. 1942-50.

41. Luna-Munoz, J., et al., *Regional conformational change involving phosphorylation of tau protein at the Thr231, precedes the structural change detected by Alz-50 antibody in Alzheimer's disease.* J Alzheimers Dis, 2005. **8**(1): p. 29-41.

42. Wang, J.Z., X. Gao, and Z.H. Wang, *The physiology and pathology of microtubule-associated protein tau.* Essays Biochem, 2014. **56**: p. 111-23.

43. Liu, F., et al., *O-GlcNAcylation regulates phosphorylation of tau: a mechanism involved in Alzheimer's disease.* Proc Natl Acad Sci U S A, 2004. **101**(29): p. 10804-9.

44. Alonso, A., et al., *Hyperphosphorylation induces self-assembly of tau into tangles of paired helical filaments/straight filaments.* Proc Natl Acad Sci U S A, 2001. **98**(12): p. 6923-8.

45. Jeganathan, S., et al., *Global hairpin folding of tau in solution.* Biochemistry, 2006. **45**(7): p. 2283-93.

46. Jeganathan, S., et al., *Proline-directed pseudo-phosphorylation at AT8 and PHF1 epitopes induces a compaction of the paperclip folding of Tau and generates a pathological (MC-1) conformation.* J Biol Chem, 2008. **283**(46): p. 32066-76.

47. Braak, H. and E. Braak, *Neuropathological stageing of Alzheimer-related changes.* Acta Neuropathol, 1991. **82**(4): p. 239-59.

48. Ward, S.M., et al., *Tau oligomers and tau toxicity in neurodegenerative disease.* Biochem Soc Trans, 2012. **40**(4): p. 667-71.

49. Braak, H. and K. Del Tredici, *The pathological process underlying Alzheimer's disease in individuals under thirty.* Acta Neuropathol, 2011. **121**(2): p. 171-81.

50. Bennett, D.A., et al., *Neuropathology of older persons without cognitive impairment from two community-based studies.* Neurology, 2006. **66**(12): p. 1837-44.

51. Braak, H., et al., *Stages of the pathologic process in Alzheimer disease: age categories from 1 to 100 years.* J Neuropathol Exp Neurol, 2011. **70**(11): p. 960-9.

52. Crary, J.F., et al., *Primary age-related tauopathy (PART): a common pathology associated with human aging.* Acta Neuropathol, 2014. **128**(6): p. 755-66.

53. Saman, S., et al., *Exosome-associated tau is secreted in tauopathy models and is selectively phosphorylated in cerebrospinal fluid in early Alzheimer disease.* J Biol Chem, 2012. **287**(6): p. 3842-9.

54. Yamada, K., et al., *In vivo microdialysis reveals age-dependent decrease of brain interstitial fluid tau levels in P301S human tau transgenic mice.* J Neurosci, 2011. **31**(37): p. 13110-7.

55. Pooler, A.M., et al., *Physiological release of endogenous tau is stimulated by neuronal activity.* EMBO Rep, 2013. **14**(4): p. 389-94.

56. Liu, L., et al., *Trans-synaptic spread of tau pathology in vivo.* PLoS One, 2012. **7**(2): p. e31302.

57. Clavaguera, F., et al., *Transmission and spreading of tauopathy in transgenic mouse brain.* Nat Cell Biol, 2009. **11**(7): p. 909-13.

58. Ahmed, Z., et al., *A novel in vivo model of tau propagation with rapid and progressive neurofibrillary tangle pathology: the pattern of spread is determined by connectivity, not proximity.* Acta Neuropathol, 2014. **127**(5): p. 667-83.

59. Dujardin, S., et al., *Neuron-to-neuron wild-type Tau protein transfer through a trans-synaptic mechanism: relevance to sporadic tauopathies.* Acta Neuropathol Commun, 2014. **2**: p. 14.

60. Lasagna-Reeves, C.A., et al., *Alzheimer brain-derived tau oligomers propagate pathology from endogenous tau.* Sci Rep, 2012. **2**: p. 700.

61. Espinoza, M., et al., *Differential incorporation of tau isoforms in Alzheimer's disease.* J Alzheimers Dis, 2008. **14**(1): p. 1-16.

62. Holton, J.L., et al., *Familial Danish dementia: a novel form of cerebral amyloidosis associated with deposition of both amyloid-Dan and amyloid-beta.* J Neuropathol Exp Neurol, 2002. **61**(3): p. 254-67.

63. Ghetti, B., et al., *Gerstmann-Straussler-Scheinker disease and the Indiana kindred.* Brain Pathol, 1995. **5**(1): p. 61-75.

64. Arai, T., et al., *Distinct isoforms of tau aggregated in neurons and glial cells in brains of patients with Pick's disease, corticobasal degeneration and progressive supranuclear palsy.* Acta Neuropathol, 2001. **101**(2): p. 167-73.

65. Sergeant, N., et al., *Dysregulation of human brain microtubule-associated tau mRNA maturation in myotonic dystrophy type 1.* Hum Mol Genet, 2001. **10**(19): p. 2143-55.

66. Goedert, M. and R. Jakes, *Mutations causing neurodegenerative tauopathies.* Biochim Biophys Acta, 2005. **1739**(2-3): p. 240-50.

67. van Swieten, J.C., S.M. Rosso, and P. Heutink, *MAPT-Related Disorders*, in *GeneReviews(R)*, R.A. Pagon, et al., Editors. 1993: Seattle (WA).

68. Murray, M.E., et al., *Clinicopathologic assessment and imaging of tauopathies in neurodegenerative dementias.* Alzheimers Res Ther, 2014. **6**(1): p. 1.

69. Vidal, R., et al., *A stop-codon mutation in the BRI gene associated with familial British dementia.* Nature, 1999. **399**(6738): p. 776-81.

70. Murrell, J., et al., *A mutation in the amyloid precursor protein associated with hereditary Alzheimer's disease.* Science, 1991. **254**(5028): p. 97-9.

71. Sherrington, R., et al., *Cloning of a gene bearing missense mutations in early-onset familial Alzheimer's disease.* Nature, 1995. **375**(6534): p. 754-60.

72. Goate, A., et al., *Segregation of a missense mutation in the amyloid precursor protein gene with familial Alzheimer's disease.* Nature, 1991. **349**(6311): p. 704-6.

73. Levy-Lahad, E., et al., *Candidate gene for the chromosome 1 familial Alzheimer's disease locus.* Science, 1995. **269**(5226): p. 973-7.

74. Rogaev, E.I., et al., *Familial Alzheimer's disease in kindreds with missense mutations in a gene on chromosome 1 related to the Alzheimer's disease type 3 gene.* Nature, 1995. **376**(6543): p. 775-8.

75. Giaccone, G., et al., *Neurofibrillary tangles of the Indiana kindred of Gerstmann-Straussler-Scheinker disease share antigenic determinants with those of Alzheimer disease.* Brain Res, 1990. **530**(2): p. 325-9.

76. Holton, J.L., et al., *Regional distribution of amyloid-Bri deposition and its association with neurofibrillary degeneration in familial British dementia.* Am J Pathol, 2001. **158**(2): p. 515-26.

77. Karran, E., M. Mercken, and B. De Strooper, *The amyloid cascade hypothesis for Alzheimer's disease: an appraisal for the development of therapeutics.* Nat Rev Drug Discov, 2011. **10**(9): p. 698-712.

78. McKhann, G., et al., *Clinical diagnosis of Alzheimer's disease: report of the NINCDS-ADRDA Work Group under the auspices of Department of Health and Human Services Task Force on Alzheimer's Disease.* Neurology, 1984. **34**(7): p. 939-44.

79. Iqbal, K. and I. Grundke-Iqbal, *Mechanism of Alzheimer neurofibrillary degeneration and the formation of tangles.* Mol Psychiatry, 1997. **2**(3): p. 178-80.

80. Dickson, D.W., *Neuropathology of Alzheimer's disease and other dementias.* Clin Geriatr Med, 2001. **17**(2): p. 209-28.

81. Lee, V.M., M. Goedert, and J.Q. Trojanowski, *Neurodegenerative tauopathies.* Annu Rev Neurosci, 2001. **24**: p. 1121-59.

82. Spillantini, M.G. and M. Goedert, *Tau protein pathology in neurodegenerative diseases.* Trends Neurosci, 1998. **21**(10): p. 428-33.

83. Ebneth, A., et al., *Overexpression of tau protein inhibits kinesin-dependent trafficking of vesicles, mitochondria, and endoplasmic reticulum: implications for Alzheimer's disease.* J Cell Biol, 1998. **143**(3): p. 777-94.

84. Hardy, J.A. and G.A. Higgins, *Alzheimer's disease: the amyloid cascade hypothesis.* Science, 1992. **256**(5054): p. 184-5.

85. Selkoe, D.J., *The molecular pathology of Alzheimer's disease.* Neuron, 1991. **6**(4): p. 487-98.

86. Braak, H., et al., *Staging of Alzheimer disease-associated neurofibrillary pathology using paraffin sections and immunocytochemistry.* Acta Neuropathol, 2006. **112**(4): p. 389-404.

87. Nelson, P.T., et al., *Correlation of Alzheimer disease neuropathologic changes with cognitive status: a review of the literature.* J Neuropathol Exp Neurol, 2012. **71**(5): p. 362-81.

88. Arriagada, P.V., et al., *Neurofibrillary tangles but not senile plaques parallel duration and severity of Alzheimer's disease.* Neurology, 1992. **42**(3 Pt 1): p. 631-9.

89. Shoji, M., et al., *Production of the Alzheimer amyloid beta protein by normal proteolytic processing.* Science, 1992. **258**(5079): p. 126-9.

90. Cai, H., et al., *BACE1 is the major beta-secretase for generation of Abeta peptides by neurons.* Nat Neurosci, 2001. **4**(3): p. 233-4.

91. Thal, D.R., et al., *Phases of A beta-deposition in the human brain and its relevance for the development of AD.* Neurology, 2002. **58**(12): p. 1791-800.

92. Petersen, R.C., *Mild cognitive impairment as a diagnostic entity.* J Intern Med, 2004. **256**(3): p. 183-94.

93. Corder, E.H., et al., *Gene dose of apolipoprotein E type 4 allele and the risk of Alzheimer's disease in late onset families.* Science, 1993. **261**(5123): p. 921-3.

94. Karch, C.M., C. Cruchaga, and A.M. Goate, *Alzheimer's disease genetics: from the bench to the clinic.* Neuron, 2014. **83**(1): p. 11-26.

95. Kauwe, J.S., et al., *Variation in MAPT is associated with cerebrospinal fluid tau levels in the presence of amyloid-beta deposition.* Proc Natl Acad Sci U S A, 2008. **105**(23): p. 8050-4.

96. Kim, J.E., et al., *PARP1 activation/expression modulates regional-specific neuronal and glial responses to seizure in a hemodynamic-independent manner.* Cell Death Dis, 2014. **5**: p. e1362.

97. Kettunen, P., et al., *Genetic Variants of GSK3B are Associated with Biomarkers for Alzheimer's Disease and Cognitive Function.* J Alzheimers Dis, 2015. **44**(4): p. 1313-22.

98. Jack, C.R., Jr., et al., *Tracking pathophysiological processes in Alzheimer's disease: an updated hypothetical model of dynamic biomarkers.* Lancet Neurol, 2013. **12**(2): p. 207-16.

99. Edelman, R.R. and S. Warach, *Magnetic resonance imaging (2).* N Engl J Med, 1993. **328**(11): p. 785-91.

100. Edelman, R.R. and S. Warach, *Magnetic resonance imaging (1).* N Engl J Med, 1993. **328**(10): p. 708-16.

101. Frisoni, G.B., et al., *The clinical use of structural MRI in Alzheimer disease.* Nat Rev Neurol, 2010. **6**(2): p. 67-77.

102. Deters, K.D., et al., *Cerebral hypometabolism and grey matter density in MAPT intron 10 +3 mutation carriers.* Am J Neurodegener Dis, 2014. **3**(3): p. 103-14.

103. Risacher, S.L., et al., *Baseline MRI predictors of conversion from MCI to probable AD in the ADNI cohort.* Curr Alzheimer Res, 2009. **6**(4): p. 347-61.

104. Risacher, S.L., et al., *Longitudinal MRI atrophy biomarkers: relationship to conversion in the ADNI cohort.* Neurobiol Aging, 2010. **31**(8): p. 1401-18.

105. Fjell, A.M., et al., *CSF biomarkers in prediction of cerebral and clinical change in mild cognitive impairment and Alzheimer's disease.* J Neurosci, 2010. **30**(6): p. 2088-101.

106. McDonald, C.R., et al., *Regional rates of neocortical atrophy from normal aging to early Alzheimer disease.* Neurology, 2009. **73**(6): p. 457-65.

107. Whitwell, J.L., et al., *3D maps from multiple MRI illustrate changing atrophy patterns as subjects progress from mild cognitive impairment to Alzheimer's disease.* Brain, 2007. **130**(Pt 7): p. 1777-86.

108. Murray, M.E., et al., *Clinicopathologic and 11C-Pittsburgh compound B implications of Thal amyloid phase across the Alzheimer's disease spectrum.* Brain, 2015.

109. Muehllehner, G. and J.S. Karp, *Positron emission tomography.* Phys Med Biol, 2006. **51**(13): p. R117-37.

110. Kato, T., et al., *Brain fluorodeoxyglucose (FDG) PET in dementia.* Ageing Res Rev, 2016.

111. Villemagne, V.L., et al., *Amyloid imaging with (18)F-florbetaben in Alzheimer disease and other dementias.* J Nucl Med, 2011. **52**(8): p. 1210-7.

112. Vandenberghe, R., et al., *18F-flutemetamol amyloid imaging in Alzheimer disease and mild cognitive impairment: a phase 2 trial.* Ann Neurol, 2010. **68**(3): p. 319-29.

113. Wong, D.F., et al., *In vivo imaging of amyloid deposition in Alzheimer disease using the radioligand 18F-AV-45 (florbetapir [corrected] F 18).* J Nucl Med, 2010. **51**(6): p. 913-20.

114. Ikonomovic, M.D., et al., *Post-mortem correlates of in vivo PiB-PET amyloid imaging in a typical case of Alzheimer's disease.* Brain, 2008. **131**(Pt 6): p. 1630-45.

115. Klunk, W.E., et al., *Imaging brain amyloid in Alzheimer's disease with Pittsburgh Compound-B.* Ann Neurol, 2004. **55**(3): p. 306-19.

116. Xia, C.F., et al., *[(18)F]T807, a novel tau positron emission tomography imaging agent for Alzheimer's disease.* Alzheimers Dement, 2013. **9**(6): p. 666-76.

117. Sander, K., et al., *Characterization of tau positron emission tomography tracer [F]AV-1451 binding to postmortem tissue in Alzheimer's disease, primary tauopathies, and other dementias.* Alzheimers Dement, 2016.

118. Motter, R., et al., *Reduction of beta-amyloid peptide42 in the cerebrospinal fluid of patients with Alzheimer's disease.* Ann Neurol, 1995. **38**(4): p. 643-8.

119. Vandermeeren, M., et al., *Detection of tau proteins in normal and Alzheimer's disease cerebrospinal fluid with a sensitive sandwich enzyme-linked immunosorbent assay.* J Neurochem, 1993. **61**(5): p. 1828-34.

120. Mattsson, N., et al., *Cerebrospinal fluid tau, neurogranin, and neurofilament light in Alzheimer's disease.* EMBO Mol Med, 2016. **8**(10): p. 1184-1196.

121. Sunderland, T., et al., *Decreased beta-amyloid1-42 and increased tau levels in cerebrospinal fluid of patients with Alzheimer disease.* JAMA, 2003. **289**(16): p. 2094-103.

122. Shaw, L.M., et al., *Cerebrospinal fluid biomarker signature in Alzheimer's disease neuroimaging initiative subjects.* Ann Neurol, 2009. **65**(4): p. 403-13.

123. Schraen-Maschke, S., et al., *Tau as a biomarker of neurodegenerative diseases.* Biomark Med, 2008. **2**(4): p. 363-84.

124. Rosso, S.M., et al., *Total tau and phosphorylated tau 181 levels in the cerebrospinal fluid of patients with frontotemporal dementia due to P301L and G272V tau mutations.* Arch Neurol, 2003. **60**(9): p. 1209-13.

125. O'Dowd, S.T., et al. *CSF total-tau and phospho-tau levels are low in pallidopontonigral degeneration (PPND)*. in *Movement Disorders*. 2012. Dublin, Ireland.

126. Gisslen, M., et al., *Plasma Concentration of the Neurofilament Light Protein (NFL) is a Biomarker of CNS Injury in HIV Infection: A Cross-Sectional Study.* EBioMedicine, 2016. **3**: p. 135-40.

127. Randall, J., et al., *Tau proteins in serum predict neurological outcome after hypoxic brain injury from cardiac arrest: results of a pilot study.* Resuscitation, 2013. **84**(3): p. 351-6.

128. Mattsson, N., et al., *Plasma tau in Alzheimer disease.* Neurology, 2016.

129. Mattsson, N., et al., *Association of Plasma Neurofilament Light With Neurodegeneration in Patients With Alzheimer Disease.* JAMA Neurol, 2017.

130. Rojas, J.C., et al., *Plasma neurofilament light chain predicts progression in progressive supranuclear palsy.* Ann Clin Transl Neurol, 2016. **3**(3): p. 216-25.

131. Swaminathan, S., et al., *Association of plasma and cortical amyloid beta is modulated by APOE epsilon4 status.* Alzheimers Dement, 2014. **10**(1): p. e9-e18.

132. He, W., et al., *Meta-analytic comparison between PIB-PET and FDG-PET results in Alzheimer's disease and MCI.* Cell Biochem Biophys, 2015. **71**(1): p. 17-26.

133. Minoshima, S., et al., *Metabolic reduction in the posterior cingulate cortex in very early Alzheimer's disease.* Ann Neurol, 1997. **42**(1): p. 85-94.

134. Kim, E.J., et al., *Glucose metabolism in early onset versus late onset Alzheimer's disease: an SPM analysis of 120 patients.* Brain, 2005. **128**(Pt 8): p. 1790-801.

135. Mosconi, L., et al., *Hypometabolism exceeds atrophy in presymptomatic early-onset familial Alzheimer's disease.* J Nucl Med, 2006. **47**(11): p. 1778-86.

136. Drzezga, A., et al., *Cerebral glucose metabolism in patients with AD and different APOE genotypes.* Neurology, 2005. **64**(1): p. 102-7.

137. Mosconi, L., et al., *Multicenter standardized 18F-FDG PET diagnosis of mild cognitive impairment, Alzheimer's disease, and other dementias.* J Nucl Med, 2008. **49**(3): p. 390-8.

138. Mosconi, L., et al., *MCI conversion to dementia and the APOE genotype: a prediction study with FDG-PET.* Neurology, 2004. **63**(12): p. 2332-40.

139. Perani, D., et al., *A survey of FDG- and amyloid-PET imaging in dementia and GRADE analysis.* Biomed Res Int, 2014. **2014**: p. 785039.

140. Vemuri, P., et al., *Effect of intellectual enrichment on AD biomarker trajectories: Longitudinal imaging study.* Neurology, 2016.

141. Knopman, D.S., et al., *18F-fluorodeoxyglucose positron emission tomography, aging, and apolipoprotein E genotype in cognitively normal persons.* Neurobiol Aging, 2014. **35**(9): p. 2096-106.

142. Mosconi, L., et al., *Maternal family history of Alzheimer's disease predisposes to reduced brain glucose metabolism.* Proc Natl Acad Sci U S A, 2007. **104**(48): p. 19067-72.

143. Ewers, M., et al., *Reduced FDG-PET brain metabolism and executive function predict clinical progression in elderly healthy subjects.* Neuroimage Clin, 2014. **4**: p. 45-52.

144. Habeck, C., et al., *Relationship between baseline brain metabolism measured using [(1)(8)F]FDG PET and memory and executive function in prodromal and early Alzheimer's disease.* Brain Imaging Behav, 2012. **6**(4): p. 568-83.

145. Landau, S.M., et al., *Amyloid deposition, hypometabolism, and longitudinal cognitive decline.* Ann Neurol, 2012. **72**(4): p. 578-86.

146. Minoshima, S., et al., *Alzheimer's disease versus dementia with Lewy bodies: cerebral metabolic distinction with autopsy confirmation.* Ann Neurol, 2001. **50**(3): p. 358-65.

147. Womack, K.B., et al., *Temporoparietal hypometabolism in frontotemporal lobar degeneration and associated imaging diagnostic errors.* Arch Neurol, 2011. **68**(3): p. 329-37.

148. Rabinovici, G.D., et al., *Amyloid vs FDG-PET in the differential diagnosis of AD and FTLD.* Neurology, 2011. **77**(23): p. 2034-42.

149. Kerrouche, N., et al., *18FDG PET in vascular dementia: differentiation from Alzheimer's disease using voxel-based multivariate analysis.* J Cereb Blood Flow Metab, 2006. **26**(9): p. 1213-21.

150. Knopman, D.S. and R.O. Roberts, *Estimating the number of persons with frontotemporal lobar degeneration in the US population.* J Mol Neurosci, 2011. **45**(3): p. 330-5.

151. Rohrer, J.D., et al., *The heritability and genetics of frontotemporal lobar degeneration.* Neurology, 2009. **73**(18): p. 1451-6.

152. Poorkaj, P., et al., *Frequency of tau gene mutations in familial and sporadic cases of non-Alzheimer dementia.* Arch Neurol, 2001. **58**(3): p. 383-7.

153. Cruts, M., S. Kumar-Singh, and C. Van Broeckhoven, *Progranulin mutations in ubiquitin-positive frontotemporal dementia linked to chromosome 17q21.* Curr Alzheimer Res, 2006. **3**(5): p. 485-91.

154. Cruts, M., et al., *Null mutations in progranulin cause ubiquitin-positive frontotemporal dementia linked to chromosome 17q21.* Nature, 2006. **442**(7105): p. 920-4.

155. Baker, M., et al., *Mutations in progranulin cause tau-negative frontotemporal dementia linked to chromosome 17.* Nature, 2006. **442**(7105): p. 916-9.

156. Murrell, J.R., et al., *Familial multiple-system tauopathy with presenile dementia is localized to chromosome 17.* Am J Hum Genet, 1997. **61**(5): p. 1131-8.

157. Spillantini, M.G., T.D. Bird, and B. Ghetti, *Frontotemporal dementia and Parkinsonism linked to chromosome 17: a new group of tauopathies.* Brain Pathol, 1998. **8**(2): p. 387-402.

158. Goedert, M., et al., *Multiple isoforms of human microtubule-associated protein tau: sequences and localization in neurofibrillary tangles of Alzheimer's disease.* Neuron, 1989. **3**(4): p. 519-26.

159. Neary, D., et al., *Frontotemporal lobar degeneration: a consensus on clinical diagnostic criteria.* Neurology, 1998. **51**(6): p. 1546-54.

160. Rascovsky, K., et al., *Sensitivity of revised diagnostic criteria for the behavioural variant of frontotemporal dementia.* Brain, 2011. **134**(Pt 9): p. 2456-77.

161. Spina, S., et al., *The tauopathy associated with mutation +3 in intron 10 of Tau: characterization of the MSTD family.* Brain, 2008. **131**(Pt 1): p. 72-89.

162. Kanda, T., et al., *Comparison of grey matter and metabolic reductions in frontotemporal dementia using FDG-PET and voxel-based morphometric MR studies.* Eur J Nucl Med Mol Imaging, 2008. **35**(12): p. 2227-34.

163. Ishii, K., et al., *Cerebral glucose metabolism in patients with frontotemporal dementia.* J Nucl Med, 1998. **39**(11): p. 1875-8.

164. Jeong, Y., et al., *18F-FDG PET findings in frontotemporal dementia: an SPM analysis of 29 patients.* J Nucl Med, 2005. **46**(2): p. 233-9.

165. Hoffmann, M., *Frontal network syndrome testing: clinical tests and positron emission tomography brain imaging help distinguish the 3 most common dementia subtypes.* Am J Alzheimers Dis Other Demen, 2013. **28**(5): p. 477-84.

166. Bastin, C., et al., *Frontal and posterior cingulate metabolic impairment in the behavioral variant of frontotemporal dementia with impaired autonoetic consciousness.* Hum Brain Mapp, 2012. **33**(6): p. 1268-78.

167. Teune, L.K., et al., *Typical cerebral metabolic patterns in neurodegenerative brain diseases.* Mov Disord, 2010. **25**(14): p. 2395-404.

168. Peters, F., et al., *Orbitofrontal dysfunction related to both apathy and disinhibition in frontotemporal dementia.* Dement Geriatr Cogn Disord, 2006. **21**(5-6): p. 373-9.

169. Salmon, E., et al., *Predominant ventromedial frontopolar metabolic impairment in frontotemporal dementia.* Neuroimage, 2003. **20**(1): p. 435-40.

170. Lindquist, S.G., et al., *Alzheimer disease-like clinical phenotype in a family with FTDP-17 caused by a MAPT R406W mutation.* Eur J Neurol, 2008. **15**(4): p. 377-85.

171. Arvanitakis, Z., et al., *Clinical-pathologic study of biomarkers in FTDP-17 (PPND family with N279K tau mutation).* Parkinsonism Relat Disord, 2007. **13**(4): p. 230-9.

172. Lossos, A., et al., *Frontotemporal dementia and parkinsonism with the P301S tau gene mutation in a Jewish family.* J Neurol, 2003. **250**(6): p. 733-40.

173. Whitwell, J.L., et al., *Neuroimaging signatures of frontotemporal dementia genetics: C9ORF72, tau, progranulin and sporadics.* Brain, 2012. **135**(Pt 3): p. 794-806.

174. Whitwell, J.L., et al., *Voxel-based morphometry patterns of atrophy in FTLD with mutations in MAPT or PGRN.* Neurology, 2009. **72**(9): p. 813-20.

175. Bateman, R.J., et al., *Clinical and biomarker changes in dominantly inherited Alzheimer's disease.* N Engl J Med, 2012. **367**(9): p. 795-804.

176. McKhann, G.M., et al., *Clinical and pathological diagnosis of frontotemporal dementia: report of the Work Group on Frontotemporal Dementia and Pick's Disease.* Arch Neurol, 2001. **58**(11): p. 1803-9.

177. Risacher, S.L., et al., *The role of apolipoprotein E (APOE) genotype in early mild cognitive impairment (E-MCI).* Front Aging Neurosci, 2013. **5**: p. 11.

178. Reiman, E.M., et al., *Preclinical evidence of Alzheimer's disease in persons homozygous for the epsilon 4 allele for apolipoprotein E.* N Engl J Med, 1996. **334**(12): p. 752-8.

179. Miyoshi, M., et al., *In vivo detection of neuropathologic changes in presymptomatic MAPT mutation carriers: a PET and MRI study.* Parkinsonism Relat Disord, 2010. **16**(6): p. 404-8.

180. Whitwell, J.L., et al., *Magnetic resonance imaging signatures of tissue pathology in frontotemporal dementia.* Arch Neurol, 2005. **62**(9): p. 1402-8.

181. Rohrer, J.D. *Imaging in familial FTD: results of the Genetic FTD Initiative* in *9th International Conference on Frontotemporal Dementias*. 2014. Vancouver, Canada.

182. Rosen, H.J., et al., *Patterns of brain atrophy in frontotemporal dementia and semantic dementia.* Neurology, 2002. **58**(2): p. 198-208.

183. Ibanez, V., et al., *Regional glucose metabolic abnormalities are not the result of atrophy in Alzheimer's disease.* Neurology, 1998. **50**(6): p. 1585-93.

184. Chien, D.T., et al., *Early clinical PET imaging results with the novel PHF-tau radioligand [F18]-T808.* J Alzheimers Dis, 2014. **38**(1): p. 171-84.

185. Chien, D.T., et al., *Early clinical PET imaging results with the novel PHF-tau radioligand [F-18]-T807.* J Alzheimers Dis, 2013. **34**(2): p. 457-68.

186. Hsiao, K., et al., *Linkage of a prion protein missense variant to Gerstmann-Straussler syndrome.* Nature, 1989. **338**(6213): p. 342-5.

187. Goldgaber, D., et al., *Mutations in familial Creutzfeldt-Jakob disease and Gerstmann-Straussler-Scheinker's syndrome.* Exp Neurol, 1989. **106**(2): p. 204-6.

188. Hsiao, K., et al., *Mutant prion proteins in Gerstmann-Straussler-Scheinker disease with neurofibrillary tangles.* Nat Genet, 1992. **1**(1): p. 68-71.

189. Farlow, M.R., et al., *Gerstmann-Straussler-Scheinker disease. I. Extending the clinical spectrum.* Neurology, 1989. **39**(11): p. 1446-52.

190. Unverzagt, F.W., et al., *Neuropsychological function in patients with Gerstmann-Straussler-Scheinker disease from the Indiana kindred (F198S).* J Int Neuropsychol Soc, 1997. **3**(2): p. 169-78.

191. Ghetti, B., et al., *Hereditary prion protein amyloidoses.* Clin Lab Med, 2003. **23**(1): p. 65-85, viii.

192. Dlouhy, S.R., et al., *Linkage of the Indiana kindred of Gerstmann-Straussler-Scheinker disease to the prion protein gene.* Nat Genet, 1992. **1**(1): p. 64-7.

193. Ghetti, B., et al., *Gerstmann-Straussler-Scheinker disease. II. Neurofibrillary tangles and plaques with PrP-amyloid coexist in an affected family.* Neurology, 1989. **39**(11): p. 1453-61.

194. Tanaka, Y., et al., *A Japanese family with a variant of Gerstmann-Straussler-Scheinker disease.* J Neurol Neurosurg Psychiatry, 1997. **62**(5): p. 454-7.

195. Achury, C., et al., *Findings in the Gerstmann-Straussler-Scheinker syndrome in an 18F-FDG PET-CT study.* Rev Esp Med Nucl Imagen Mol, 2012. **31**(6): p. 352-3.

196. Kepe, V., et al., *PET of brain prion protein amyloid in Gerstmann-Straussler-Scheinker disease.* Brain Pathol, 2010. **20**(2): p. 419-30.

197. Plate, A., et al., *Atypical parkinsonism due to a D202N Gerstmann-Straussler-Scheinker prion protein mutation: first in vivo diagnosed case.* Mov Disord, 2013. **28**(2): p. 241-4.

198. Villemagne, V.L., et al., *11C-PiB PET ABri imaging in Worster-Drought syndrome (familial British dementia): a case report.* J Alzheimers Dis, 2010. **19**(2): p. 423-8.

199. Klunk, W.E., et al., *Uncharged thioflavin-T derivatives bind to amyloid-beta protein with high affinity and readily enter the brain.* Life Sci, 2001. **69**(13): p. 1471-84.

200. Ishikawa, K., et al., *Amyloid imaging probes are useful for detection of prion plaques and treatment of transmissible spongiform encephalopathies.* J Gen Virol, 2004. **85**(Pt 6): p. 1785-90.

201. Boxer, A.L., et al., *Amyloid imaging in distinguishing atypical prion disease from Alzheimer disease.* Neurology, 2007. **69**(3): p. 283-90.

202. Villemagne, V.L., et al., *11C-PiB PET studies in typical sporadic Creutzfeldt-Jakob disease.* J Neurol Neurosurg Psychiatry, 2009. **80**(9): p. 998-1001.

203. Hyare, H., et al., *11C-PiB PET does not detect PrP-amyloid in prion disease patients including variant Creutzfeldt-Jakob disease.* J Neurol Neurosurg Psychiatry, 2012. **83**(3): p. 340-1.

204. Okamura, N., et al., *In vivo detection of prion amyloid plaques using [(11)C]BF-227 PET.* Eur J Nucl Med Mol Imaging, 2010. **37**(5): p. 934-41.

205. Brett, M., et al., *Region of interest analysis using an SPM toolbox [abstract]*, in *Presented at the 8th International Conference on Functional Mapping of the Human Brain, June 2-6, 2002*. 2002: Sendai, Japan.

206. Johnson, S.C., et al., *Amyloid burden and neural function in people at risk for Alzheimer's Disease.* Neurobiol Aging, 2014. **35**(3): p. 576-84.

207. Yi, D., et al., *Beta-amyloid associated differential effects of APOE epsilon4 on brain metabolism in cognitively normal elderly.* Am J Geriatr Psychiatry, 2014. **22**(10): p. 961-70.

208. Renard, D., et al., *Fluorine 18-labeled fluorodeoxyglucose positron emission tomography in familial Creutzfeldt-Jakob disease.* Arch Neurol, 2008. **65**(10): p. 1390-1.

209. Eckert, T., et al., *FDG PET in the differential diagnosis of parkinsonian disorders.* Neuroimage, 2005. **26**(3): p. 912-21.

210. Piccini, P., et al., *Familial progressive supranuclear palsy: detection of subclinical cases using 18F-dopa and 18fluorodeoxyglucose positron emission tomography.* Arch Neurol, 2001. **58**(11): p. 1846-51.

211. Ghetti, B., et al., *Familial Gerstmann-Straussler-Scheinker disease with neurofibrillary tangles.* Mol Neurobiol, 1994. **8**(1): p. 41-8.

212. Deters, K.D., et al., *[(11)C]PiB PET in Gerstmann-Straussler-Scheinker disease.* Am J Nucl Med Mol Imaging, 2016. **6**(1): p. 84-93.

213. Miyazono, M., et al., *Colocalization of prion protein and beta protein in the same amyloid plaques in patients with Gerstmann-Straussler syndrome.* Acta Neuropathol, 1992. **83**(4): p. 333-9.

214. Bugiani, O., et al., *Beta PP participates in PrP-amyloid plaques of Gerstmann-Straussler-Scheinker disease, Indiana kindred.* J Neuropathol Exp Neurol, 1993. **52**(1): p. 64-70.

215. Brier, M.R., et al., *Tau and Abeta imaging, CSF measures, and cognition in Alzheimer's disease.* Sci Transl Med, 2016. **8**(338): p. 338ra66.

216. Ewers, M., et al., *Prediction of conversion from mild cognitive impairment to Alzheimer's disease dementia based upon biomarkers and neuropsychological test performance.* Neurobiol Aging, 2012. **33**(7): p. 1203-14.

217. Olsson, B., et al., *CSF and blood biomarkers for the diagnosis of Alzheimer's disease: a systematic review and meta-analysis.* Lancet Neurol, 2016. **15**(7): p. 673-84.

218. Dage, J.L., et al., *Levels of tau protein in plasma are associated with neurodegeneration and cognitive function in a population-based elderly cohort.* Alzheimers Dement, 2016.

219. Zetterberg, H., et al., *Plasma tau levels in Alzheimer's disease.* Alzheimers Res Ther, 2013. **5**(2): p. 9.

220. De Bock, M., et al., *The dual face of connexin-based astroglial Ca(2+) communication: a key player in brain physiology and a prime target in pathology.* Biochim Biophys Acta, 2014. **1843**(10): p. 2211-32.

221. Ashburner, J. and K.J. Friston, *Voxel-based morphometry--the methods.* Neuroimage, 2000. **11**(6 Pt 1): p. 805-21.

222. Rohrer, J.D., et al., *Serum neurofilament light chain protein is a measure of disease intensity in frontotemporal dementia.* Neurology, 2016. **87**(13): p. 1329-36.

223. Zetterberg, H., et al., *Association of Cerebrospinal Fluid Neurofilament Light Concentration With Alzheimer Disease Progression.* JAMA Neurol, 2016. **73**(1): p. 60-7.

224. Brett, M., et al. *Region of interest analysis using an SPM toolbox.* in *Human Brain Mapping*. 2002. Sendai, Japan.

225. Dale, A.M., B. Fischl, and M.I. Sereno, *Cortical surface-based analysis. I. Segmentation and surface reconstruction.* Neuroimage, 1999. **9**(2): p. 179-94.

226. Fischl, B., M.I. Sereno, and A.M. Dale, *Cortical surface-based analysis. II: Inflation, flattening, and a surface-based coordinate system.* Neuroimage, 1999. **9**(2): p. 195-207.

227. Jack, C.R., Jr., et al., *An operational approach to National Institute on Aging-Alzheimer's Association criteria for preclinical Alzheimer disease.* Ann Neurol, 2012. **71**(6): p. 765-75.

228. Greicius, M.D., et al., *Default-mode network activity distinguishes Alzheimer's disease from healthy aging: evidence from functional MRI.* Proc Natl Acad Sci U S A, 2004. **101**(13): p. 4637-42.

229. Yan, Z., J. Flores-Hernandez, and D.J. Surmeier, *Coordinated expression of muscarinic receptor messenger RNAs in striatal medium spiny neurons.* Neuroscience, 2001. **103**(4): p. 1017-24.

230. Motts, S.D. and B.R. Schofield, *Cholinergic and non-cholinergic projections from the pedunculopontine and laterodorsal tegmental nuclei to the medial geniculate body in Guinea pigs.* Front Neuroanat, 2010. **4**: p. 137.

231. Gomez-Ramos, A., et al., *Extracellular tau promotes intracellular calcium increase through M1 and M3 muscarinic receptors in neuronal cells.* Mol Cell Neurosci, 2008. **37**(4): p. 673-81.

232. Gomez-Ramos, A., et al., *Characteristics and consequences of muscarinic receptor activation by tau protein.* Eur Neuropsychopharmacol, 2009. **19**(10): p. 708-17.

233. Mersiyanova, I.V., et al., *A new variant of Charcot-Marie-Tooth disease type 2 is probably the result of a mutation in the neurofilament-light gene.* Am J Hum Genet, 2000. **67**(1): p. 37-46.

234. Figlewicz, D.A., et al., *Variants of the heavy neurofilament subunit are associated with the development of amyotrophic lateral sclerosis.* Hum Mol Genet, 1994. **3**(10): p. 1757-61.

235. Lavedan, C., et al., *A mutation in the human neurofilament M gene in Parkinson's disease that suggests a role for the cytoskeleton in neuronal degeneration.* Neurosci Lett, 2002. **322**(1): p. 57-61.

236. Trojanowski, J.Q., N. Walkenstein, and V.M. Lee, *Expression of neurofilament subunits in neurons of the central and peripheral nervous system: an immunohistochemical study with monoclonal antibodies.* J Neurosci, 1986. **6**(3): p. 650-60.

237. Zhu, Q., S. Couillard-Despres, and J.P. Julien, *Delayed maturation of regenerating myelinated axons in mice lacking neurofilaments.* Exp Neurol, 1997. **148**(1): p. 299-316.

238. Fernandez-Martos, C.M., et al., *Neurofilament light gene deletion exacerbates amyloid, dystrophic neurite, and synaptic pathology in the APP/PS1 transgenic model of Alzheimer's disease.* Neurobiol Aging, 2015. **36**(10): p. 2757-67.

239. Vickers, J.C., et al., *Alterations in neurofilament protein immunoreactivity in human hippocampal neurons related to normal aging and Alzheimer's disease.* Neuroscience, 1994. **62**(1): p. 1-13.

240. Idland, A.V., et al., *CSF neurofilament light levels predict hippocampal atrophy in cognitively healthy older adults.* Neurobiol Aging, 2017. **49**: p. 138-144.

241. Sperling, R.A., et al., *Toward defining the preclinical stages of Alzheimer's disease: recommendations from the National Institute on Aging-Alzheimer's Association workgroups on diagnostic guidelines for Alzheimer's disease.* Alzheimers Dement, 2011. **7**(3): p. 280-92.

242. Hansson, O., et al., *Blood-based NfL: A biomarker for differential diagnosis of parkinsonian disorder.* Neurology, 2017. **88**(10): p. 930-937.

243. Deters, K.D., et al., *Plasma Tau Association with Brain Atrophy in Mild Cognitive Impairment and Alzheimer's Disease.* J Alzheimers Dis, 2017.

244. Hirschhorn, J.N. and M.J. Daly, *Genome-wide association studies for common diseases and complex traits.* Nat Rev Genet, 2005. **6**(2): p. 95-108.

245. Escott-Price, V., et al., *Polygenic score prediction captures nearly all common genetic risk for Alzheimer's disease.* Neurobiol Aging, 2017. **49**: p. 214 e7-214 e11.

246. Lalli, M.A., et al., *Whole-genome sequencing suggests a chemokine gene cluster that modifies age at onset in familial Alzheimer's disease.* Mol Psychiatry, 2015. **20**(11): p. 1294-300.

247. Ma, X. and L. Gao, *Biological network analysis: insights into structure and functions.* Brief Funct Genomics, 2012. **11**(6): p. 434-42.

248. Barabasi, A.L. and Z.N. Oltvai, *Network biology: understanding the cell's functional organization.* Nat Rev Genet, 2004. **5**(2): p. 101-13.

249. Bruckner, A., et al., *Yeast two-hybrid, a powerful tool for systems biology.* Int J Mol Sci, 2009. **10**(6): p. 2763-88.

250. Rapaport, F., et al., *Classification of microarray data using gene networks.* BMC Bioinformatics, 2007. **8**: p. 35.

251. Bar-Joseph, Z., et al., *Computational discovery of gene modules and regulatory networks.* Nat Biotechnol, 2003. **21**(11): p. 1337-42.

252. Cline, M.S., et al., *Integration of biological networks and gene expression data using Cytoscape.* Nat Protoc, 2007. **2**(10): p. 2366-82.

253. Robertson, L.A., K.L. Moya, and K.C. Breen, *The potential role of tau protein O-glycosylation in Alzheimer's disease.* J Alzheimers Dis, 2004. **6**(5): p. 489-95.

254. Warde-Farley, D., et al., *The GeneMANIA prediction server: biological network integration for gene prioritization and predicting gene function.* Nucleic Acids Res, 2010. **38**(Web Server issue): p. W214-20.

255. Stark, C., et al., *BioGRID: a general repository for interaction datasets.* Nucleic Acids Res, 2006. **34**(Database issue): p. D535-9.

256. Wong, A.K., et al., *IMP: a multi-species functional genomics portal for integration, visualization and prediction of protein functions and networks.* Nucleic Acids Res, 2012. **40**(Web Server issue): p. W484-90.

257. Szklarczyk, D., et al., *STRING v10: protein-protein interaction networks, integrated over the tree of life.* Nucleic Acids Res, 2015. **43**(Database issue): p. D447-52.

258. Ashburner, M., et al., *Gene ontology: tool for the unification of biology. The Gene Ontology Consortium.* Nat Genet, 2000. **25**(1): p. 25-9.

Curriculum Vitae

Kacie Danielle Deters

Education

PhD in Medical Neuroscience August 2017
Indiana University Indianapolis, IN
Dissertation: "Tau and neurodegeneration: neuroimaging, genes, and biomarkers."
Advisor: Andrew J Saykin, PsyD

MS in Biology August 2012
California State University, Dominguez Hills Carson, CA
Thesis title: "Association analysis of variance within the microtubule associated protein-tau (MAPT) gene and phenotypes of Alzheimer's disease."
Advisor: Andrew J Saykin, PsyD

BS in Biology May 2008
University of Alabama at Birmingham Birmingham, AL

Research Funding

Current
1R36AG053445-01
National Institute on Aging
Role: PI
"Investigation of the Tau Gene Network and Quantitative Alzheimer's Disease Biomarker Phenotypes."
09/01/2016-07/31/2017
Total direct: $43,376

Honors/Awards

Indiana University School of Medicine Travel Award April 2017
Indiana University School of Medicine Travel Award April 2016
Alzheimer's Association International Conference Travel Fellowship, Alzheimer's Association April 2016
Larry Kays Fellowship, Indiana University School of Medicine September 2015
SPINES Neuroscience Symposium Travel Award September 2015
Trainee Professional Development Award, Society for Neuroscience August 2015
Neuroscience Scholars Program Associate August 2015
Indiana University School of Medicine Travel Award June 2015
Alzheimer's Imaging Consortium Travel Fellowship, Alzheimer's Association April 2015
American Society of Human Genetics Conference Travel Award, FASEB MARC Program August 2014
Best Poster Presentation, CSUDH Student Research Day February 2011
Bridge to the Doctorate, National Institute of Health May 2010 - 2012

Professional Memberships

Toastmaster's International Member 2015
Alzheimer's Association International Society to Advance Alzheimer's Research and Treatment (ISTAART) Student Member 2015
Society for Neuroscience (SfN) Student Member 2014
American Society for Human Genetics (ASHG) Student Member 2014

Research Experience

Doctoral Research 2013 - 2017
IU Center for Neuroimaging Department of Radiology and Imaging Sciences
Indianapolis, IN
Principal Investigator: Andrew J Saykin, PsyD

- Characterizing the neuroimaging signatures of familial tauopathies.
- Evaluation of plasma tau across the Alzheimer's disease spectrum, as well as associations with cognition, brain structure, and cerebrospinal fluid analytes.
- Investigating the tau gene network and quantitative Alzheimer's disease biomarker phenotypes.

Clinical Research Coordinator Assistant 2011 - 2012
University of Texas Southwestern Medical Center Dallas, TX

- Assist breast cancer research coordinators with sample collection and processing, and data entry.

Student Research, Department of Anatomy and Neurobiology 2010-2011
University of California, Irvine Irvine, CA
Principal Investigator: Oswald Steward, PhD

- Studied the effects of the phosphatase and tensin homolog (*PTEN*) gene deletion on neuronal regeneration after spinal cord injury in rodent models.

Master's Research 2010 - 2012
IU Center for Neuroimaging Department of Radiology and Imaging Sciences
Indianapolis, IN
Principal Investigator: Andrew J Saykin, PsyD

- Genetic association of the tau gene with neuroimaging measures and cerebrospinal fluid measures in participants with Alzheimer's disease and mild cognitive impairment.

Publications

Original manuscripts

- **Deters KD**, Risacher SL, Farlow MR, Unverzagt FW, Kareken DA, Hutchins GD, Yoder KK, Murrell JR, Spina S, Epperson F, Saykin AJ, and Ghetti B. Cerebral hypometabolism in carriers of the intron 10 + 3 *MAPT* mutation. *American Journal of Neurodegenerative Disease.* 2014; 3(3): 103-114.

- **Deters K.D.***, Risacher S.L.**, Yoder K.K., Oblak A.L., Unverzagt F.W., Murrell J.R., Epperson F., Tallman E.F., Quaid K.A., Farlow M.R., Saykin A.J., and Ghetti B. [11-C]PiB PET in Gerstmann–Sträussler–Scheinker Disease. *American Journal of Nuclear Medicine and Molecular Imaging.* 2016; 6(1):84-93. *****Dual first authors
- **Deters KD**, Risacher SL, Kim S, Nho K, West JD, Blennow K, Zetterberg H, Crane PK, Shaw L, Trojanowski J, Weiner MW, and Saykin AJ for the Alzheimer Disease Neuroimaging Initiative. Plasma tau association with atrophy in mild cognitive impairment and Alzheimer's disease. *Journal of Alzheimer's Disease.* 2017 May 25. doi: 10.3233/JAD-161114.
- **Deters KD**, Risacher SL, Kim S, Nho K, Ramanan V, Saykin AJ, and the Alzheimer Disease Neuroimaging Initiative. Genetic influence on language performance using genome-wide association studies. *Brain & Language*. 2017 May 31. https://doi.org/10.1016/j.bandl.2017.04.008.

In preparation

- **Deters KD**, Risacher SL, Farlow MR, Unverzagt FW, Hutchins GD, Yoder KK, Murrell JR, Epperson F, Saykin AJ, and Ghetti B. Glucose hypometabolism in Gerstmann–Sträussler–Scheinker Patients with the F198S mutation.
- **Deters KD,** Risacher SL, Blennow K, Zetterberg H, Weiner MW, and Saykin AJ for the Alzheimer Disease Neuroimaging Initiative. Elevated plasma neurofilament light chain is association with reduced grey matter density in AD and MCI.
- **Deters KD**, Risacher SL, Parks R, Saykin AJ. PET in Alzheimer's disease. *Neuropsychology of Alzheimer's disease and other dementias (2nd edition).*

Ad Hoc Reviewer

Brain Imaging and Behavior

Academic/Leadership Experience

Indiana University Graduate School Exhibitor 2016
Annual Biomedical Research Conference for Minority Students Tampa, FL

- Met with and discussed research and graduate school opportunities during and beyond the undergraduate years.

Graduate School and Career Workshop 2016
California State University, Dominguez Hills Carson, CA

- Speaker representing Indiana University and the Bridge to the Doctorate Program.
- Discussed my journey to, and during, graduate school.

Brain and Beyond 2015 – 2017
Indiana University School of Medicine, Neuroscience Center Indianapolis, IN

- Delivered presentations using PowerPoint and plastic models to discuss the broad field of neuroscience to middle and high school students in Indiana with the goal to stimulate interest in neuroscience disciplines.
- Participated in the Brain and Beyond Annual science fair for the students.

Guest Lecturer, Undergraduate Neuroscience Program 2015 – 2017
Indiana University – Purdue University Indianapolis Indianapolis, IN
Mentor: Stephen Boehm II, PhD

- Planned and led PowerPoint presentations for undergraduate students in various upper class courses: Systems Neuroscience (PSY-B 301), Drugs and Behavior (PSY-B 394), and Behavioral Neuroscience (PSY-B 320).
- Created and graded test questions for the lectures taught.
- Met with Dr. Boehm regularly to discuss my performance and ways to improve.

Medical Neuroscience Representative 2015 – 2017
Indiana University School of Medicine, Biomedical Gateway Program Indianapolis, IN

- Participate in Graduate Professional Student Government council meetings.
- Took part in the Graduate Curriculum Committee where I gave feedback regarding the current and future planning of graduate requirements, both for current courses and for graduation.
- Reviewed travel grants for fellow graduate students and disseminated funds as the group saw appropriate.

Hoosier Science and Engineering Fair Judge 2015
Science Education Foundation of Indiana Indianapolis, IN

- Judged science projects from elementary to high school levels.

Adjunct Faculty, Biology Department 2010 – 2011
California State University, Dominguez Hills Carson, CA

- Taught General Biology Laboratory (BIO103).
- Created course syllabus and planned lessons and tests based on the course objectives.

Graduate Teaching Assistant 2009
California State University, Dominguez Hills Carson, CA

- Taught several lectures, graded papers, homework assignments, and tests throughout the semester for the Personal, Social and Intellectual Development (UNV101) course for first-year college students.

Student Teaching, Biology Department 2007 – 2008
University of Alabama at Birmingham Birmingham, AL
Course Director: Dennis Kearns

- Taught Human Anatomy Laboratory (BY115L) using PowerPoint presentations, human cadavers, plastic models, and A.D.A.M. Interactive Anatomy software.
- Created and graded tests and homework assignments based on course objectives.
- Took part in the dissection of the human cadavers used for this course.

Conferences/Presentations

Oral Presentations

Deters KD. (December 2016) Tau protein in Alzheimer's disease. Stark Neuroscience Research Institute Seminar Series, Indianapolis, IN.

Deters KD, Risacher SL, Nho K, Kim S, West JD, Blennow K, Zetterberg H, Weiner MW, and Saykin AJ for the Alzheimer's Disease Neuroimaging Initiative. (November 2016) Comparison of CSF and plasma tau biomarker associations with atrophy on magnetic resonance imaging in Alzheimer's disease and mild cognitive impairment. Society for Neuroscience, San Diego, CA.

Deters KD, Risacher SL, Nho K, Kim S, Saykin AJ, and the Alzheimer's Disease Neuroimaging Initiative. (July 2016) Plasma tau levels in mild cognitive impairment and Alzheimer's disease. Alzheimer's Association International Conference, Toronto, Canada.

Deters KD, Nho K, Risacher SL, Kim S, Vidal R, Saykin AJ, and the Alzheimer's Disease Neuroimaging Initiative. (October 2015) *BRI3* allelic variants are associated with cerebrospinal fluid levels of phosphorylated-tau in Alzheimer's disease. Toyo University and IUPUI International Scientific Exchange Symposium, Indianapolis, IN.

Poster Presentations

Deters K.D, Nho K, Risacher S.L., Kim S, Vidal R, Saykin AJ, and the Alzheimer's Disease Neuroimaging Initiative. (October 2015) *BRI3* allelic variants are associated with cerebrospinal fluid levels of phosphorylated-tau in Alzheimer's disease. Society for Neuroscience Annual Meeting, Chicago, IL.

Deters KD, Nho K, Risacher SL, Kim S, Ramanan VK, Crane PK, Apostolova L, Saykin AJ, and the Alzheimer's Disease Neuroimaging Initiative. (July 2015) Genome-wide association study of language performance in Alzheimer's disease. Alzheimer's Association International Conference, Washington D.C.

Deters KD, Risacher SL, Farlow MR, Unverzagt FW, Hutchins GD, Yoder KK, Murrell JR, Epperson F, Saykin AJ, and Ghetti B. (Julys 2015) Glucose hypometabolism in Gerstmann–Sträussler–Scheinker Patients with the F198S mutation. Alzheimer's Imaging Consortium, Washington D.C. Nominated for best poster.

Deters KD, Nho K, Kim S, Weiner MW, Foroud T, Trojanowski JQ, Shaw LM, Green RC, Toga AW, Saykin AJ, and the Alzheimer's Disease Neuroimaging Initiative. (October 2014) Association Analysis of *MAPT* with Cerebrospinal Fluid Tau Using Targeted Sequencing Data in Older Adults with Mild Cognitive Impairment or Alzheimer's Disease. The American Society of Human Genetics Conference, San Diego, CA.

Deters KD, Nho K, Kim S, Weiner MW, Foroud T, Trojanowski JQ, Shaw LM, Green RC, Toga AW, Saykin AJ, and the Alzheimer's Disease Neuroimaging Initiative. (October 2014) Association Analysis of *MAPT* with Cerebrospinal Fluid Tau Using Targeted Sequencing Data in Older Adults with Mild Cognitive Impairment or Alzheimer's Disease. Indianapolis Chapter of the Society for Neuroscience Annual Meeting, Indianapolis, IN.

Deters KD, Risacher SL, Farlow MR, Unverzagt FW, Kareken DA, Hutchins GD, Yoder KK, Murrell JR, Spina S, Epperson F, Saykin AJ, and Ghetti B. (April 2014) Cerebral hypometabolism in carriers of the intron 10 + 3 *MAPT* mutation. IUPUI Research Day, Indianapolis, IN.

Deters KD, Risacher SL, Farlow MR, Unverzagt FW, Kareken DA, Hutchins GD, Yoder KK, Murrell JR, Spina S, Epperson F, Saykin AJ, and Ghetti B. (March 2014) Cerebral hypometabolism in carriers of the intron 10 + 3 *MAPT* mutation. Indiana Alzheimer's Disease Center Scientific Symposium on AD, Indianapolis, IN.

Deters KD, Risacher SL, Farlow MR, Unverzagt FW, Kareken DA, Hutchins GD, Yoder KK, Murrell JR, Spina S, Epperson F, Saykin AJ, and Ghetti B. (October 2013) Cerebral hypometabolism in carriers of the intron 10 + 3 *MAPT* mutation. The Indiana Neuroimaging Symposium, Bloomington, IN.

Deters KD, Risacher SL, Farlow MR, Unverzagt FW, Kareken DA, Hutchins GD, Yoder KK, Murrell JR, Spina S, Epperson F, Saykin AJ, and Ghetti B. (October 2013) Cerebral hypometabolism in carriers of the intron 10 + 3 *MAPT* mutation. Indianapolis Chapter of the Society for Neuroscience Annual Meeting, Indianapolis, IN.

Deters KD, Nho K, Kim S, Swaminathan S, Risacher SL, Foroud T, Shen L, Saykin AJ, and the Alzheimer's Disease Neuroimaging Initiative. (November 2011) CSF association with *MAPT* polymorphisms and haplotypes. Annual Biomedical Research Conference for Minorities, St. Louis, MO.

Deters KD, Nho K, Kim S, Swaminathan S, Risacher SL, Foroud T, Shen L, Saykin AJ, and the Alzheimer's Disease Neuroimaging Initiative. (July 2011) CSF association with *MAPT* polymorphisms and haplotypes. IUPUI Research Symposium, Indianapolis, IN.

Deters KD, Nho K, Kim S, Swaminathan S, Risacher SL, Foroud T, Shen L, Saykin AJ, and the Alzheimer's Disease Neuroimaging Initiative. (February 2011) Association of haplotypes of the *MAPT* gene with Alzheimer's Disease and Quantitative Neuroimaging Phenotypes. CSUDH Student Research Day, Carson, CA. Best poster presentation winner.

Deters KD, Nho K, Kim S, Swaminathan S, Risacher SL, Foroud T, Shen L, Saykin AJ, and the Alzheimer's Disease Neuroimaging Initiative. (November 2010) Association of haplotypes of the *MAPT* gene with Alzheimer's Disease and Quantitative Neuroimaging Phenotypes. Annual Biomedical Research Conference for Minorities, Charlotte, NC.

Deters KD, Nho K, Kim S, Swaminathan S, Risacher SL, Foroud T, Shen L, Saykin AJ, and the Alzheimer's Disease Neuroimaging Initiative. (July 2010) Association of haplotypes of the *MAPT* gene with Alzheimer's Disease and Quantitative Neuroimaging Phenotypes. IUPUI Research Symposium**,** Indianapolis, IN.